EVALUATION OF IMAGE TUBES IN ASTRONOMY

A Thesis

Presented for the Degree of Doctor of Philosophy

by

PETER W. J. L. BRAND

UNIVERSITY OF EDINBURGH

May 1967

C O N T E N T S

		Page
Acknowledgments		
Introduction		1
	PART I	
Chapter I	Discussion of Detector Analysis: Equivalent Quantum Efficiency, Granularity, Fourier Analysis, Information Theory	9
Chapter II	Measurement of Granularity	27
Chapter III	Absolute Sensitivity and Modulation Transfer Function Measures	42
Chapter IV	Linearity of Response of Electronography: G5 Emulsion Model	54
Results of Part I		70
	PART II	
Chapter V	Mounting on a Cassegrain Spectrograph	73
Chapter VI	Astronomical Program: Width of Profile of Interstellar Band at 4430A	85
Conclusions		92
Appendix		
References		

ACKNOWLEDGMENTS

I extend my sincere thanks to my supervisors for helping to make this project a success. Professor Brück has at all times shown a stimulating interest in the research, and frequently has been able to remove material hurdles from its path. Dr Smyth has ably guided the project and helped me to circumvent the hiatuses encountered.

I am grateful to the University of Edinburgh for a Studentship during my first year, and to the Cormack Bequest Committee of the Royal Society of Edinburgh for a Fellowship during my second year.

I also wish to thank Dr Baker of the British Scientific Instrument Research Association and the staff of the Optical Metrology Department of the National Physical Observatory for helpful discussions; Mr Nilsen of Tartu Observatory, Estonia, who stayed at the Observatory for some months, and who advised me on regression methods applied to the analysis of profiles; and the staff of the Observatory, particularly Mr Matthews and the staff of the workshop, almost all of whom at one time or another have helped to advance the work.

Especial thanks are due to Professor McGee and his staff at Imperial College, who made and supplied the tubes (once at very short notice indeed) and who have shown interest in the work done at the Observatory.

Last, and most, I thank my wife, who not only encouraged me when difficulties arose, but also typed this thesis under most trying circumstances.

P.W.J.L.B.

INTRODUCTION

Of the sciences, astronomy occupies, in its nature, a unique position - it is entirely observational. The phenomena studied are *a priori* beyond our interference. Even today, as science advances, those parts of the universe accessible to man cease to be the object of astronomical study, and become instead a part of experimental physics.

Thus, the tools of the astronomer are essentially observational tools, and an analysis of their efficacy is a consideration of their value as receivers of signals. For, however we may improve our instrumental techniques, we cannot improve on the information contained in the signal received. The proper approach to this problem already exists; it is Information Theory, created to deal with problems of intercommunication and warfare, by Wiener, Shannon and others.

The signals to be dealt with by the astronomer are radiations of all types from parts of the universe too distant to be investigated by more direct means, and the vital necessity of evaluating astronomical detectors is due to the fact that most of these radiations are of such low intensity that their effects are not large compared with background disturbances of local origin.

The detectors used to meet these conditions, once visual observation was superseded, have been photographic emulsions and photoelectric cells. The electromagnetic radiation studied has been that in or near the visible waveband, and later also radio wavelengths, these limitations being dictated, until the recent advent of space astronomy, by the transparency of the atmosphere to different wavelengths of radiation.

These two separate methods have had their own advantages; photographic emulsions, though not efficient detectors of light, can register and store a large amount of information, highly resolved with respect to position on the detector; photoelectric cells on the other hand, particularly photomultipliers, can efficiently detect light falling on them, but have no resolution in the above sense, i.e. have only one 'channel'.

The concept of using a photocathode as detector and emulsion as recorder is due to Lallemand,[1] who first used such a device for astronomy in 1936, thus pioneering the research of which this thesis is a part.

Since then, Lallemand has been the instigator of a continued project, the Camera Electronique, which is now a most refined instrument, and is used, with detectors derived from it, all over the world. The chief drawback to the Camera Electronique is its complexity, which stems

from the fact that the photocathode and photographic (more strictly electronographic) emulsion are in the same evacuated compartment. Descriptions of the Camera Electronique have appeared in numerous publications, for instance the Report of the Second Symposium on Photoelectronic Imaging Devices[2]; so it has not been considered advantageous to describe it here.

Since Lallemand's first trial of astronomical photography with an image intensifying system, many different methods have been used. These may be divided into three categories:

(a) Scanning systems (T.V.)

(b) Optical output (phosphor screen intensifiers)

(c) Electronographic systems (electron beam 'writes' on emulsion)

Of these, the most promising are storage cameras in category (a), cascaded systems in category (b), and the Camera Electronique, and derivatives of it, and the Spectracon (of which more will be written below) in category (c). Category (a) systems, by virtue of their electrical signal output, are suited to certain specialised applications, such as rocketry, but are otherwise not as efficient as others, due to effects such as storage decay, beam bending, beam noise, etcetera and since such systems were not subjected to study by

the author, will not further be considered. Discussion of their properties, and of present development may be found in the Third Symposium Report.[3]

The cascaded intensifier with phosphor output is being extensively developed by the Carnegie Image Tube Committee in America, and by Professor McGee and EMI Electronics Limited, and seems to have considerable promise as a means of amplifying signals to an extent that the signal-to-noise ratio in the recorder is large. The main drawback at present seems to be the difficulty of designing suitable transfer optics,[4] which, being an implicit part of the system, will limit the information throughput. However, a considerable amount of astronomical work[5] has been done with this tube, and with the secondary electron transmission tube, also developed by Professor McGee.

Despite improvements in these devices, it seems to the author that, since each process in the recording of an image must reduce the information carried in the original signal,[6] a method of electronographic recording must give the highest equivalent quantum efficiency, since so few signal transfer processes are involved. This certainly applies until the noise added, and spatial frequency response degradation, at each stage for the other types of tube has been reduced to negligible

proportions. To investigate these properties, an approach such as that set forth in Chapter I must be used, since the whole purpose of an intensifier system, if not used merely for convenience (i.e. as a signal transducer) must be to increase informational throughput, and this can only be studied in the terms of Chapter I, as done, for instance, by Beckman.[7]

This present report is concerned with one type of tube only - the electronographic tube devised by Professor McGee, and christened the Spectracon. This tube has now reached such a stage of development that its routine use in astronomical spectrophotometric programs could become commonplace, as this report is intended to demonstrate (Part II).

The Spectracon is designed to overcome the chief difficulty associated with the Camera Electronique, that is, the location of emulsion in the same evacuated compartment as the photocathode. This feature means that the photocathode must frequently be replaced, and a complex pumping system and emulsion cooling system employed in use. By contrast, the Spectracon needs no further preparation once in position on the telescope. The means by which this advantage is achieved is by the logical extension of the idea used for instance by Hiltner[8] of placing a thin protective membrane between

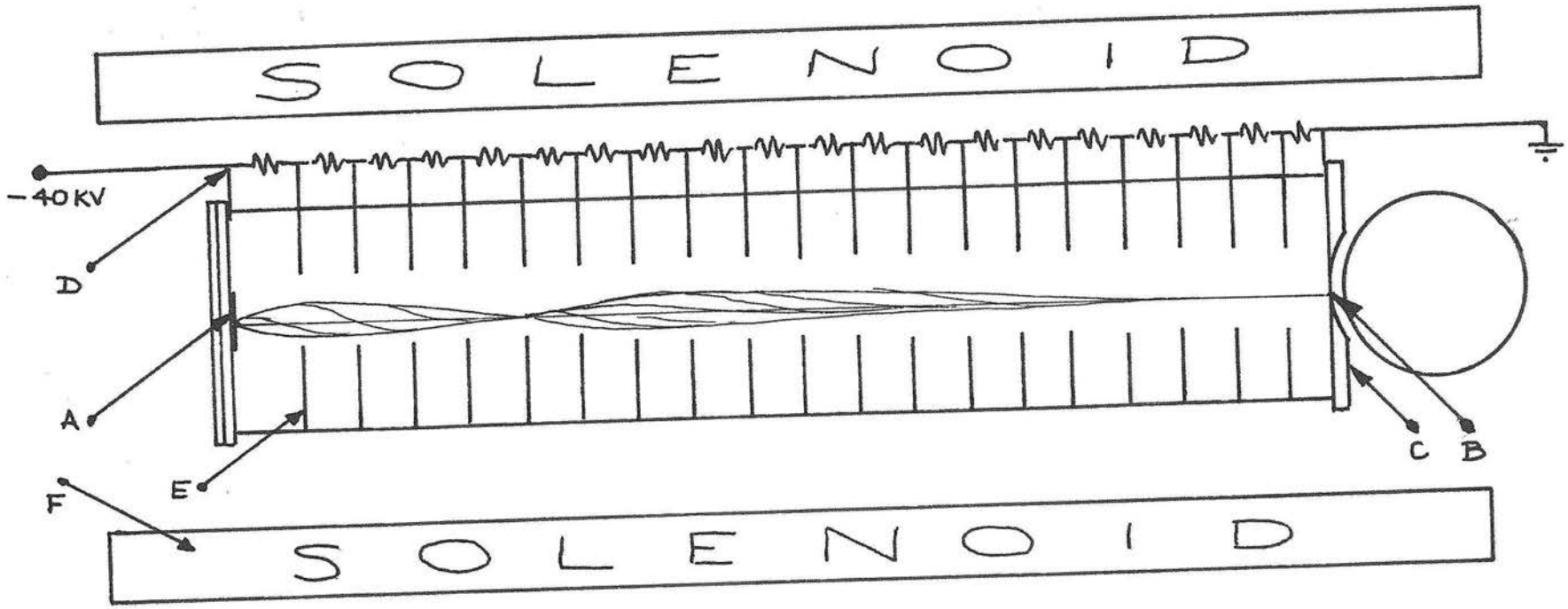

Figure 1 Diagram of the Spectracon

cathode and emulsion (since the membrane cannot withstand atmospheric pressure a complex system of vacuum locks and pumps must be used for this tube). In the tube designed by Professor McGee, use is made of the remarkable lateral strength of thin mica sheet, which forms both the protective membrane for the cathode and, since it can easily withstand atmospheric pressure when thin enough to allow electrons to pass through it, part of the evacuated envelope. In this way, the emulsion is always outside the tube, being exposed to the signal beam by being pressed in contact with the mica window.

Figure 1 is a diagram of the Spectracon, showing (A) the photocathode, type S11 ($SbCs_3$) at present, but capable of being infrared sensitive or, in the future, a trialkali cathode. Electrons emitted by the cathode are accelerated by a potential of about 40 KV between the cathode and aluminium backed thin mica window (B), which is attached with solderglass to a cylindrical depression in the chrome iron end piece (C) (later models use titanium here, to avoid magnetic distortion).

The cylindrical depression, in the centre of which is the 1cm x 3cm exit slot, ensures that the mica is subjected to curvature in one direction only, avoiding stress at the edges of the slot. The potential on the tube is rendered uniform by a bleeder chain (D) connected

to the ring annodes (E) in which are cut slots to match the shape of cathode and mica window. These not only improve field uniformity, but also prevent stray electrons from causing ion emission from the glass walls, which would increase background. The electrons are constrained to perform helical trajectories (see Chapter V), by the solenoid (F) and two loop focussing is employed, to reduce S-distortion.

A more detailed description is given by Professor McGee in the Third Symposium Report,[3] and the description of the tube's experimental development in a thesis by Khogali.[9]

The aim of the work to be described is to evaluate an example of this tube informationally, according to unique principles described in Chapter I, and expanded in Part I, and to show that the tube is a useful instrument in routine spectrophotometry, which work is described in Part II.

P A R T I

CHAPTER I

Discussion of Detector Analysis : Equivalent Quantum Efficiency, Granularity, Fourier Analysis, Information Theory

(i) Equivalent Quantum Efficiency

The concept of equivalent quantum efficiency was introduced by Rose[10] and named by Fellgett[11] and developed for use in the case of photographic detectors by him and by Clark Jones[12] (who calls it detective quantum efficiency).

Photon interactions between a beam of radiation and matter (such as a detecting surface in the beam) obey Bose-Einstein statistics, from which can be derived (Lewis[13]) the equation for mean squared deviation of photon numbers of a given frequency in a beam of radiation interacting with the detecting surface

$$\overline{\Delta n_f}^2 = \overline{n_f}\left(1 + \frac{n_f}{N}\right) \qquad 1.1$$

where $\overline{n_f}$ is the mean number of frequency f, and N is the occupation number in phase space.

Since the second term is negligible for visible radiation, in such cases,

$$\overline{\Delta n}^2 = \overline{n} \qquad 1.2$$

and the photon statistics behave like those of randomly arriving particles, obeying the Poisson distribution law.

Now consider a detector which counts photons in a beam arriving from a source of such intensity that in a given time the number of photons detectable is n, and the average over many such time intervals $\bar{n}$. If the detector were ideal, it would count all these photons, and only these, and its signal-to-noise ratio is then

$$\bar{n} / \sqrt{\overline{\Delta n^2}} = \sqrt{\bar{n}} \qquad 1.3$$

This then expresses the ultimate accuracy of any such measurement, and any real detector would produce a lower signal-to-noise ratio in such circumstances.

Thus there is a figure of merit which is never greater than 1, but approaches 1 for nearly ideal detectors, - the ratio of actual to ideal signal-to-noise powers. The square of signal-to-noise ratio is used, rather than the first power for the following reasons. In the above case, to achieve a signal-to-noise ratio R, an ideal detector requires $n = R^2$ photons, while any actual detector will require exposure to a greater number m photons to produce the same signal-to-noise ratio R. The ratio n/m is the <u>equivalent quantum efficiency</u> E_e of the detector. This fits intuitive ideas of efficiency as may be seen thus: If an ideal detector is placed behind a filter of transmission (efficiency) equal to E_e, the signal-to-noise ratio will be $\sqrt{mE_e} = \sqrt{n}$ if m photons are available, and this is the

signal-to-noise ratio produced by an actual detector with equivalent quantum efficiency E_e exposed to m photons. We can write

$$E_e = (\text{signal:noise})^2_{\text{detected}} \,/\, (\text{signal:noise})^2_{\text{ideal}} \qquad 1.4$$

Also, $R^2 = N$ may be regarded as the noise equivalent number of photons required to produce a signal-to-noise ratio R, and N will henceforth be called the equivalent photon storage of the measurement.

(ii) Granularity

The study of photographic granularity has undergone a confused course since Selwyn's[14] pioneer work, due to initial investigations being directed largely towards subjective ends, the correlation of graininess with granularity. Granularity is measured as a mean squared deviation in density, graininess is the visual appearance of a photograph, subjectively judged as the 'roughness' of the uniform areas in the pictures. That these are opposed approaches may be brought home by the fact that a photographic emulsion carrying the maximum amount of information (that is, having maximum signal: noise optimally coded) would look like a uniformly exposed area with accentuated graininess.

An interesting paper by O'Neill[15] compares Jones and Higgins'[16] for graininess with an emulsion model,

and suggests from the similarity of graininess vs. density and entropy (see Section (iv)) that the eye is an 'information detector'.

Granularity is the 'noise' in any given measure of density or transmission, and hence a thorough understanding of it is vital to the assessment of equivalent quantum efficiencies of films.

The studies of Fellgett,[17] Clark Jones,[18] Marriage and Pitts[19] and Zweig[20] have shown how granularity may be analysed using the methods applied to electronic systems, and when these methods are applied properly, ambiguity as to expected noise values (cf. Schade[21]) disappears.

The application of these methods will now be described.

(iii) Fourier Analysis Applied to Granularity : the Wiener Spectrum

The following normalisation (R. Woodward[22]) of the 2-dimensional Fourier transform pairs will be used

$$g(u,v) = \iint f(x,y)\ e^{+2\pi i(ux+vy)}\,dx\,dy$$

$$f(x,y) = \iint g(u,v)\ e^{-2\pi i(ux+vy)}\,du\,dv$$

To discuss granularity, we shall base consideration upon the following experimental conditions. A uniformly exposed photographic emulsion is scanned with a finite aperture projected on to the film with a microscope objective and values of density or transmittance are

sampled at different positions. The average of these values is the mean density or transmittance, and the limiting values that would be measured if the aperture were infinitesimally small and the optics perfect (producing no degradation of detail) will be called the 'true' values of these quantities. And with the choice of density or transmittance, transmittance will be used as the variable, since this is the one measured in the experiments, and since this choice renders some of the results below somewhat less approximately (in particular the averaging effect of the aperture, see below e.g. (1.6).

If $\bar{T}$ is the mean value of transmittance over the film, and $\Delta T = T - \bar{T}$, then the Fourier transform over the film is

$$F(u,v) = \int_A \Delta T(x,y)\ e^{2\pi i(ux+vy)}\, dx\, dy \qquad 1.5$$

If the film is scanned with a finite aperture and physically realisable optics, then there will exist an aperture function $a(x'y')$ where $(x'y')$ is the co-ordinate system with axes parallel to those of the emulsion co-ordinates, but whose origin is defined by a point in the aperture projected on the emulsion. This function $a(x'y')$ is determined by the projected size of the aperture, and by the image spread introduced by the optics. (This last point has been largely overlooked in earlier experimental work on granularity).

The subscript 'a' will be used to denote values derived from measures with such a system, as opposed to those relating to 'true' values.

Then,

$$\Delta T_a(x,y) = \int_A \Delta T(x+x',y+y')\ a(x',y')dx'dy' \qquad 1.6$$

is the observed fluctuation in transmittance.

By the convolution theorem, if $b(u,v)$ is the Fourier transform of $a(x'y')$, then the Fourier transform of $\Delta T_a(x,y)$ is $F(u,v)b(u,v)$, and $b(u,v)$ may be called the aperture filter function, in analogy with electrical usage, or the modulation transfer function of the aperture in conformity with recommendations by the Sub-Committee for Image Assessment Problems of the I.C.O., July 1961. This modulation transfer function will be dealt with more fully later (Chapter II, section ii).

So far, only a finite piece of photographic emulsion has been considered, and equation (1.5) raises no mathematical difficulties. However, the function $F(u,v)$ contains a deal of information regarding phase relationships which are not relevant to the statistical properties of the film, but arise out of the particular measurements made. More useful quantities are the noise spectrum, or Wiener spectrum (so named by Clark Jones), which is defined

$$n(u,v) = \frac{1}{A} \left| F(u,v) \right|^2 \qquad 1.7$$

and the autocorrelation function

$$\varphi(x,y) = \frac{1}{A} \int_A \Delta T(X+x, Y+y)\, \Delta T(X,Y)\, dX dY \qquad 1.8$$

Since

$$n(u,v) = \frac{1}{A} F(u,v) F^{+}(u,v) \qquad 1.9$$

where $^{+}$ denotes complex conjugation, the Fourier transform of $n(u,v)$ is

$$\frac{1}{A} \Delta T(x,y) * \Delta T(-x,-y) = \varphi(x,y) \qquad 1.10$$

where * denotes convolution

$$\text{i.e. } \varphi(x,y) = \int_A n(u,v)\, e^{-2\pi i(ux+vy)} du dv \qquad 1.11$$

$$\text{and } n(u,v) = \int_A \varphi(x,y)\, e^{2\pi i(ux+vy)} dx dy \qquad 1.12$$

Note that $n(u,v)$ and (x,y) are even functions, so that equations (1.11) and (1.12) may be written:

$$\varphi(x,y) = 4 \int_{+A} n(u,v) \cos 2\pi(ux+vy)\, du dv \qquad 1.11a$$

$$n(u,v) = 4 \int_{+A} \varphi(x,y) \cos 2\pi(ux+vy)\, dx dy \qquad 1.12a$$

with the integrations taken over positive values of (u,v), (x,y).

These results still apply only to the particular piece of film measured, but if the physical postulate is made that the statistical properties of the emulsion are a sample of the properties of the ensemble of all such pieces, then the generalised harmonic analysis of

Wiener[23] may be applied, and equations (1.7), (1.8) still hold as limits in the mean, although such equations as (1.5) no longer exist. Equation (1.7) becomes

$$n(u,v) = \underset{A \to \infty}{\text{l.i.m.}} \frac{1}{A} |F(u,v)|^2 \qquad 1.13$$

and (1.8) becomes

$$\varphi(x,y) = \underset{A \to \infty}{\text{l.i.m.}} \frac{1}{A} \int_A \Delta T(X+x,Y+y)\, \Delta T(X,Y)\, dX\underline{dY} \qquad 1.14$$

and equations (1.7) and (1.8) are estimates of these quantities.

Thus the noise power spectrum and autocorrelation function are the proper functions with which to deal with granularity. It should be noticed that these functions are still Fourier transforms of one another, and therefore contain the same information with regard to granularity.

From the definitions of noise spectrum and aperture function, the noise spectrum measured with a given aperture and projection optics is

$$n_a(u,v) = |b(u,v)|^2\, n(u,v)$$

since

$$\varphi(o,o) = \underset{A \to \infty}{\text{l.i.m.}} \frac{1}{A} \int \Delta T(x,y)^2\, dxdy \qquad 1.15$$

and $$\varphi(o,o) = \int n(u,v)\, dudv \qquad 1.16$$

from equations (1.14) and (1.11) respectively,

and $$\varphi_a(o,o) = \text{l.i.m.}\ \frac{1}{A}\int \Delta T_a(x,y)^2\, dxdy \qquad 1.17$$

$$\varphi_a(o,o) = \int |b(u,v)|^2\, n(u,v)\, dudv \qquad 1.18$$

and since the first and third of these equations are the 'true' and 'measured' mean squared deviations in transmission, as statistical properties of the film, σ_t^2 and $\sigma_{t_a}^2$,

$$\sigma_t^2 = \int n(u,v)\, dudv \qquad 1.19$$

$$\sigma_{t_a}^2 = \int |b(u,v)|^2\, n(u,v)\, dudv \qquad 1.20$$

where the integrations extend over the whole planes. The actual measurements are over a finite portion of film, and the derived values of σ_t^2 will be estimates, whose accuracy will be considered in Chapter II, section ii.

Thus we can estimate the 'noise' in any experimental arrangement, if we know the noise spectrum, and the modulation transfer function b(u,v) for the scanning system.

It is particularly interesting to compare equation (1.20) with Selwyn's definition of a granularity coefficient,[14]

$$S^2 = 2a.\sigma_d^2 \qquad 1.21$$

where a is the area of the scanning aperture. To

compare it with results so far derived, (1.21) must be transformed to refer to σ_t^2.

For $\sigma_D/\bar{D}$ small, which is generally the case,

$$\sigma_D = \frac{\sigma_t}{\bar{T}} \times .4343$$

and the coefficient may be redefined

$$S'^2 = 2a.\sigma_t^2 \qquad 1.22$$

Selwyn showed that under certain simplifying assumptions, S^2 (or equivalently S'^2) is independent of a.

If n(u,v) is 'flat' (i.e. if the noise spectrum is independent of frequency), (1.20) becomes

$$\sigma_{t_a}^2 = n\iint |b(u,v)|^2 \, dudv$$

Since b(o,o) = 1, and using Parseval's theorem,

$$\sigma_{t_a}^2 = n/a \qquad 1.23$$

where a is the equivalent scanning aperture.

The condition on n(u,v) can be relaxed to the condition that n(u,v) is 'flat' to frequencies beyond which b(u,v) is effectively zero.

Then equation (1.23) shows that if a is the equivalent scanning aperture (taking account of optical degradation), and the noise spectrum is flat enough, then Selwyn's coefficient of granularity is indeed independent of a. The failure of this relationship

in Jones and Higgins' series of papers[16] for moderate apertures ($a > 200\mu^2$) can be attributed to their neglect of the effect of the optics in degrading the aperture function of their scanning system.

(iv) Information in an Optical Image

The Fourier treatment of granularity has been described separately from an overall analysis of information, largely because it forms the most intractable part of the analysis, but also because granularity has been subject to study whose intensity has, in part, been due to a failure to realise the relevance of the methods that have just been described.

What will now be shown is that the equations deduced above accord with a rigorous treatment of the ability of photographic systems to store information, and that equivalent quantum efficiency can be expressed as a quantity whose factors relate to sensitivity, granularity and resolution respectively, in a unique and unambiguous way.

The proper approach to the problem has been dealt with by Fellgett and Linfoot in a classic paper entitled "On the Assessment of Optical Images"[24], in which the parts relevant to this section are based on Information Theory as developed by Shannon.[6]

Shannon defined a quantity H which he called entropy, and which measures the amount of information conveyed by the result of a particular choise from a set of possible events with given probabilities. In particular, if there are N equiprobable possibilities, the result being any one will convey the information H = -log N. He showed that, if a continuous signal were frequency-limited, and contained noise, then only a finite amount of information could be conveyed in a finite time. When this is applied to an optical image, we see that diffraction at a finite aperture, abberations, and turbidity of the photographic emulsion produce spatial frequency limitations on the image, and photon fluctuations and granularity of the emulsion act as noise in the signal. The frequency limitations mean that samples of the value of transmittance at a finite number of points gives as complete a knowledge of the incident signal as possible, and the further effect of noise is to limit the number of distinguishable values of transmittance at any such sampling point. This gives a finite total number N of sets of point values arising from any signal, and so a finite information increase on finding a particular set of point values.

On considering the situation in detail, and basing their calculations on certain assumptions, Fellgett and

Linfoot arrive at a value for the information content of an image, the relation of interest being their equation (3.70) which will be rewritten:

$$I = \int \log_2 \sqrt{1 + \frac{P(u,v)\,|b(u,v)|^2}{n(u,v)}}\, dudv \qquad 1.24$$

This is the information content in 'bits' resulting from the exposure of an emulsion with noise spectrum n(u,v) and modulation transfer function b(u,v) to a signal whose power spectrum is P(u,v), assuming all processes are linear. In fact, the transfer function for the photographic process is not linear, but the results hold if they are applied to low contrast signals, (which is the interesting case, since there is no difficulty in discerning signals of high contrast). If this is done, a conversion factor must be included in equation (1.24) since n(u,v) is defined in terms of emulsion variables, but P(u,v) is defined in terms of signal variables.

$$P(u,v) = \underset{A \to \infty}{\text{l.i.m.}}\ \frac{1}{A} \left| \int \Delta Q(x,y)\ e^{2\pi i(ux+vy)}\, dxdy \right|^2 \qquad 1.25$$

where Q is the number of photons.

These results can be applied to photographic emulsions in the following way. The mean transmittance (or density) of the emulsion is related to the total exposure, to the wavelengths to which it was exposed, and to the time of the exposure (reciprocity failure). If low-contrast

signals only are considered, then the transfer of these signals will be approximately linear, and the transfer factor will be the gradient of the curve relating the exposure to the transmittance (or density) at the point representing the mean value. Thus we can relate a given transmittance (or density) fluctuation to a corresponding incident signal fluctuation and equation (1.24) may be rewritten for the photographic case:

$$I = \int \log_2 \sqrt{1 + \frac{k^2 P(u,v) |b(u,v)|^2}{n(u,v)}}\, dudv \qquad 1.26$$

where k is the gradient of the macroscopic transmittance (or density) versus exposure curve, at the mean exposure of the emulsion

$$k = \frac{dT}{dQ} \quad \text{or} \quad k = \frac{dD}{dQ} \qquad 1.27$$

The second term in the surd in equation (1.26) can be related to the equivalent quantum efficiency and the equivalent photon storage in the following way. At a given point in the (u,v) frequency plane, the registered signal power is $k^2 P(u,v) |b(u,v)|^2$ and the noise power is $n(u,v)$, so that the signal-to-noise power ratio is

$$R^2(u,v) = \frac{k^2 P(u,v) |b(u,v)|^2}{n(u,v)} \qquad 1.28$$

For the ideal detector, the signal power is $P(u,v)$, and the noise power is produced by the complete randomness of the photon interaction in a 'cell' of phase space.

This means that the noise spectrum must be flat, and extend to infinity (this raises no conceptual difficulties, as the randomness is not complete - see the argument leading to equation (1.2)) otherwise a tendency for photons to interact at a particular distance from each other, or within certain limits, would be implied.

For a random process producing $\bar{Q}$ events in an area A, the response to each event being G(x,y) then the power spectrum of the process will be

$$P_Q(u,v) = \bar{Q} |H(u,v)|^2 \qquad 1.29$$

where H(u,v) is the Fourier transform of G(x,y). Now for a photon, and within the limits indicated in Section (i),

$G(x,y) = \delta(x)\delta(y)$, and so

$$P_Q(u,v) = \bar{Q} \qquad 1.30$$

(see, for instance, Carson[25]).

Then the power signal-to-noise ratio of an ideal detector under the same conditions would be

$$R_1^2(u,v) = \frac{P(u,v)}{\bar{Q}} \qquad 1.31$$

where the subscript 1 denotes an ideal detector ($E_e = 1$). So

$$E_e(u,v) = \frac{k^2 |b(u,v)|^2 \bar{Q}}{n(u,v)} \qquad 1.32$$

and we may rewrite (1.26) as

$$I = \int \log_2 \sqrt{1 + N(u,v)}\ dudv \qquad 1.33$$

where N(u,v) is the (frequency-dependent) equivalent photon storage of the measurement. These quantities relate to the quantities discussed in Section (i) in the following way:

From equations (1.3) and (1.23) for an equivalent area a

$$E_{ea} = \frac{k^2 \bar{Q}^2}{(\Delta \bar{T}^2)_a} \Big/ a.\bar{Q}$$

$$= \frac{k^2\ \bar{Q}}{a(\Delta \bar{T}^2)_a} \qquad 1.34$$

and from (1.32)

$$E_e(o,o) = \frac{k^2\ \bar{Q}}{n(o,o)} \qquad 1.35$$

now the conditions that these expressions are the same are just those mentioned in connection with the Selwyn granularity coefficient (i.e. n(u,v) is flat while $|b(u,v)|^2$ is sensibly different from zero and that this holds has been amply demonstrated[26,27]).

The incident signal is the output of the spectrograph, and is the convolution of the power spectrum of the incident radiation with the (incoherent radiation) modulation transfer function (MTF). If the radiation spectrum is carrying 'spectroscopic' information, this

may be represented by the mean squared deviation of the mean (photon average) signal, which may in turn be written as a fraction κ of the photon noise mean squared deviation. Thus, the squared signal to noise ratio of the incident spectrum is

$$R^2 = \kappa \qquad 1.36$$

or the mean signal spectrum is $\kappa\bar{Q}$ and the spatial frequency spectrum presented to the detector is

$$\kappa \bar{Q}\, b_s(u,v) \qquad 1.37$$

In the usual case, the spectrograph is slit limited, and

$$b_s(u,v) = \mathrm{sinc}^2 au \qquad 1.38$$

Hence equation (1.26) may be written

$$I = \int \log_2 \sqrt{1 + \frac{k^2\, \bar{Q} b_s |b(u,v)|^2}{n(u,v)}}\, dudv \qquad 1.39$$

$$= \int \log_2 \sqrt{1 + b_s(u,v)\, E_e(u,v)}\, dudv \qquad 1.40$$

$$= \sqrt{H} \int \log_2 \sqrt{1 + b_s(u)\, E_e(u)}\, du \qquad 1.41$$

where $E_e(u)$ is written for $E_e(\sqrt{u^2+v^2})$ and H is the spectrograph slit height and

$$E_e(u) = \sqrt{H} \cdot \frac{k^2 |b(u)|^2}{n(u,v)} \qquad 1.42$$

Note that the conditions on such equations as (1.24) are strict, requiring linearity, stationarity, entropy maximisation, and signal not too large compared with noise.

These conditions are only very approximately adhered to, but equation (1.24) will give an upper bound to information density.

CHAPTER II

Measurement of Granularity

In Chapter I there was an intentional vagueness as to the use of density or transmittance as the variable to be measured. This was for the following reason. If it were possible to measure the transmittance or density at a point in the emulsion, the transmittance would have a value close to 0 or 1, and the corresponding density would be close to 0 or very large indeed. Thus the scan of density by a small aperture would consist of wild excursions from the mean, whose magnitude would be largely determined by the response of the measuring instrument. It is therefore more sensible to measure transmittance. However, it is fairly well established that, for a given emulsion, density is proportional to the number of developed grains.[28,29,30,31,32] Thus a theoretical treatment of results is simpler in terms of density measures.

(i) Measuring equipment

Since, as will be seen below, a large amount of data is required to define granularity, the most suitable reduction of results is by computer. At the Observatory, a Hilger and Watts microphotometer has been converted by the Astronomical Instrumentation Division, to provide digital output. (Described in the Observatory Publications[33]).

This equipment scans the specimen table through a slit projected and demagnified by a microscope objective, the transmitted light being measured by photomultiplier whose output is sampled at intervals determined by a Moire fringe system, and punched out in 5-hole Edsac code.

The strips of nuclear emulsion to be measured were placed between glass plates, and scanned. The tapes produced were analysed on a KDF9 computer.

(ii) Measurement of Granularity with a Slit Aperture

The required accuracy in determining granularity specifies the number of independent samples of transmittance to be made. If we assume that fluctuations form a normal distribution, which assumption was used by Selwyn in his derivation of equation (1.20), and seems well borne out by the results of Thompson[34], then if

$$v = (T-\bar{T})^2/2\sigma^2$$

where $(\bar{T}, \sigma^2)$ are the parameters of the normal distribution,

$$p(v) = \frac{v^{-\frac{1}{2}}e^{-v}}{\Gamma(\frac{1}{2})}$$

i.e. v is a $\gamma(\frac{1}{2})$ variate.[35]

Hence,

$\sum_{1}^{n}(T-\bar{T})^2/2\sigma^2$ is a $\gamma(n/2)$ variate.

So if $s^2 = 1/N \sum(T_i - \bar{T})^2$ is an estimate of σ^2,

then $X = Ns^2/\sigma^2$ is distributed as $\chi^2(N-1)$.

For large N, $\sqrt{2X} - \sqrt{2N}$ forms a normal distribution, parameters (0,1).

Now confidence limits can be established on estimates of variance s^2.

$$\text{Prob}\ (\sigma^2(1-k)^2 < s^2 < \sigma^2(1+k)^2)$$

$$= \text{Prob}\ (N(1-k)^2 < X < N(1+k)^2)$$

$$= \text{Prob}\ (\sqrt{2N}\,(-k) < \sqrt{2X} - \sqrt{2N} < \sqrt{2N}\,(+k))$$

$$= 2\text{erf}\ (\sqrt{2N}\,k).$$

This is the probability that the estimate of variance lies within $\pm$ 100k% of true variance. A table of N for a range of values of this probability P and k follows.

	P						
	.98	.95	.90	.80	.75	.70	.65
.01	27000	19000	13500	8200	6600	5400	3500
.02	6750	4800	3400	2050	1650	1350	880
k .05	1080	770	540	330	264	216	140
.10	270	190	135	82	66	54	35
.25	43	31	21	13	10	9	6

It is seen that the number of samples necessary rises steeply as P increases and k diminishes, and for P = .98 rapidly becomes unmanagable with k .05. A value of 1000 was taken for N, giving for P = .98, k = .05.

The above analysis presupposes independent samples. The emulsion is scanned with a slit moving in the direction of its smaller dimension. To decide how frequently samples should be taken so as to be independent, the modulation transfer function (MTF) of the microphotometer must be investigated. This enters the calculations as equation (1.19). If it is assumed[26,27] that $n(u,v)$ is flat where $b(u,v) \neq o$, then

$$n(u,v) = n$$

The aperture function of the slit is 1, $|x,y| \leqslant a/2, b/2$

0 otherwise.

Taking $A = ah$ to be the area, a to be the width, h is taken to be so large that

$$b(u,v) = b(u)\,\delta(v)$$

where $\delta(v)$ is the Dirac delta function.

If the MTF of the microphotometer optics is $b_o(u,v)$

then $$b(u,v) = \frac{b_o(u)}{h} \cdot \frac{\sin^2 \pi au}{(\pi au)^2}$$

and then equation (1.19) becomes

$$\sigma_{t_a}^2 = \frac{n}{h} \int b_o^2(u) \frac{\sin^2 \pi au}{(\pi au)^2} \, du \qquad 2.1$$

It has not been possible to measure the MTF of the optical train in the microphotometer, but an estimate may be made using the results of Schade.[21] Typical lens

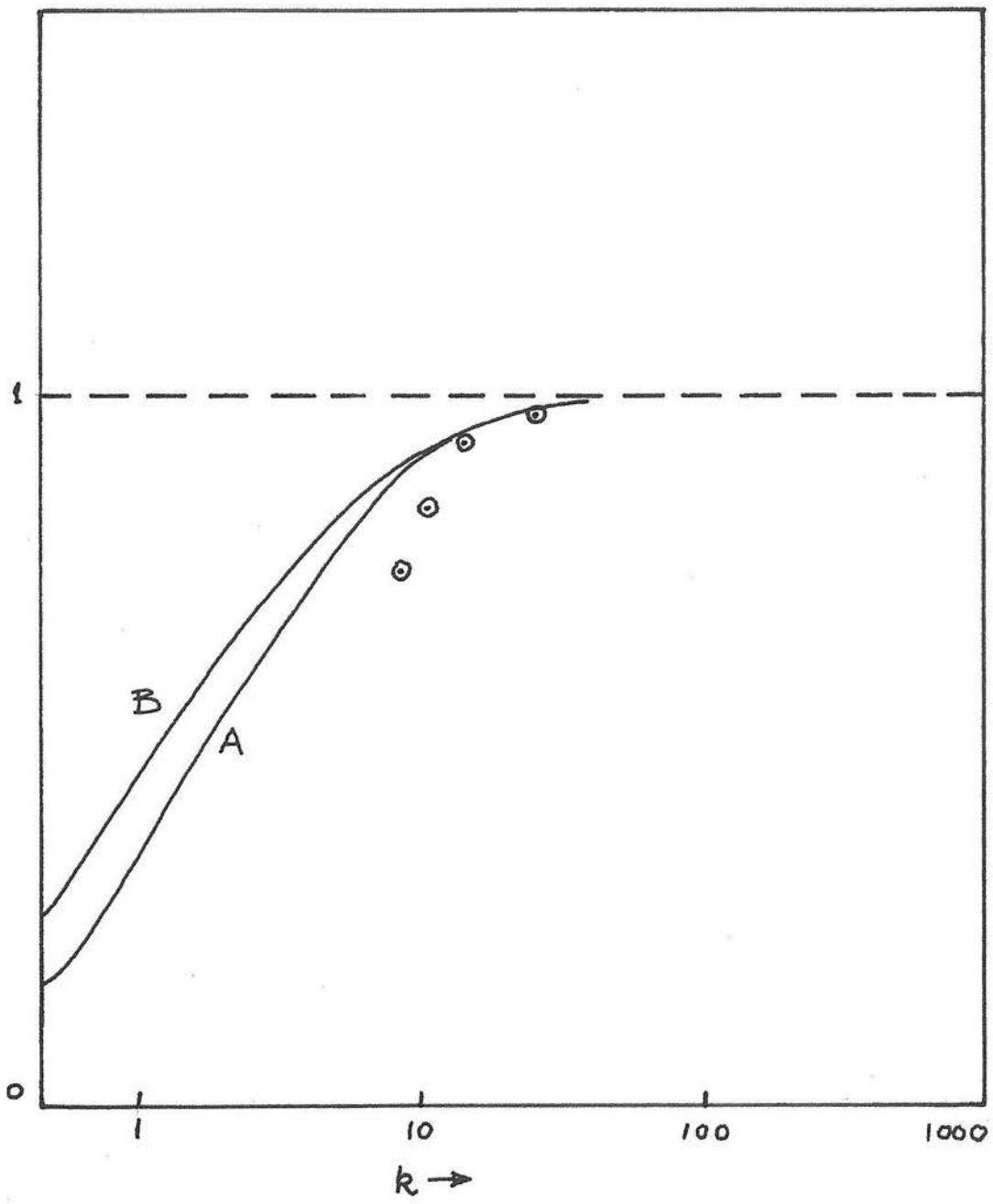

Figure 2 $A\sigma^2_{t_a} / n(o,o)$ as a function of k

MTFs lie between the functions $1-u/c$ and $e^{-u/c}$ where e is chosen to fit the slope of the MTF at low spatial frequencies. The effect on equation (2.1) of putting $b_o^2(u) = 1-u/c$ and $b_o^2(u) = \exp(-u/c)$ can be calculated.

(a) $b_o^2(u) = 1-u/c$

$$\sigma_{t_a}^2 = \frac{2n}{\pi A}\int_o^k \frac{\sin^2 f}{f^2}\,df - \frac{1}{k}\int_o^k \frac{\sin^2 f}{f}\,df$$

where $f = \pi au$, $k = \pi ac$

$$\therefore \sigma_{t_a}^2 = \frac{2n}{\pi A}\left[\left(Si(2k) - \frac{\sin^2 k}{k}\right) - \frac{1}{2k}\int^{2k}\frac{1-\cos f}{f}\,df\right]$$

$$\therefore A\sigma_{t_a}^2 = \frac{2n}{\pi}\left[Si(2k) - \frac{\sin^2 k}{k} - \frac{.577 + \ln(2k) - Ci(2k)}{2k}\right] \qquad 2.2$$

(b) $b_o^2(u) = \exp(-u/c)$

$$A\sigma_{t_a}^2 = \frac{n}{\pi}\int_o^\infty \frac{(1-\cos 2f)e^{-f/k}}{f^2}\,df$$

and by expanding cos2f and integrating term by term and equating the series to the definite integral

$$\int_o^{2k}\frac{\ln(1+y^2)}{y^2}\,dy$$

$$A\sigma_{t_a}^2 = 2\arctan(2k) - \ln(1+4k^2)/2k \qquad 2.3$$

These two determinations of $A\sigma_{t_a}^2$ are shown in figure 2 as functions of k, labelled A and B respectively. The value of c was estimated, from values for a variety of lenses in Schade's paper, to be about 300. From

figure 2 it may be seen that for either curve A or B, the deviation of $A\sigma_{t_a}^2$ from n is less than the variance of the measures estimated in the last section, when $2k = 50$. Since these two curves are bounds upon the shape of the MTF, it is reasonable to suppose that at $2k = 50$, measures of $\sigma_{t_a}^2$ will be a good estimate of n/A. In particular, $c = 300$ implies that $a = 20\,\mu m$.

If the output from the microphotometer were measured as a continuous waveform, it would be frequency-limited by the MTF of the slit and optical train. The electrical output is frequency-limited by a matching filter to eliminate noise introduced by the circuitry.[33] So the waveform sampling theorem (see e.g. Woodward[22]) may be employed to estimate the smallest sampling interval for which samples are independent. If the output is frequency-limited to u_o, and the output is represented by $T(x)$, the filtered point transmission, then

$$T(x) = \sum T(n/2u_o) \text{ since } 2u_o(x-n/2u_o) \qquad 2.4$$

The first zero of the slit MTF occurs at $u = 1/a$ and the optics degrade the frequency response further so the overall MTF will be zero at $u_o = r/a = 1/a'$ where $r < 1$, and $T(x)$ is determined by values spaced $a/2r$ apart.

By good fortune, the sample distance on the Hilger microphotometer is $12\frac{1}{2}\,\mu m$, which is the value that would have been chosen from the above consideration. The

length of the slit h was taken to be 180 μm.

The sampling theorem then gives

$$\text{l.i.m.}\ \frac{1}{X}\int_0^X T^2(x)dx = \frac{a'}{2X}\sum T_n^2 \qquad 2.5$$

where X is the length of emulsion measured, and $X = N\Delta x$ where Δx is the sample spacing.

This is the required estimate of σ_t^2

$$\overline{T^2} = \frac{a'}{2\Delta x} \cdot \frac{1}{N}\sum T_n^2 \qquad 2.6$$

and $a' = 2\Delta x$, so

$$\overline{T^2} = 1/N \sum T_n^2 \qquad 2.7$$

(iii) Computer reduction of measures

Early attempts to define estimates of σ^2 were frustrated by the incidence of marks on the cathode and mica window, and blemishes in the emulsions as supplied backed with Melinex. In the terms of Chapter I these defects correspond to low frequency components in the noise power spectrum. This may be most readily visualised in terms of the autocorrelation function, the real Fourier transform of the noise power spectrum. The autocorrelation function of the grains of halide in the emulsion exposed with the image tube tends to zero at a distance corresponding to the mean diameter of

a grain clump produced by an electron. This distance (see Chapter IV) is typically less than 10 μm. The autocorrelation function of the defects mentioned, however, will generally extend a greater distance, and the autocorrelation function of the emulsion is the sum of these two components. A device for correcting the measures has been adopted, which is essentially a high-pass filter on the noise power spectrum. By subtracting the autocorrelation function of T_i at a distance equal to the microphotometer sampling step ($12\frac{1}{2}\mu$m), the fluctuations due to defects with sizes greater than $12\frac{1}{2}\mu$m are considerably damped, while grain-dependent fluctuations are unaffected. If σ'^2_g represents the total variance of microphotometer output values g_i, with $g_i \propto T_i$, and σ_g^2 is the corrected variance,

$$\sigma_g^2 = \sigma'^2_g - \varphi_g(d) \qquad 2.8$$

where $d = 12\frac{1}{2}\mu m$

$$\varphi_g = 1/N \sum \Delta g_i \, \Delta g_{i+1}$$

$$= 1/N \sum g_i g_{i+1} - \bar{g}^2 \qquad 2.9$$

so, from (2.8) and (2.9)

$$\sigma_g^2 = 1/N \sum g_i^2 - 1/N \sum g_i g_{i+1} \qquad 2.10$$

also, if $\bar{g}_o$ is the microphotometer mean output through clear plate,

$$\bar{D} = \log_{10}\bar{g}_o - \log_{10}\bar{g} \qquad 2.11$$

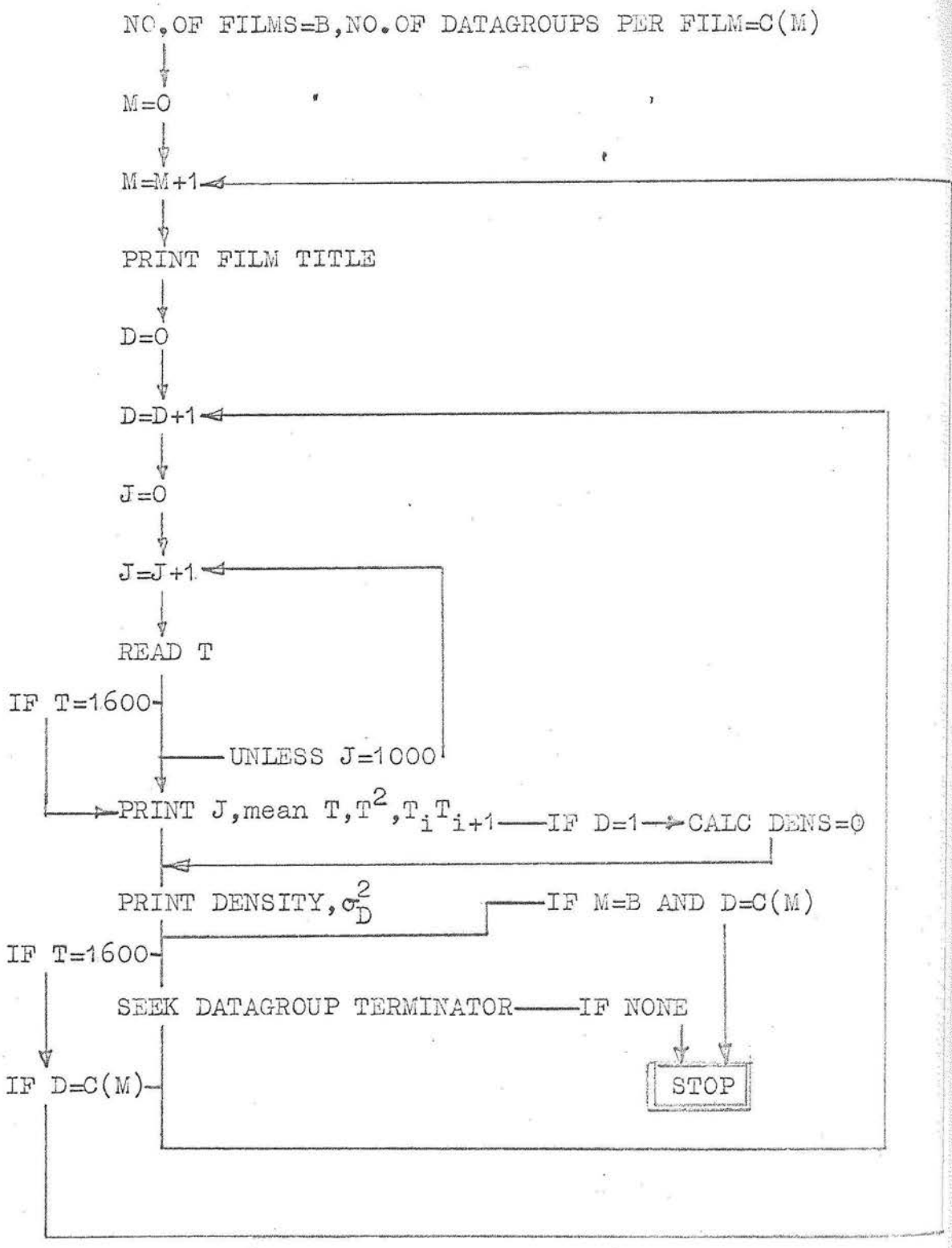

Figure 3. Flow diagram for "PHOTOGRAN Y"

and so

$$\sigma_D^2 = (.4343)^2 \sigma_g^2/\bar{g}^2 \qquad 2.12$$

assuming (as is borne out by the measurements) that the fluctuations in g are small compared with the mean value.

Finally, (2.12) and (2.10) give

$$\sigma_D^2 = .1886 \times N \left[\sum g_i^2 - \sum g_i g_{i+1}\right] \Big/ \left[\sum g_i\right]^2 \qquad 2.13$$

The use of a compensating autocorrelation function also eliminates the effect of drift in the microphotometer and uneven cathode sensitivity.

The flow diagram for the program is shown opposite (Figure 3) and a facsimile program (named PHOTOGRAN) in ISO Atlas Autocode is in the Appendix.

(iv) Instrument noise

It is obviously necessary to determine the value of the noise produced by the microphotometer itself. Such noise is separable into two parts. One part is noise due to lamp intensity fluctuations, electrical noise, and allied sources of noise, the other has been termed[36] quantisation noise. This type of noise is due to rounding errors in the digital voltmeter which feeds the paper tape punch. For example, if the instrument produced no other source of noise, and scanned a noiseless 'emulsion' whose transmittance produced an output value

midway between consecutive numbers on the digital voltmeter, the RMS deviation would be $\frac{1}{2}$ of the least significant digit. The quantisation noise in any actual case may be predicted as follows. If the value sampled by the digital voltmeter is $g = I+y$, where I is the integral part of g, then the probability of registering I is $(1-y)$, and of registering $I+1$ is y. Hence the mean squared deviation is

$$y^2(1-y)+(1-y)^2y = y(1-y) \qquad 2.14$$

The average value of quantisation noise when the sampled value is also statistically distributed over several digits will be 1/6, for it is

$$\int_0^1 y(1-y)dy = 1/6 \qquad 2.15$$

Using these results, electrical and lamp intensity noise was investigated. A photographic plate of given transmittance was supported independently of the specimen table, and placed in the focus of the measuring beam. The table drive was started at the usual value of 1mm/minute and the output punched on tape. This was done for a series of values of transmittance. On the basis of the deductions above, the expected values of quantisation-induced mean squared deviation q were calculated. These were subtracted from the measured values, and the results expressed as a percentage of q; these values are set out in the table below, which was calculated with an

earlier version of the PHOTOGRAN program, which calculated mean squared deviation in groups of 100 values. The groups have been averaged for 1,000 values, after calculating q for each group, and it is these averaged values which are displayed.

mean g	msd	q	100(msd-q)/q
1339.279	1.426	0.187	495%
451.295	0.445	0.151	195%
154.510	0.197	0.179	11%
82.487	0.168	0.102	66%
30.559	0.200	0.200	0%

The measurements took about 2 hours to run, and it is readily seen that after this time, quantisation noise plays the major part in errors in measured mean squared deviation.

(v) Confirmation of slit width value

As a check that the value chosen for the width of the scanning slit was correct, a series of measurements on the same piece of film were made, varying the slit width between runs from about 11μm to 30μm. The slit width values were checked comparing the instrument setting, and were found to agree within 5%, which was considered satisfactory. It may be seen from the table below that $A\sigma_D^2$ flattens out when $a > 20\mu$m in agreement with the value predicted in Section (ii). Values of 'a' greater than 30μm were not studied, as this introduces

new problems of non-independent sampling.

Slit width	$A\sigma_D^2$	Mean output value
11	3.025	210.1
15.5	3.51	283.4
20	4.10	366.5
30	4.30	577.8

Thus it seems fairly certain that the estimate of σ_D^2 will be an accurate one, within the limits given in Section (ii).

(vi) Results

The results are gratifyingly reproducible, within the limits predicted, and the relation between $n(o,o) = n$ and density is linear in most cases, the only important deviation from this rule being G5 at high density, where the noise seems to grow more rapidly than D. Few observations have been made with G5 for densities greater than 0.6, since, as will be seen in the results at the end of Part I of this thesis, the equivalent quantum efficiency has dropped considerably. The results are exhibited as Figure 4 for G5, XM and IIaO. The values have been corrected for quantisation noise. There is a slight spread of values of $n(o,o)$ at fog density, this being due to uneven Melinex support, or in the case of XM emulsion, different fog densities from emulsion to emulsion, and, since the program PHOTOGRAN sets fog

readings to D = 0, there will be a slight shift in the vertical direction for the graphs.

The linear relationship is most interesting, especially in view of recent discussion of this relationship[37,38,39] in the literature. The results presented accord well with Siedentopf's law for granularity. Using Nutting's[28] equation, which is borne out by many references,[29,31,32]

$$D = .43\ na/A \qquad 2.16$$

where a is projected grain area, and A is area of scanning aperture,

$$\sigma_D^2 = (.43\ na/A)^2 \sigma^2(n) \qquad 2.17$$

If the grains are distributed randomly, then $\sigma^2(n) = \bar{n}$, and

$$\sigma_D^2 = (.43\ a/A).\bar{D} \qquad 2.18$$

or $$A.\sigma_D^2 = .43\ a.\bar{D} \qquad 2.18a$$

If the clumps of grains produced by electrons in the nuclear emulsion are of mean number $\bar{m}$, and m is Poisson distributed (cf Rogers et al[40]) then if r electrons impinge randomly in A, with mean number $\bar{r}$ then

$$\begin{aligned} \sigma_n^2 &= \bar{r}\sigma_m^2 + \bar{m}^2\sigma_r^2 \\ &= \bar{r}\ \bar{m}(1 + \bar{m}) \\ &= \bar{n}(1 + \bar{m}) \end{aligned} \qquad 2.19$$

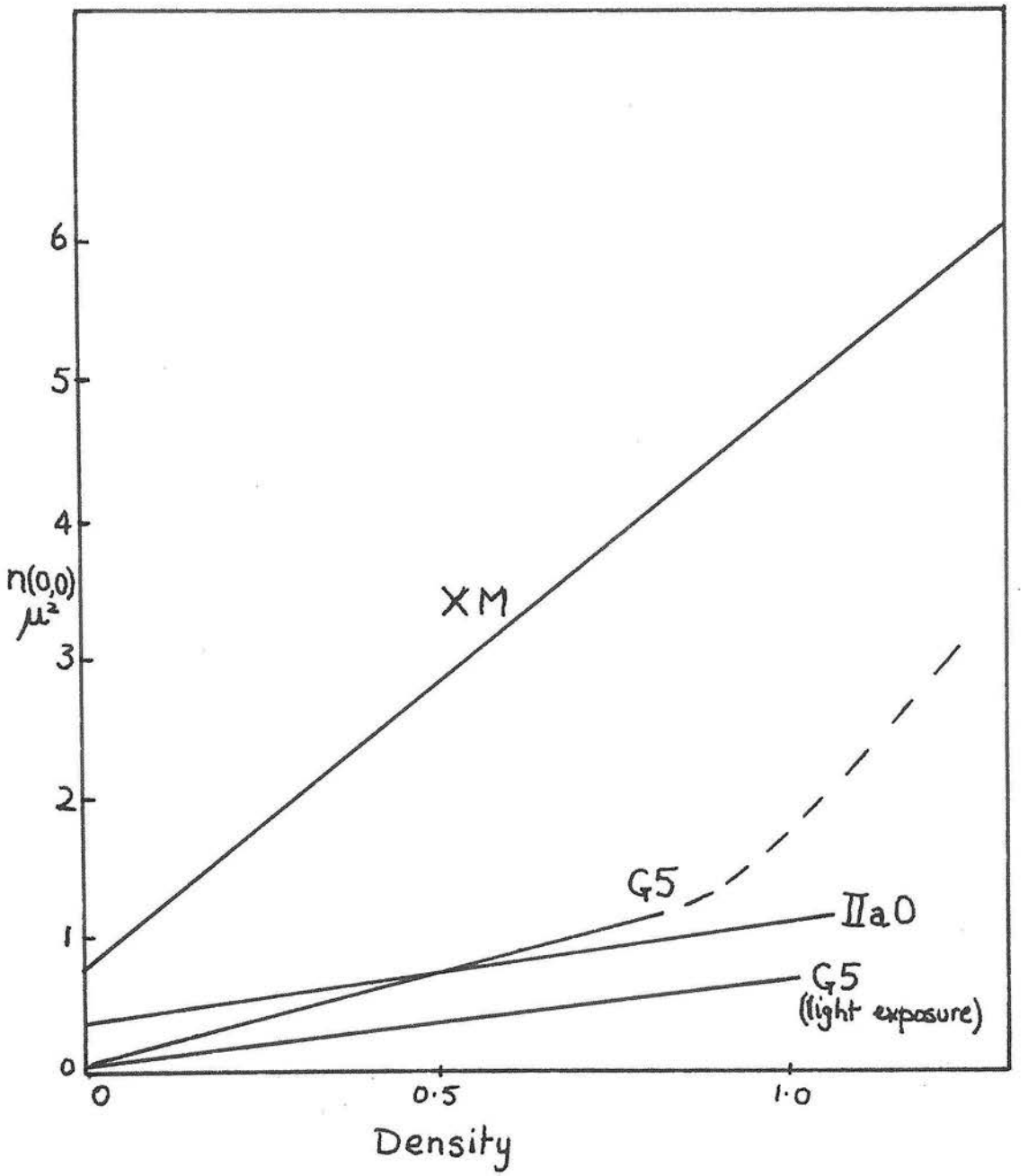

Figure 4 Noise power at zero frequency for IIaO, XM, G5 and G5 exposed to light

so $A\sigma_D^2 = .43a(1 + \bar{m})\ \bar{D}$ 2.20

and if the clumps are all of the same number of grains,

$$A\sigma_D^2 = .43a\bar{m}D \qquad 2.21$$

For G5, $A\sigma_D^2 = 1.36\bar{D}$

which gives a value for $a(1 + \bar{m})$ of $3.14\mu^2$ If we take Nutting's value of .43 for the constant in equation (2.16) then 'a' is the projected area of the developed grain, and from equation (2.20)

$$1.36 = .43a(1+\bar{m})$$

taking m = 7 from Rogers' paper,

$$a = .40\mu^2$$

and the diameter of the equivalent circular grain is

$$d = (4 \times .40/\pi)^{\frac{1}{2}}$$

$$= .71\mu$$

and since the quoted value for the mean diameter of grains in G5 emulsion is $.27\mu$[41], the amplification in linear size of a grain, caused by development, is $2\frac{1}{2}$ times. Strips of G5 exposed to light were also measured and the result plotted in Figure 4. From the slope, and the assumption of single grain statistics rather than clumps, the amplification in this case is approximately 1μ, i.e. the linear amplification is about $3\frac{1}{2}$.

The results certainly imply that for moderate densities (less than 1) $D \propto n$, and the events are in random clumps.

The values taken from the graph give the values of noise power spectrum at zero frequency:

for IIaO	$n(o,o) = 0.44\ \bar{D} + .80$	
for G5	$n(o,o) = 1.31\ \bar{D} + .08$	2.22
for XM	$n(o,o) = 5.26\ \bar{D} + .815$	

with an accuracy of $\pm 5\%$, taking into account (i) sample numbers, (ii) determination of equivalent sampling area, (iii) reduction of individual errors in values by fitting a straight line to σ_D^2 vs. D.

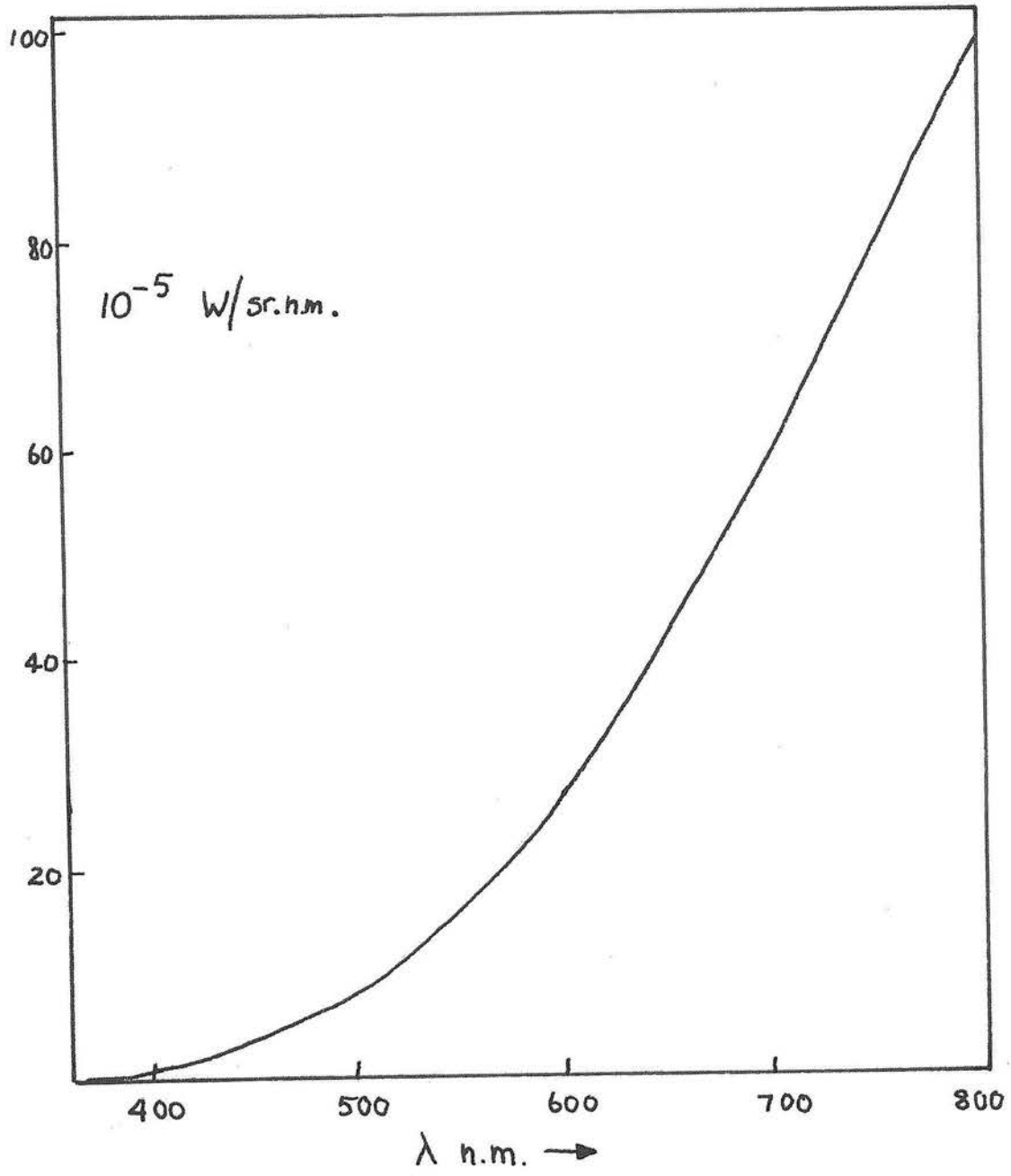

Figure 5 Wavelength calibration for Wotan lamp (watts per steradian nanometre)

CHAPTER III

Absolute Sensitivity and Modulation Transfer Function Measures

While the results of Chapter II provide sufficient data for the calculation of photon storage per unit area $N = R^2$ (see Chapter I), to evaluate equivalent quantum efficiency it is necessary to know the absolute radiation flux producing the density at which N is calculated, and it is also necessary to determine the modulation transfer function (MTF) of the image tube/emulsion combination.

(i) Absolute Light Flux

A 'Wotan' Wi41/V lamp (serial no. SoBWi281) calibrated in watts/steradian nanometer was obtained from the Munich Laboratories of Osram Limited. The colour temperature of the lamp is 2,200°K at 14.83 volts, 3.72 amps. The calibration is reproduced as Figure 5 and was converted to photons/steradian n.m.sec. After consultation with the National Physical Laboratory's Optical Metrology Department, it was decided to run the lamp from a voltage stabiliser. The stabiliser used was a Coutant Electronics Unit capable of delivering 10 amps at 30 volts with an accuracy in voltage of 1:5,000. The output was calibrated by means of a Solartron digital voltmeter. Secondary leads soldered to the lamp

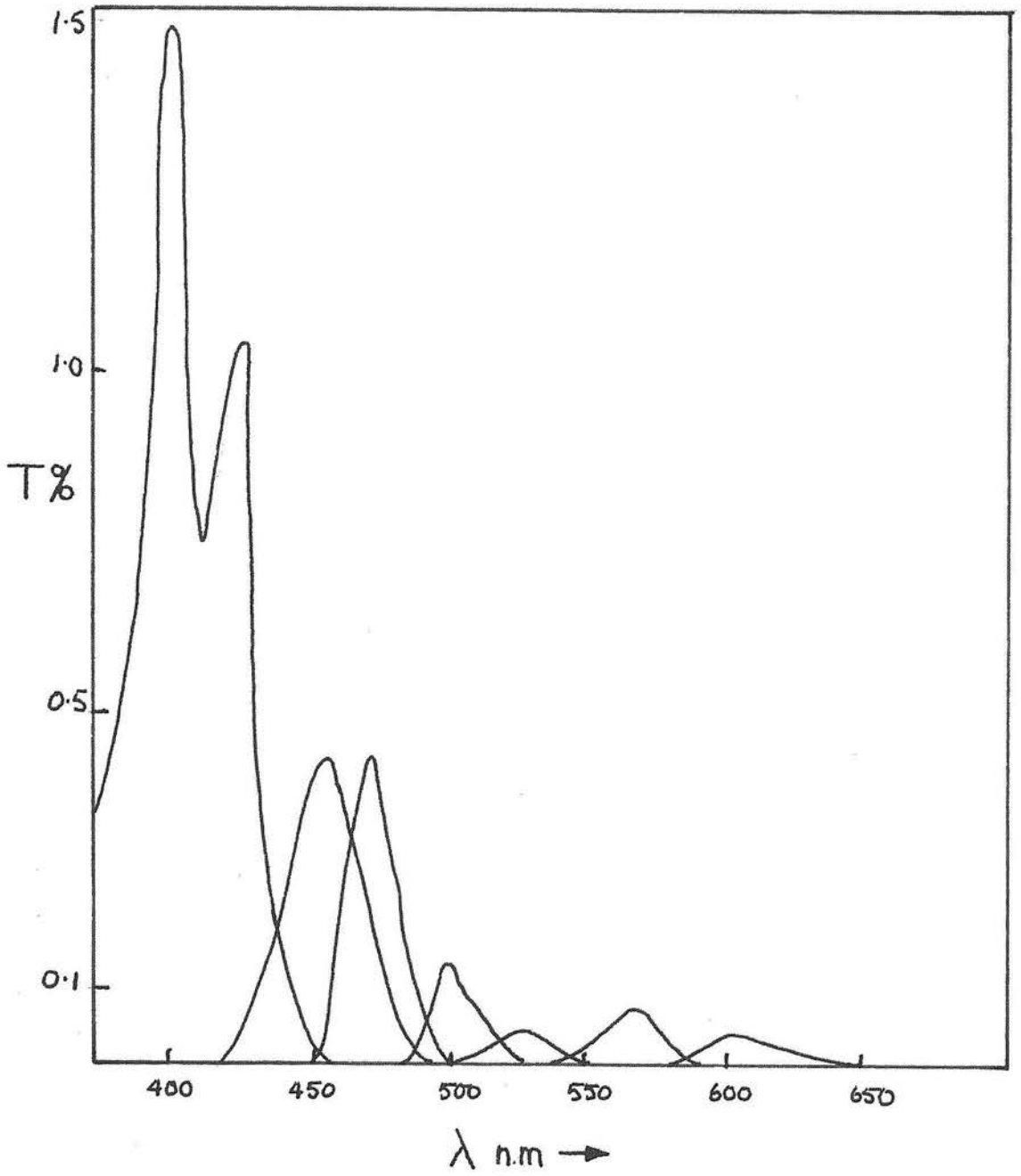

Figure 6 Wavelength calibration of transmission of filters

terminals connected the voltage across the lamp to the feedback system of the power supply, thereby compensating for voltage drop in the power lines to the lamp.

(ii) Filter Calibration

In order to investigate the wavelength response of the image tube, a series of colour filters (Ilford Spectrum filters 600 - 607) were obtained. To achieve a sufficiently narrow bandwidth, these, together with a red filter (referred to as R), were used in successive pairs, covering a wavelength range from 420 n.m. to 610 n.m. The filters were calibrated in pairs with one of the spectrographs used by the Department for undergraduate teaching. The spectrograph in the configuration used consists of a Hilger and Watts adjustable slit, Bausch and Lamb $2\frac{1}{2}$" grating, and a photometer head containing an RCA 1P21 photomultiplier. The collimator and camera lenses are 2" doublets. The spectrograph was first calibrated for wavelength using discharge lamps. A pyrometer (tungsten ribbon filament) lamp was focussed onto the slit, the convergent beam having a low aperture ratio in order to simulate conditions for the filters in use, and the output of the photometer head was measured with a Keithley electrometer micro-micro-ammeter. The ratio of output with the filters in the beam to that without filters was measured at a series of

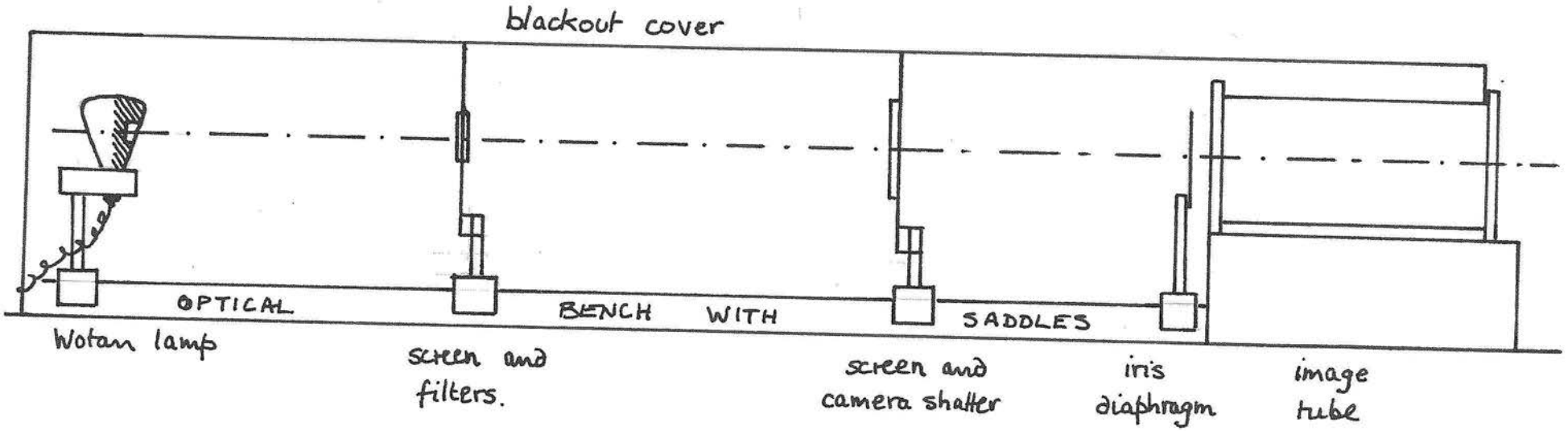

Figure 7 Optical bench for measuring absolute sensitivity

wavelengths (and in that order, to allow for variation of lamp intensity), and this was taken to be the transmission function of the filter combination measured. The error in wavelength determination is small enough to be negligible, and that of point transmission (the filters were used close to the condenser at the slit) certainly better than 5%.

The transmission curves for the filters in pairs, and for a 'grey' filter (denoted G) used with some combinations, are shown in Figure 6.

The output of the lamp in photons/steradian n.m. sec. and the filter transmissions were multiplied together to obtain the output of the combination in photons/steradian sec., and the RMS bandwidth and mean wavelength were also calculated. These were calculated by computer, with the program named FILTER PARAMETER (see Appendix) in which the table of values of E(i) gives the output of the lamp in photons/steradian n.m. sec. at intervals of 20 n.m. The argument (0) corresponds to 380 n.m.

(iii) Experimental Arrangements for Sensitivity Measures

Figure 7 shows the layout of the equipment used during the measurement of absolute sensitivity of the image tube. Two 1-metre optical benches were screwed down parallel with the axis of the tube in contact with one another,

and the lamp was mounted on a saddle, so that the centre of its filament was on the image tube axis. Angular orientation of the Wotan lamp is not critical, as the directed intensity is constant to about $\pm 5^{\circ}$ from the filament perpendicular.[42] Two screens with apertures were placed between the lamp and the tube. The filter mounts were placed in the first aperture, and in the second a camera iris shutter with an internal aperture of 2". Any additional filters (e.g. the gray filter) were mounted before the first aperture. An iris aperture was placed over the front of the image tube, to permit only light coming directly from the lamp to arrive at the photocathode. The lamp was used at a distance of 1.935 metres from the photocathode.

When the same arrangement is used for exposing IIaO emulsion, the emulsion can be placed in the position previously occupied by the cathode by the use of a special plateholder mounting, and the use of a test pattern projector whose construction will be described in Chapter V. The front of the mounting is identical with the faceplate of the tube focussing coil, which can be unambiguously located with respect to the optical bench. The projector is first focussed on the image tube, and then transferred to the plateholder mounting, and the plateholder moved into the focus of the aerial image of

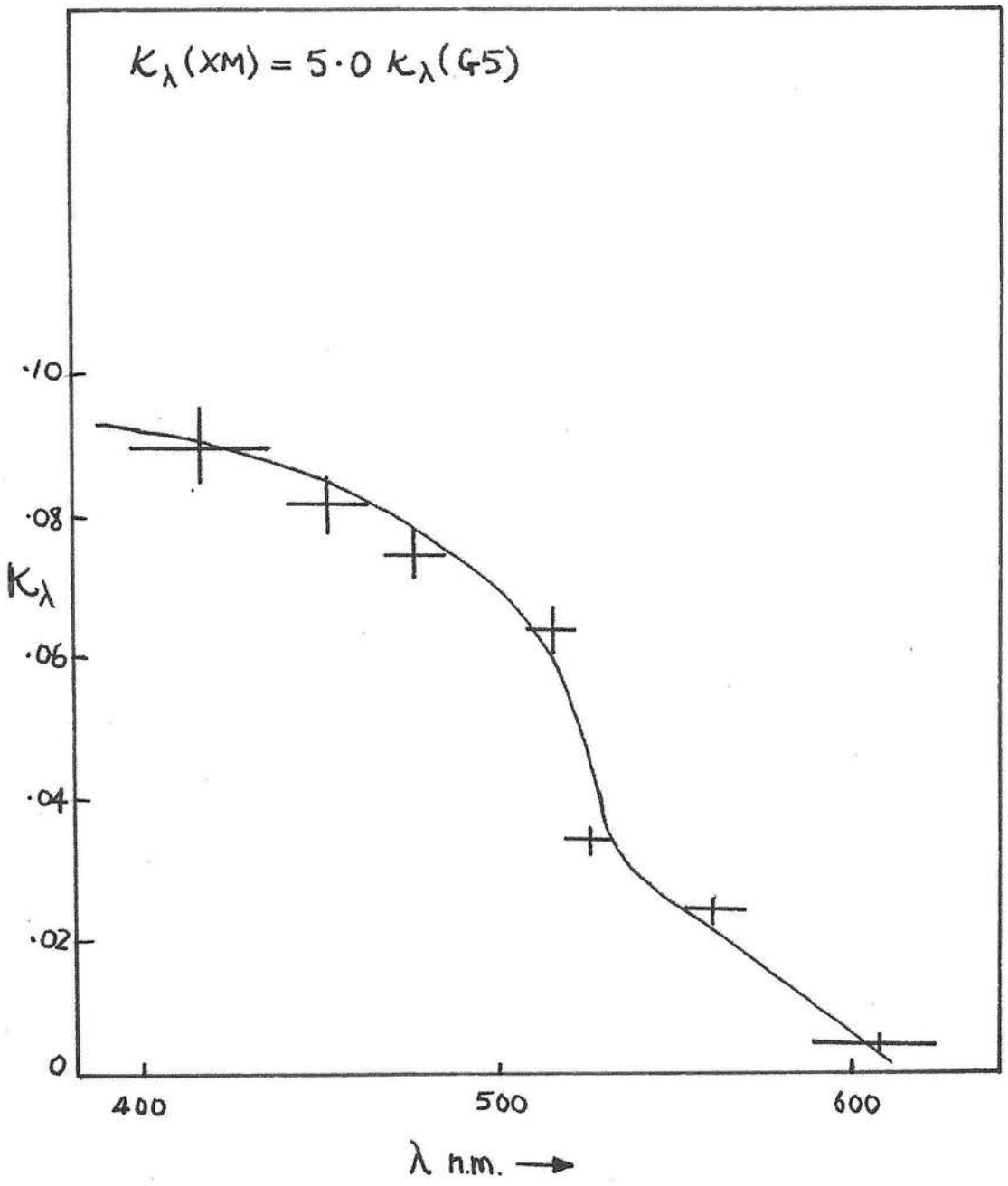

Figure 8 Sensitivity of Spectracon B24 with G5 in density per photon per square micron

the test pattern. Then the lamp/emulsion distance will be identical with that previously between lamp and tube photocathode.

The complete test bench is covered with blackout material draped over a framework of Dexion.

Timed exposures were made with the various filters (the grey filter was introduced when the exposure for moderate densities without it would be too short to give accurate timing) up to 60 seconds, with the maximum density produced being about 1.3. These densities were plotted on a Joyce-Loebl microdensitometer with a large scanning aperture, and from these plots the value of density/second deduced for the various filter combinations.

(iv) Absolute Sensitivity Results

The following table lists the filter numbers (F), mean wavelengths of lamp/filter output in n.m. ($\bar{\lambda}$), light intensity in photons/μ^2sec.(n_λ), density/sec. produced (D/t), and sensitivity in density μ^2/sec. (κ_λ) for a series of measurements. The measurements were made after the tube voltage had remained set for two hours, and the lamp voltage for between 10 and 20 minutes. In no case did the value of κ_λ deviate from the values given below by more than the estimated error of $\pm$ 5%. (Note that this excludes errors in the manufacturers' calibration of the lamp - evaluating this error, which

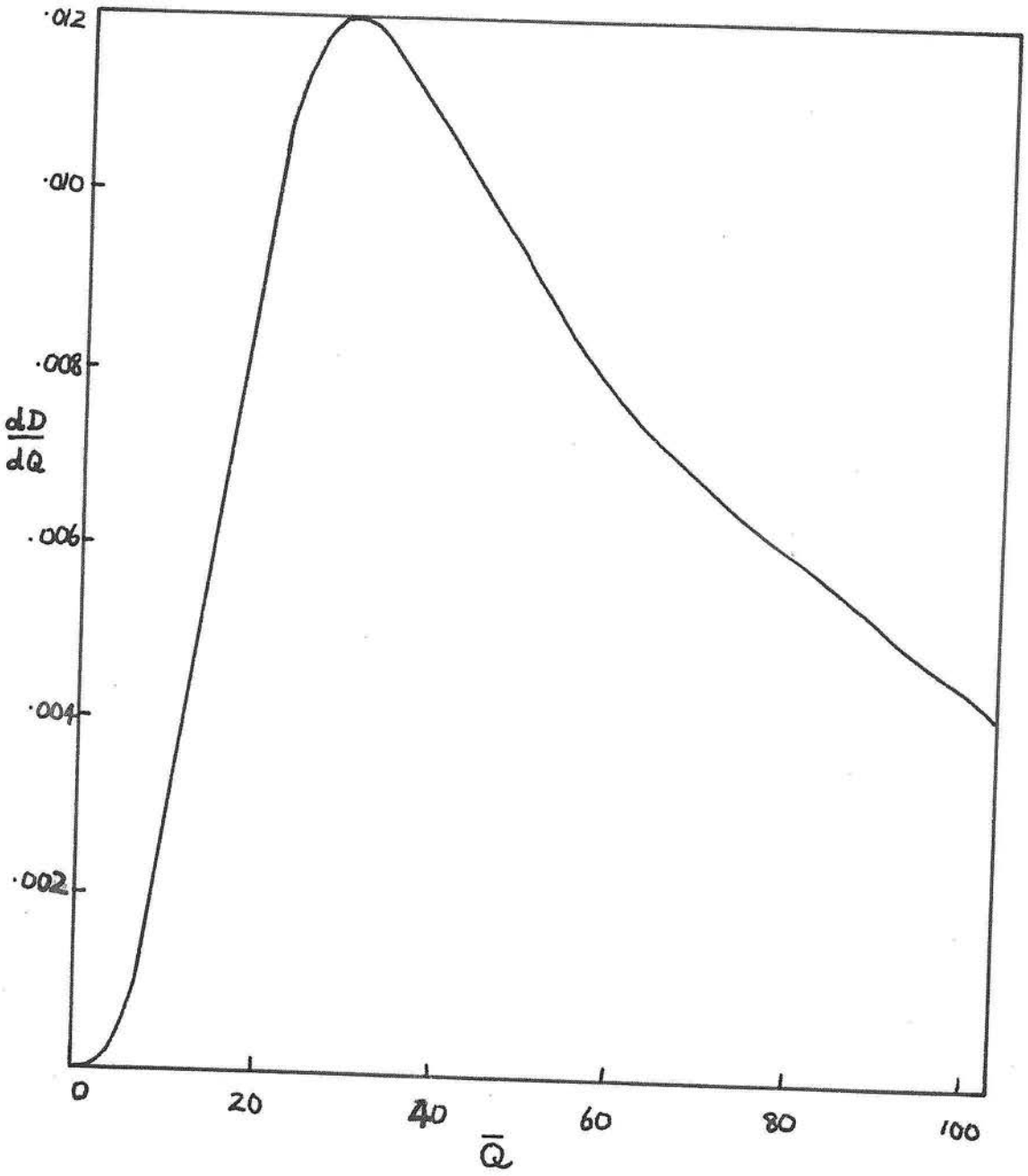

Figure 9 Sensitivity of unbaked IIa0

however is not likely to exceed one or two per cent, is a problem of an altogether different magnitude). The value of κ_λ as a function of wavelength has been drawn through the values derived below, and plotted, together with the estimated error in κ_λ and RMS bandwidth of the filter combination, in Figure 8.

F	$\bar{\lambda}$	n_λ	(D/t)	κ_λ
600/G	420	.669	.0600	.0899
601/2/G	453	.352	.0286	.0814
602/3/G	481	.446	.0325	.0730
603/4/G	508	.222	.0143	.0640
604/5	528	.780	.0249	.0318
605/6	562	1.58	.0378	.0239
606/R	608	5.02	.0260	.0052

The absolute sensitivity of unbaked IIaO was measured at 420 n.m. only, since (a) density is not proportional to intensity, (b) granularity and MTF will be functions of the wavelength of the incident radiation, and hence to investigate thoroughly the equivalent quantum efficiency of light-sensitive emulsions as a function of wavelength is a problem in its own right. The sensitivity curve in the same units as that for the image tube is shown as Figure 9.

(v) Modulation Transfer Function Measures

The discussion in the literature of photographic modulation transfer functions has been long drawn out, and still, to a certain extent, inconclusive.

One of the main drawbacks to a straightforward carrying over of the corresponding results in communications theory has been the non-linearity of photographic response. Detailed consideration of this problem has been given by Langner[43] and Schade, for instance. In view of the obvious complexity of the problem (and note that some of the difficulties outlined in the literature, such as the effect of development, for instance, render in a non-linear fashion even an apparently linear process, such as the response of an electronographic image tube) and after discussion with Dr L. R. Baker of the British Scientific Instrument Research Association, whose own paper[44] on the measurement of MTFs of lenses provided a valuable stimulus, it was decided to perform a straightforward pilot experiment by projecting a slit image, and taking the resultant Fourier transform. The method used was to project the image of a Hilger and Watts 5μ slit with a low aperture ratio projection lens onto the cathode of the tube, and then to scan both the aerial image of the slit, and the resulting images on G5 and XM emulsion with a microphotometer designed for the purpose. By scanning with the same device both the aerial and developed images, it is possible to eliminate the MTF of the measuring instrument, and that of the image of the slit.

The nonlinearity of photographic (and electronographic) response complicates the issue. If the distribution of intensity in the object is I(x) (considering only the direction perpendicular to the slit) and the spread function of the imaging device (astronomical emulsion or image tube) is S(x), then, using the method of 'effective exposure'[45], the distribution of effective exposure is I(x) * S(x) where * denotes convolution. The image is scanned with a microphotometer having a spread function P(x), and the response of the imaging device is T = g(I) which gives an input signal for the photometer T(I * S). Then the output of the photometer is P(x) * T(I * S). Now the object is the image in a projection lens of a 5μ slit. The projection lens is of high quality, stopped down to a radius of $\frac{1}{2}$ cm., and used at a magnification of 1, the object distance being 20 cm. In these conditions, it is possible to regard the image produced to be the convolution of a rectangular function and the Airy diffraction pattern. From this may be deduced the function I(x) which is the object for the imaging device. Further, by scanning this device with the photometer, P(x) may be deduced, since the photometer output in this case is I * P. Thus, the necessary steps to determine S(x) or its Fourier transform $F[S]$, which on appropriate normalisation is the modulation transfer function of the

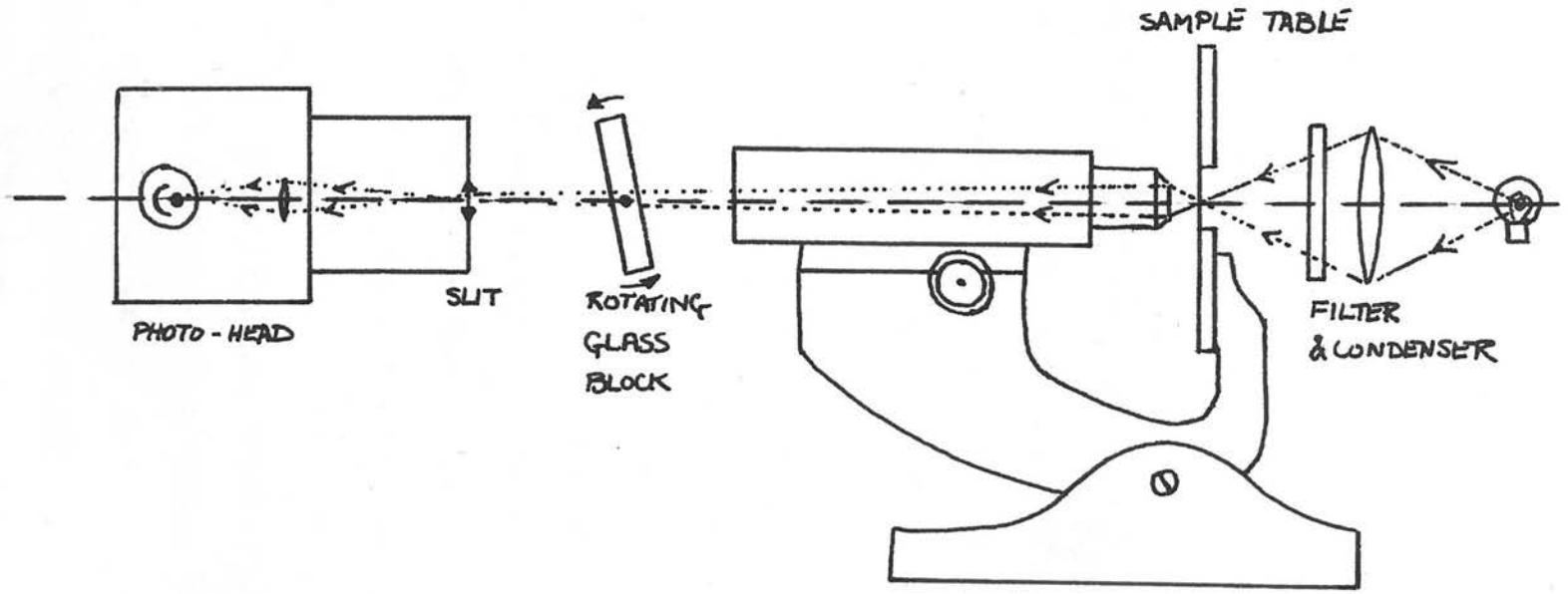

Figure 10 Diagram of MTF photometer

imaging device, are:

(i) Calculate $I(x)$; hence derive $F[I]$

(ii) Scan $I(x)$; hence derive $F[I * P] = F[I]\,F[P]$
this gives the MTF of the photometer $F[P]$

(iii) Scan the emulsion; hence derive $F[T] \cdot F[P]$
this gives $F[T]$; hence derive $T(x)$

(iv) Calculate effective exposure distribution
$T = g(S(x) * I(x))$; hence derive $F[I]\,F[S]$

(v) MTF = $F[S]$

From the data given for the slit and projection lens,[46]

$$F[I] = \frac{10}{\pi} \operatorname{sinc}^2(5u)\left[\cos^{-1}(u/.7) - (u/.7)\sqrt{1 - (u/.7)^2}\right] \quad 3.1$$

(vi) Scanning Photometer

A diagram of the photometer is shown as Figure 10. Since the functions being scanned were only of the order of 1/10 mm. broad, it was necessary to devise a means to scan them very slowly in order to have sufficient longitudinal magnification on the output trace. The method used was to place an optically flat block of glass in the beam, and rotate it about an axis parallel to the slit image, which was magnified X20 and projected through a glass block onto a calibrated slit, behind which was the photometer. The glass block was rotated by a Klaxon synchronous motor, with reduction gears, at an angular speed of .1 revolution per minute. The output

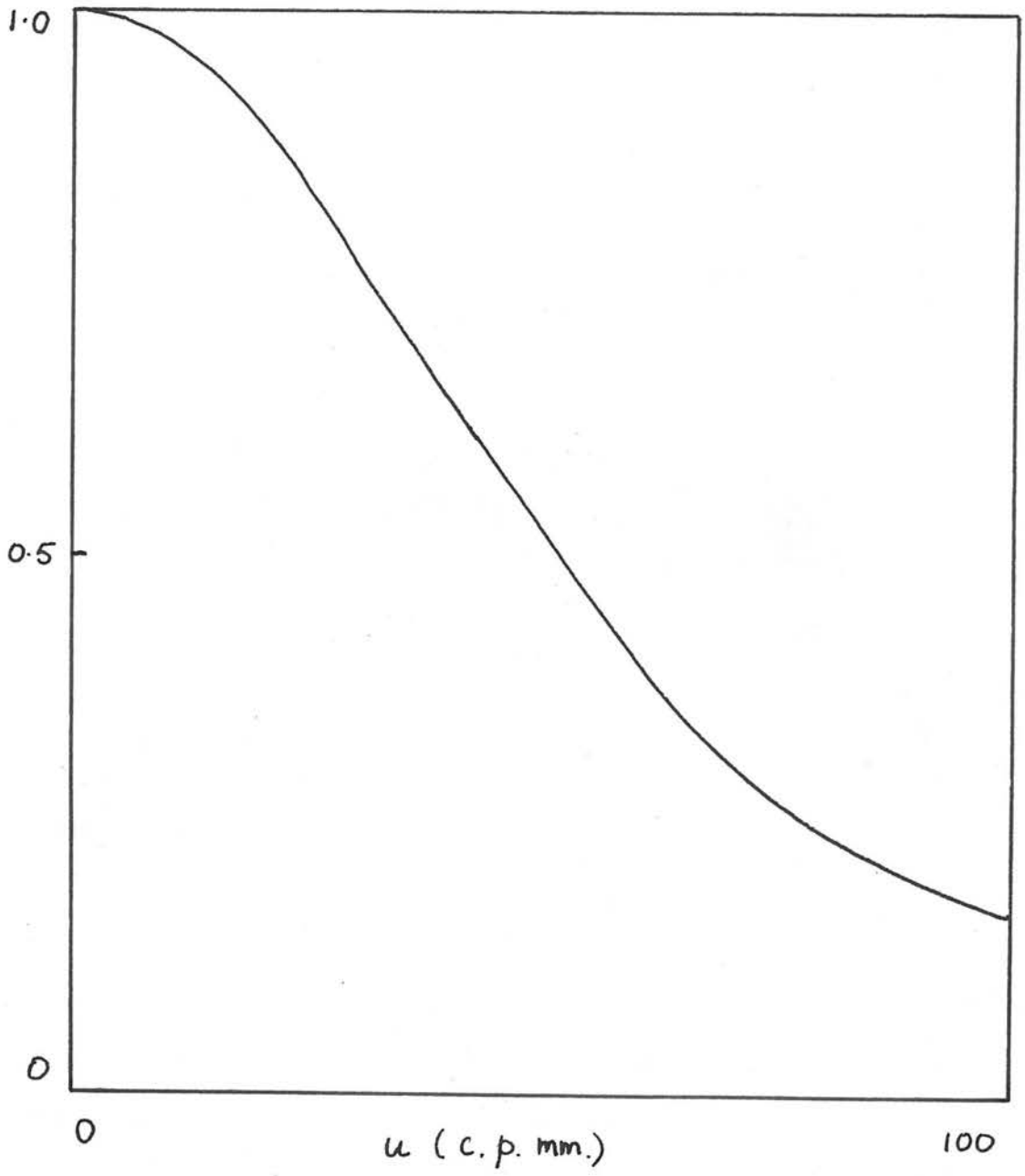

Figure 10a MTF of photometer

of the photometer was fed, via a DC amplifier, to a Beckman Chart Recorder.

The displacement of a ray of light passing through a plane parallel sided block of glass d mm. thick, at an angle of incidence θ , is

$$x = \frac{d}{2} \frac{\sin\theta\cos\theta}{\sqrt{n^2 - \sin^2\theta} + \sin^2\theta/\cos\theta} \quad \text{mm} \qquad 3.2$$

at small θ

$$\delta x = \frac{d}{2n} \delta\theta \qquad 3.3$$

where n is the refractive index of the glass. The linear relation (3.3) holds with sufficient accuracy up to angles of interest. For the particular block of glass, d = 6 mm., n = 1.55. The relation (3.3) was determined using a slit object, a spectrometer, and a travelling microscope. Then, in the relevant units, the image is displaced .036 mm/degree rotated. Given the angular speed of the drive motor, the magnification of X20, and the chart recorder speed of 1"/minute, the scale on the chart is 64.8μm/inch.

The photometer could be focussed by replacing the photometer head with an optical bench microscope, focussed onto the reverse side of the photometer slit (the slit was set at 20μm width for all measurements).

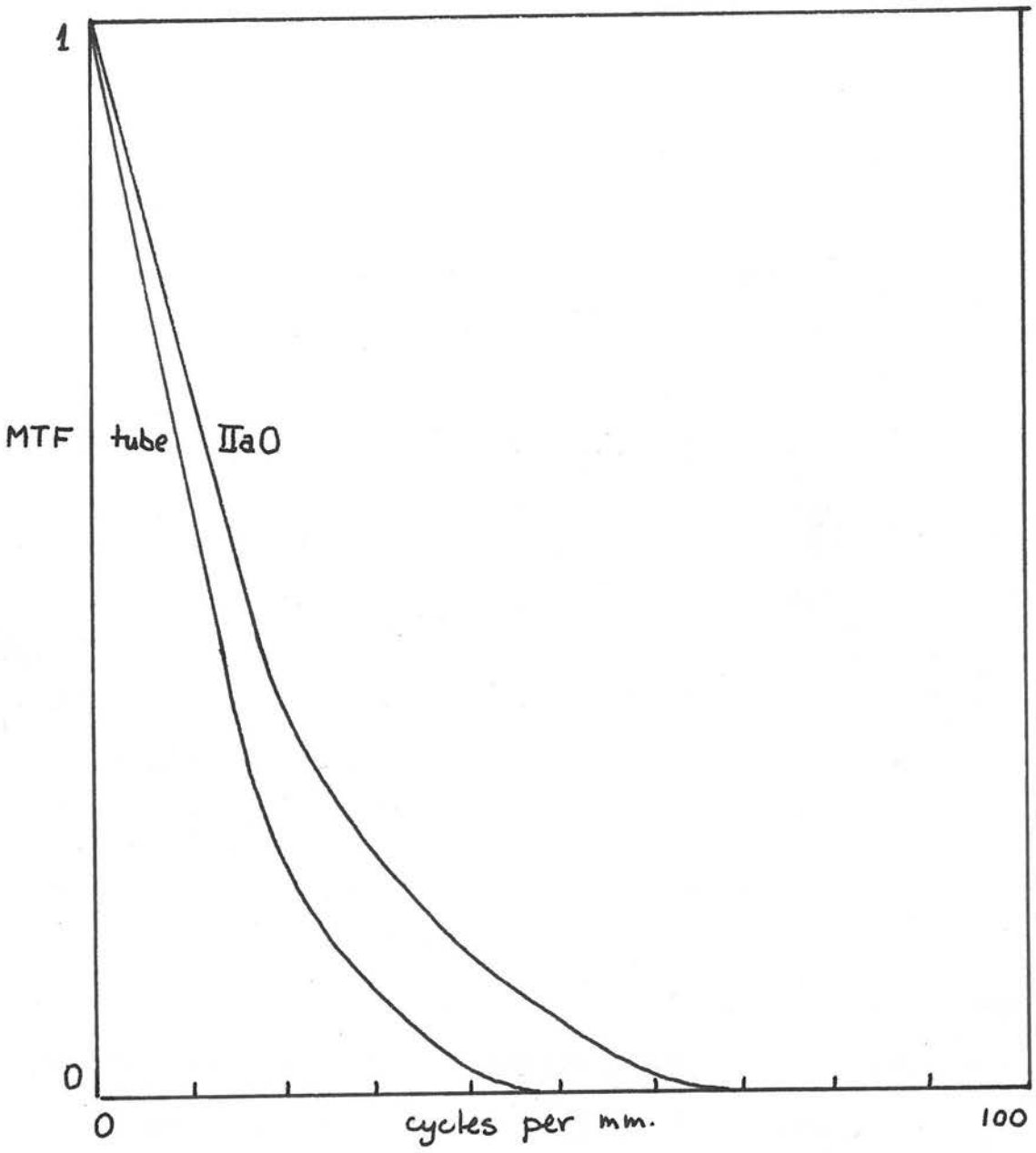

Figure 11 MTF of image tube and IIaO

(vii) Reduction of Results

$F[I]$ was calculated from equation (3.1) and $F[I * P]$ for the slit image, $F[T * P]$ for IIaO and for the tube (the photometer output was identical within experimental error for G5 and XM; this would not be the case for a Spectracon with full resolution capabilities) were calculated on a computer using a variation of numerical Fourier transformation described by Booth.[47]

If the output of the photometer is f(x), we seek a transform of f(x) with the following properties. f(x) is symmetrical about its maximum taken to be at x = 0 (since the method described above for the derivation of MTF is not highly accurate, phase information in the MTF (i.e. assymetry, if any, in f(x) is suppressed to increase the amplitude accuracy), and f(x) is zero beyond $|x| = a$, where a is of the order of 100μm since f(x) is an even function,

$$F[f] = 2\int_0^a f(x)\cos 2\pi ux\,dx \qquad 3.4$$

Requiring $F[f]$ at values of .01/μ up to .1/μ equation (3.4) is evaluated using the trapezium rule

and $$F[f]_{u=n\delta u} = In + E \qquad 3.5$$

where $$In = Z(fo/2 + f_1\cos\frac{2\pi n}{100}dx + \ldots$$

$$\ldots + f_{m-1}\cos\frac{2\pi n(m-1)}{100}dx\ ) \qquad 3.6$$

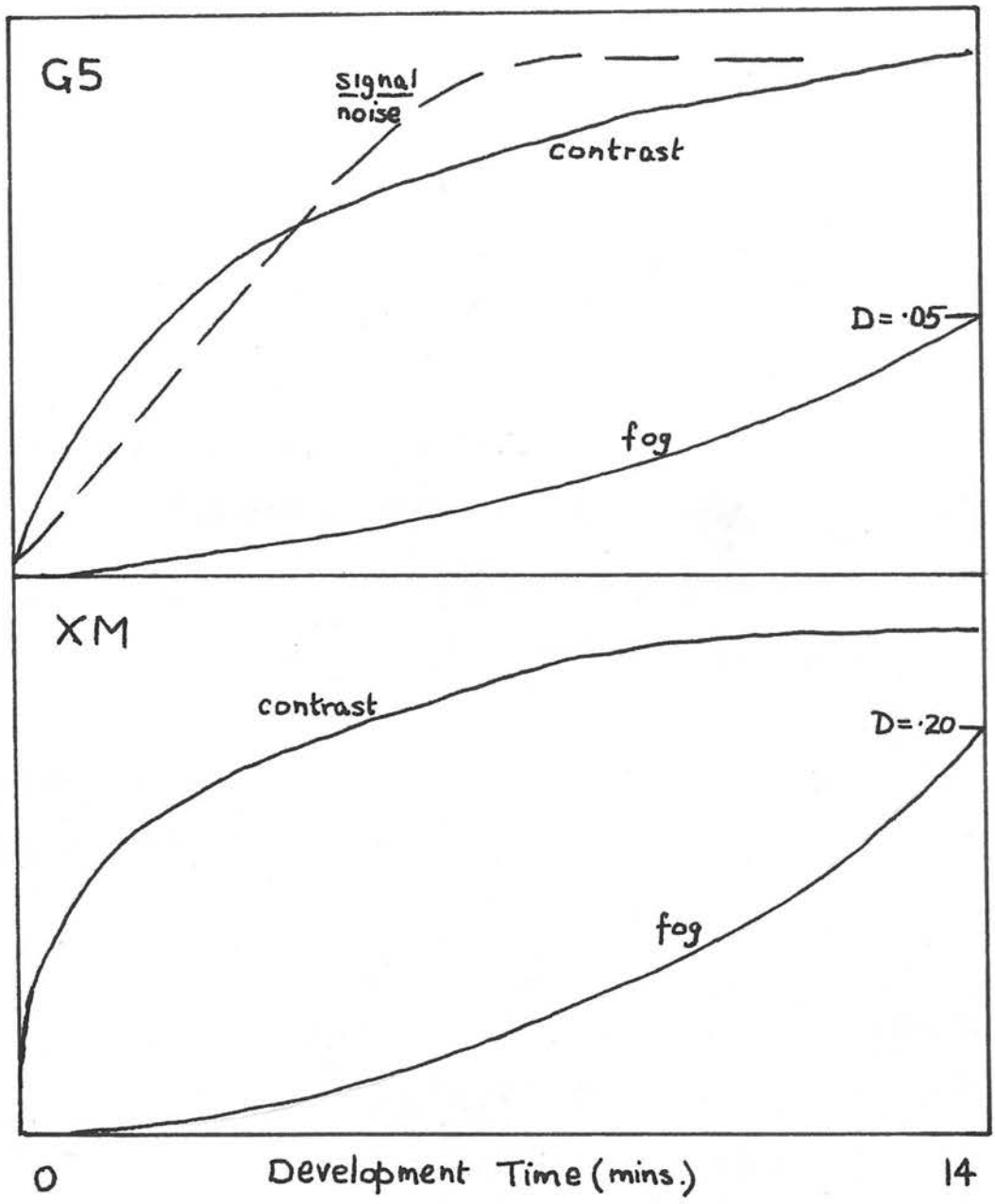

Figure 12 Parameters of G5 and XM as a function of development time

since $f_m = 0$, $m\delta x = a$, δx is the sampling interval

$$f_r = f(r\delta x), \text{ and } E = -\frac{m\delta x^3}{12} f^{11}(y) \qquad 3.7$$

where $0 < y < a$.

Since the highest frequency is .1 cycle/μ, i.e. 10 cycles per 100μ, and interval δx is 2μ there are at least 5 ordinates sampled per cycle, and the errors in negative lobes tend to compensate for those in the positive. The MTF of the photometer is shown in Figure 10a, and those of the image tube, and IIaO, in Figure 11.

(viii) Development

The development procedure was checked by measuring the slope of the D vs. exposure relation and also the chemical fogging, at a series of values of development time. The PHOTOGRAN program was run on the strips so developed, and the noise thus measured plotted as a function of density. The results are shown in Figure 12, which indicates that the optimum development time is about 5 minutes for G5 and XM, i.e. the value used in all measurements and observations.

CHAPTER IV

Linearity of Response of Electronography: G5 Emulsion Model

There has been considerable divergence of opinion on the question of the linearity of electronographic response of G5, i.e. on whether the density produced on a G5 nuclear emulsion exposed with an image tube is proportional to the incident exposure. It might be supposed that, since the cathode transduction is linear, and density is proportional to n, and any grain affected by an electron is developable (unlike the case for light exposure), the response should be linear up to densities approaching saturation density, which in this case is high, probably greater than 3 or even 4. However, this is not the case. As an example, consider a single layer emulsion consisting of grains rendered developable by single hits of randomly arriving electrons. If the mean exposure is n electrons/unit area, and the grain area is a, then the probability of a grain receiving r hits is

$$P(r) = (na)^r e^{-na}/r!$$

and the probability of a grain receiving at least one hit is

$$\sum_{1}^{\infty} P(r) = 1-e^{-na} \qquad 4.1$$

so the mean number of developable grains/unit area is proportional to this quantity. Using the proportionality of D and number of developed grains,

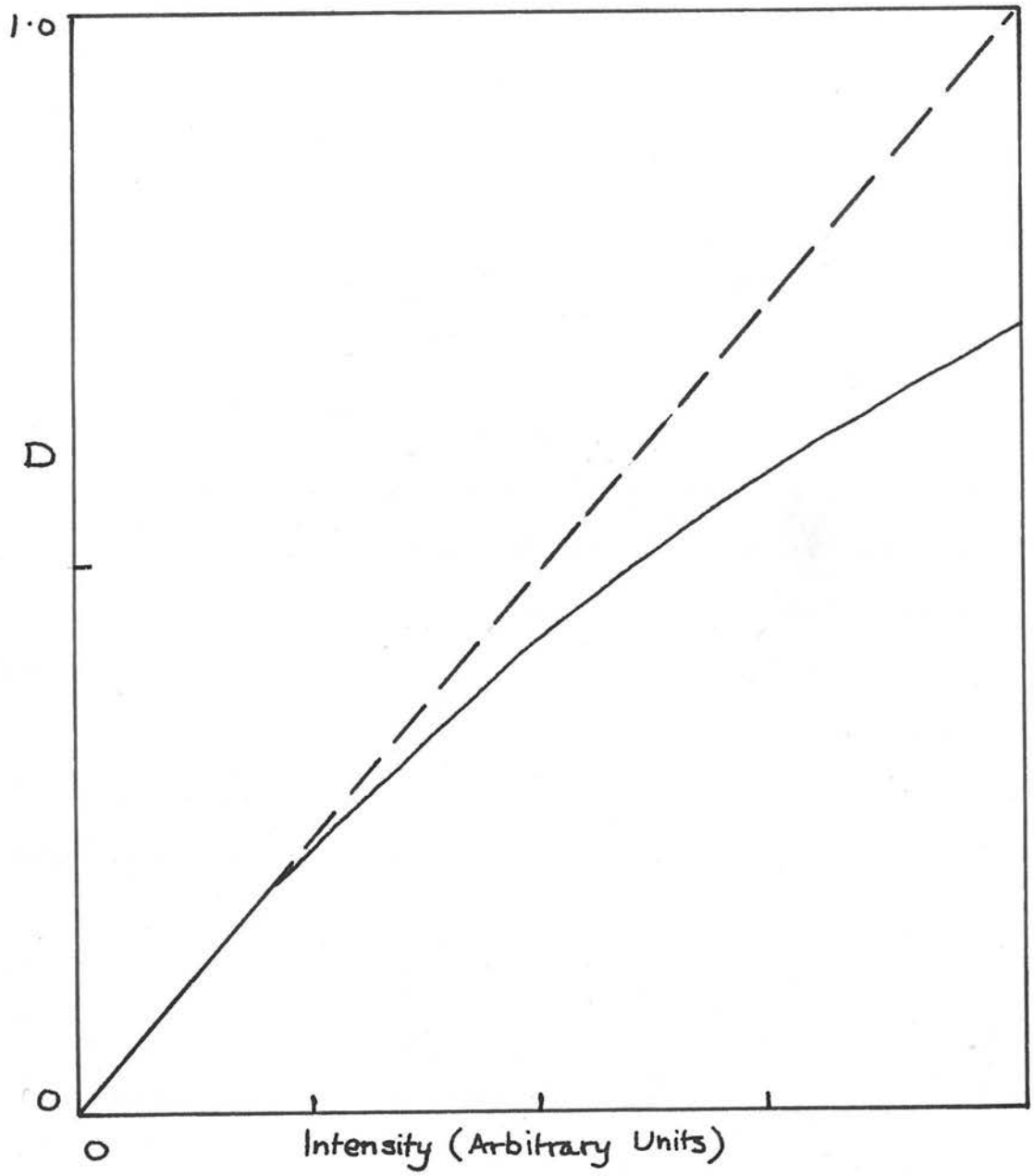

Figure 13 Nonlinearity of G5

$$D/D_{sat.} = 1-e^{-na} \qquad 4.2$$

and at an exposure of 1 electron/grain area

$$D/D_{sat.} = 1/e$$

whereas a linear relation predicts a value of unity.

(i) Experimental Results

In view of these considerations, some attention has been payed to the shape of non-linearity of response of G5. Uniform density exposure series have been made, and later measured with a Joyce-Loebl densitometer, and the graph of D vs. exposure plotted. It has not always been possible to maintain the same slope at small values of exposure, due to uncertainties of the output of the lamp used in the experiments, between series of exposures. An incandescent lamp was used, rather than for instance an electroluminescent panel, as it was desired to use fairly narrow band colour filters (the one used for these measurements was Ilford filter 806) and also because the experiments were designed to form the pilot investigation for the absolute calibration described in Chapter III. The slopes of graphs of D vs. time of exposure to the source were adjusted to a constant value by altering the horizontal scale of the graphs, and then all such results fell on the same curve with an error of $\pm$ 2%. The curve is displayed as Figure 13. The straight line

fitted to the linear portion of the curve will be called the 'linear response'. Then deviations from linear response for G5 are as follows:

D	% of linear response
.5	2% (comparable with error)
1.0	7½%
1.5	16%
2.0	28%

These values agree tolerably well with values determined by Kahan at Imperial College,[47] any lack of agreement probably being due to different development techniques. The technique of development will evidently affect the shape of the curve, since developer exhaustion will occur at high densities unless the specimen is frequently agitated. The method used has been to suspend the strip of emulsion across the dish of developer by means of two clips which slide on the sides. These clips are then slid to and fro, ensuring turbulence on the surface of the emulsion, and good developer mixing. It is hoped to devise some mechanical method of development, to standardise the process as completely as possible.

Non-linearity in XM emulsion was not investigated as thoroughly, but preliminary results indicate a non-linearity somewhat in excess of that for G5.

(ii) Emulsion Model

It now becomes interesting to discover if these results

can be explained on the basis of the mechanism of latent image formation in nuclear emulsions. Sufficient data exist for a simplified model of the emulsion Ilford G5, but not for XM. It is to be hoped that it will be possible to derive necessary data in the future. The data for the model were taken from papers by Zajac and Ross[48] on Kodak NT4 emulsion, whose properties are as similar to Ilford G5 as different batches of G5, and from the comprehensive and beautiful paper by Levi, Rogers, Bentzon and Nielsen[40] on the quantitative evaluation of autoradiograms.

The emulsion consists of small silver halide grains of nearly uniform size randomly dispersed in gelatin, and occupying about half the volume of the emulsion.

The electrons arrive nearly monoenergetically at the surface of the emulsion, penetrate it, and are scattered by the grains, and by the atoms in the gelatin.

The stopping power of the halide is twice that of the gelatin, approximately[49] (stopping power is defined as $-\frac{\overline{dE}}{dx}$). If we consider the simplified situation in which equal amounts of energy E_o are lost per collision (and take up the uncertainty of this being so in the distribution of mean free path; this will introduce errors certainly within the compass of the data errors) then

$$-\overline{\frac{dE}{dx}} = -E_0\overline{\frac{du}{dx}} \qquad 4.3$$

and $1/\overline{\frac{du}{dx}}$ may be regarded as the mean free path.

The model simulating this situation is as follows.

Electrons perform a 3-dimensional random walk in an 'emulsion' consisting of spherical 'grains' of radius a. If the end of a step in the walk lies inside a grain the grain is developable. The steps are isotropic, that is there is no preferred direction with respect to the emulsion, or to the previous step, except the assumption is made that, if an electron enters the emulsion, it remains in it.

The RMS free path varies slowly with distance through the walk. On average any step will pass through amounts of halide (stopping power S_1) and gelatin (stopping power S_2) determined by the fraction f where

$$f = 4/3.\pi ma^3 \qquad 4.4$$

and m is the mean number of grains per unit volume of emulsion.

The postulate is made that:

(a) the RMS free path $\propto 1/S$ in either material

(b) the mean stopping power in a heterogeneous material is the volume-weighted mean stopping power:

$$\bar{S} = fS_1 + (1-f)S_2 \qquad 4.5$$

Let the RMS free path in the emulsion be d_i at the i^{th} step performed by an electron which arrives at the surface of the emulsion with initial energy E KeV.

It is supposed that, since the RMS deviation in actually determined path lengths as a function of electron energy is large, and not too accurately known, it is legitimate to describe the distribution of step lengths at the i^{th} step by a gaussian distribution.

The notation $\underline{u}\,|\,d\underline{u}$ is introduced to represent the interval (volume element) between $\underline{u}$ and $\underline{u}+d\underline{u}$. Then, the probability of the i^{th} step being to $\underline{r}_i\,|\,d\underline{r}_i$ is

$$p(\underline{r}_i)d\underline{r}_i = \frac{1}{(2\pi d_i^2/3)^{3/2}} \exp(-3r_i^2/2d_i^2)d\underline{r}_i \qquad 4.6$$

The probability of the N^{th} step being $\underline{r}_N\,|\,d\underline{r}_N$ and ending in a grain is $\propto p(\underline{r}_N)d\underline{r}_N$ where

$$\propto = f \times \frac{S}{S}_1 \qquad 4.7$$

Following Chandrasekhar,[50] the probability of the electron arriving in $\underline{R}/d\underline{R}$ in N steps and being scattered at a grain is

$$^{\propto}W_N(\underline{R})d\underline{R} = \frac{\propto}{(2\ \overline{Nd^2}/3)^{3/2}} \exp(-3R^2/2N\overline{d^2}) \qquad 4.8$$

and of being scattered by gelatin is $^{1-\propto}W_N(\underline{R})d\underline{R}$ where

$$N\overline{d^2} = \sum_1^N d_i^2 \qquad 4.9$$

Now the observed path distribution is that of distances between grains in the track. This is related to the d_i in the following way. Consider a subset of random walks between two adjacent grains in the track, and suppose that the RMS free path in gelatin does not change between grain collisions, which is a trivial assumption, as the number of steps between grains on average is very small as will be shown below.

The probability of M-1 steps in gelatin from the previous grain and a final step arriving at $\underline{R}' \,|\, d\underline{R}'$ stopping at a grain is

$$W_M(\underline{R}')d\underline{R}' = \frac{\alpha(1-\alpha)^{M-1}}{(2\pi M d_i^2/3)^{3/2}} \exp(-3R'^2/2Md_i^2)\, d\underline{R}' \qquad 4.10$$

whence the mean square value of R' is

$$\bar{R}'^2 = \sum \alpha(1-\alpha)^{M-1} M d_i^2 \qquad 4.11$$

$$= \alpha d_i^2 \sum M(1-\alpha)^{M-1}$$

$$\therefore \quad \bar{R}'^2 = d_i^2/\alpha \qquad 4.12$$

and this is the observed mean squared path between grains in the track. As the fraction of halide decreases, the grains are more widely spaced, and $\bar{R}'^2 \to \infty$; as the fraction of halide tends to unite, $\bar{R}'^2 \to d_i^2$, the mean square path in halide. Thus so far the model satisfies the demands of intuition. Further, for $S_1 = 2S_2$, $f = \frac{1}{2}$, $\bar{R}'^2 = 1.5d^2$ so the assumption * above is indeed justified.

An orthogonal co-ordinate system (x,y,h) with the (x,y) plane representing the surface of the emulsion, and h directed into the emulsion. For convenience $x\underline{i} + y\underline{j}$ is written as $\underline{X}$.

The probability of a walk ending within the volume element $d\underline{X}dh$ due to all electrons arriving at h = 0 is

$$nd\underline{X}dh\int\sum W_N(X'^2+h^2)d\underline{X}' = nd\underline{X}dh.w(h) \qquad 4.13$$

where n is the mean number of electrons arriving per unit area of surface. If $d\underline{X}dh$ contains halide $W_N = {}^{\alpha}W_N$, if not, $W_N = {}^{1-\alpha}W_N$.

Thus the mean number of step endings per unit volume at $(\underline{X},h)$ is

$$\nu(h) = nw(h) \qquad 4.14$$

The volume of a grain is

$$V = \frac{4}{3}\pi a^3$$

so the probability of k steps ending in a grain with its centre in h/dh is

$$P(k) = (\nu V)^k e^{-\nu V}/k! \qquad 4.15$$

The probability of at least 1 step ending in this grain is

$$\sum_1^{\infty} P(k) = 1-e^{-\nu v} \qquad 4.16$$

So the number of grains developable per unit area throughout the thickness of the emulsion is

$$q = m\int_o (1-e^{-\nu v})dh \qquad 4.17$$

The upper bound on the integral is formally infinity, since for the situation on which the model is based, no electron will pass completely through the emulsion.

Then

$$w(h) = \int_{x'} \sum^{\infty} W_N(X'^2+h^2)\,d\underline{X}'$$

$$= \sum \frac{2\alpha}{(2\pi N\bar{d}^2/3)^{3/2}} \exp(-3h^2/2N\overline{d^2})$$

$$\times \left[\int e^{-3x^2/2N\overline{d^2}}\,dx\right]^2$$

and so

$$w(h) = \sum \frac{2\alpha}{2\pi N\overline{d^2}/3} \exp(-3h^2/2N\overline{d^2}) \qquad 4.18$$

$$= \alpha \sum w_N(h) \qquad 4.19$$

where the summation is from 1 to the mean number of grains developable per track produced by an incident electron of energy E KeV. From equation (4.17)

$$q = m\int (1-e^{-\alpha nV \sum w_N(h)})\,dh \qquad 4.20$$

and since this integral is evidently convergent, the exponential is expanded in powers, and integrated term by term. Rewriting,

$$q/m = -\sum \frac{(-\beta)^k}{k!} \cdot y^{(k)} \qquad 4.21$$

where $y^{(k)} = \int (\sum w_N(h))^k\,dh \qquad 4.22$

and $\beta = \alpha hV \qquad 4.23$

$$\text{If } S(N) = N\overline{d^2}/3 = \sum_{i}^{N} d_i^2/3 \qquad 4.24$$

$$y^{(k)} = \sum_{i(1)} \cdots \sum_{i(2)} w_{i(1)}(h) \ldots . w_{i(k)}(h)\, dh \qquad 4.25$$

$$= (2\pi)^{-k/2} \sum_{\text{all } i} \frac{1}{\sqrt{S(i(1)) \ldots S(I(k))}}$$

$$\times 2^k \int \exp\left(-\frac{h^2}{2}\left(\frac{1}{S(i(1))} + \cdots + \frac{1}{S(i(k))}\right)\right) dh \qquad 4.26$$

$$\therefore \quad y^{(k)} = \sqrt{\frac{\pi}{2}} \cdot \left(\frac{2^k}{2\pi}\right)^{k/2} SUM(k) \qquad 4.27$$

where

$$SUM(k) = \sum_{i(1)} \cdots \sum_{i(k)} \left[\frac{1}{S(i(1)) \ldots S(i(k))}\right.$$

$$\left. \times \frac{1}{1/S(i(1)) + \ldots + 1/S(i(k))}\right]^{1/2} \qquad 4.28$$

and the upper limit on all the summations is that for (4.18) and (4.19).

Equation (4.21) as a function of β is the matter in which the latent image builds up with increasing exposure.

The modulation transfer function of the film, as the Fourier transform of the spread function may also be deduced from the model.

The probability of a path ending in $\rho | d\rho$ where $\rho = \underline{X} + h\underline{k}$, and $d\rho = r\, d\varphi\, dr dh$ and $r^2 = x^2 + y^2$, if n electrons arrive at $\rho = o$ is

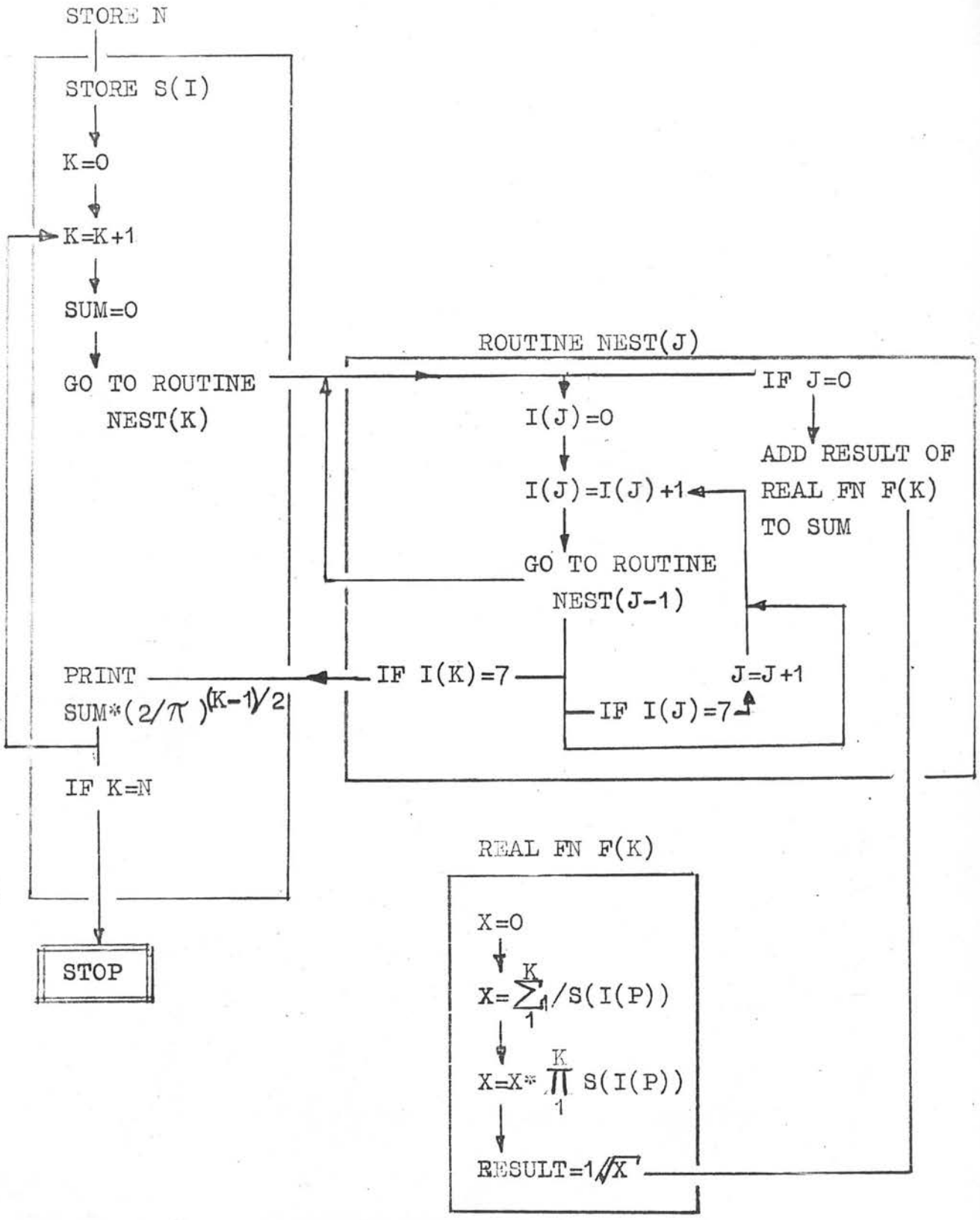

Figure 14. Flow diagram for "MODEL G5 COEFFS"

$$nrd\varphi\, dr \int \sum W_N(v^2+h^2)dh$$

$$= nrd\varphi\, dr \sum e^{-r^2/2S(N)} \cdot \int \frac{\alpha}{(2\pi S(N))^{3/2}} e^{-h^2/2S(N)} dh$$

Therefore, the probability per unit area of a step end is

$$\frac{n\alpha}{2\pi} \sum e^{-r^2/2S(N)} \cdot \frac{1}{2\pi S(N)}$$

$$= \frac{n\alpha}{4\pi} \sum \frac{\exp(-r^2/2S(N))}{S(N)} \qquad 4.29$$

and the Fourier transform (FT) of this is

$$\frac{n\alpha}{4\pi} \sum \frac{1}{S(N)} \text{ FT} \left[\exp(-r^2/2S(N)) \right]$$

$$= \frac{n\alpha}{4\pi} \sum \exp(-2\pi^2 S(N) w^2) \qquad 4.30$$

where $w^2 = u^2 + v^2$ and (u,v) are (x,y) spatial frequencies.

(iii) Model emulsion computer program

In order to solve equations (4.27) and (4.30) computer programs were written. The first, named MODEL G5 COEFFS. (see Appendix), calculates the coefficients $y^{(k)}$ of equation (4.27). The flow diagram for this program, which recursively calls a routine to form the summations, is shown in Figure 14. The other program, MODEL G5 SPREAD FN, MTF, calculates the summations in equations (4.29) and (4.30). The parameters required for the programs are

(i) the upper limit on the summations,

(ii) values for S(i).

The multiplication theorem for gaussian distributions is invoked to pass from 'emulsion space' to 'grain space' and m becomes 1/V, α becomes 1 and the parameter $(_i)$ becomes the mean number of grains produced by an electron of energy E KeV.

From the work of Khogali,[9] and from investigation of density vs. tube potential at constant exposure, the energy lost by an electron of energy 38 KeV passing through the mica window is 21.5 KeV. This is deduced from the following factors. The curve of D vs. tube potential crosses D = 0 at 21.5 KeV. In general, an electron has to have an energy of at least 5 KeV to produce a latent image in G5[49,9] and 38 + 5 - 21.5 = 21.5. Thus the mean energy of electrons impinging on the emulsion is 21.5 KeV, with a spread about this value[51,52] which is not large, and has been ignored in the model. The effect of including it would be to distribute the parameter (i) above about the mean value to be determined below.

The number of developable grains produced by an electron of 21.5 KeV is 7, according to Rogers' paper. This then is the parameter (i) in the program. From Rogers' relation (Rogers Ch. V, equation (1))

$$\log L = 1.59 \log E - 1.51$$

and $L_i = L_o - 1/g_i$

where L is the track length, and g_i is the linear grain density, and putting $1/g_i = d_i$, the table of $S(N) = \sum d_i^2/3$ is constructed

N	S(N)
1	.205
2	.391
3	.554
4	.693
5	.805
6	.885
7	.951

and these are the parameters (ii) above.

The value $\alpha = f \frac{S_1}{\bar{S}}$

$$= f_o \times 1/(1+(1-f)/f \times S_2/S_1)$$

is derived from composition values given in Ilford's[41] data sheet, and $S_2/S_1 = \frac{1}{2}$.[49]

whence

$$\alpha = 2/3$$

The volume of a grain is derived from the results of Chapter II:

$$V = .1\mu^3$$

The value derived from the Ilford data sheet is

$$V = .010\mu^3$$

(iv) Model Results

The values of $y^{(k)}$ are given below

k	$y^{(k)}$	$y^{(k)}/k!$
1	7.00	7.00
2	35.84	17.92
3	218.42	36.40
4	1425.6	56.08
5	9651.2	80.48

$$\text{then } q = 1/V\left[nVy^{(1)} - (nV)^2\frac{y^{(2)}}{2!} + (nV)^3\frac{y^{(3)}}{3!} - .....\right] \quad 4.31$$

$$= ny^{(1)} - n^2V\frac{y^{(2)}}{2!} + n^3V^2\frac{y^{(3)}}{3!} - .....$$

Taking the result of Khogali[9] that for the linear portion of the response curve density is proportional to the number of incident electrons of energy E per cm^2. and the relation between clump size and energy from Rogers' paper (supra) to convert to 38 KeV electrons, Khogali's relation is

$$D = n \quad 4.32$$

Now, writing equation (4.31) as a defect from linearity, i.e. by dividing (4.31) by the first (linear) term, and subtracting the result from unity, we have the percentage drop from linearity in the model:

$$P = 100\left[1 - q/2ny^{(1)}\right] \qquad 4.33$$

$$= \frac{100}{y^{(1)}}\left[\frac{2nVy^{(2)}}{2!} - \frac{(2nV)^2 y^{(3)}}{3!} + \frac{(2nV)^3 y^{(4)}}{4!} - \ldots\right]$$

Then, calculating this defect for D = n = .5, 1.0, 1.5, 2.0, and for V calculated from the value for mean diameter before and after development (see Chapter II, section (vi)), and comparing it with the experimental results, the following table is derived:

D	Model deviation (%) after develop.	Model deviation (%) before develop.	Experimental deviation (%)
.5	12.1	1.3	2
1.0	20.3	2.6	$7\frac{1}{2}$
1.5	34.9	3.9	16
2.0	43.2	5.2	28

The large divergence between the results is disappointing. It is seen that the experimental results are bracketed by the two sets of model results. The explanation probably lies in the fact that Nutting's relation between density and developed grains breaks down when there is a large clump formation.

This problem deserves further consideration, as (see infra) certain workers, notably those using image tubes based on LaIlemand's 'Camera Electronique', claim linear response to densities much higher than those indicated by present results.

It would be interesting to investigate in detail the methods of density measurement used and to enquire more thoroughly how Nutting's relation is affected by the various methods.

The model has been extended, using generalisation of methods described by O'Neill,[46] to provide the noise power spectrum of the image but, pending a resolution of the above problem, it has not seemed advantageous to calculate this in detail.

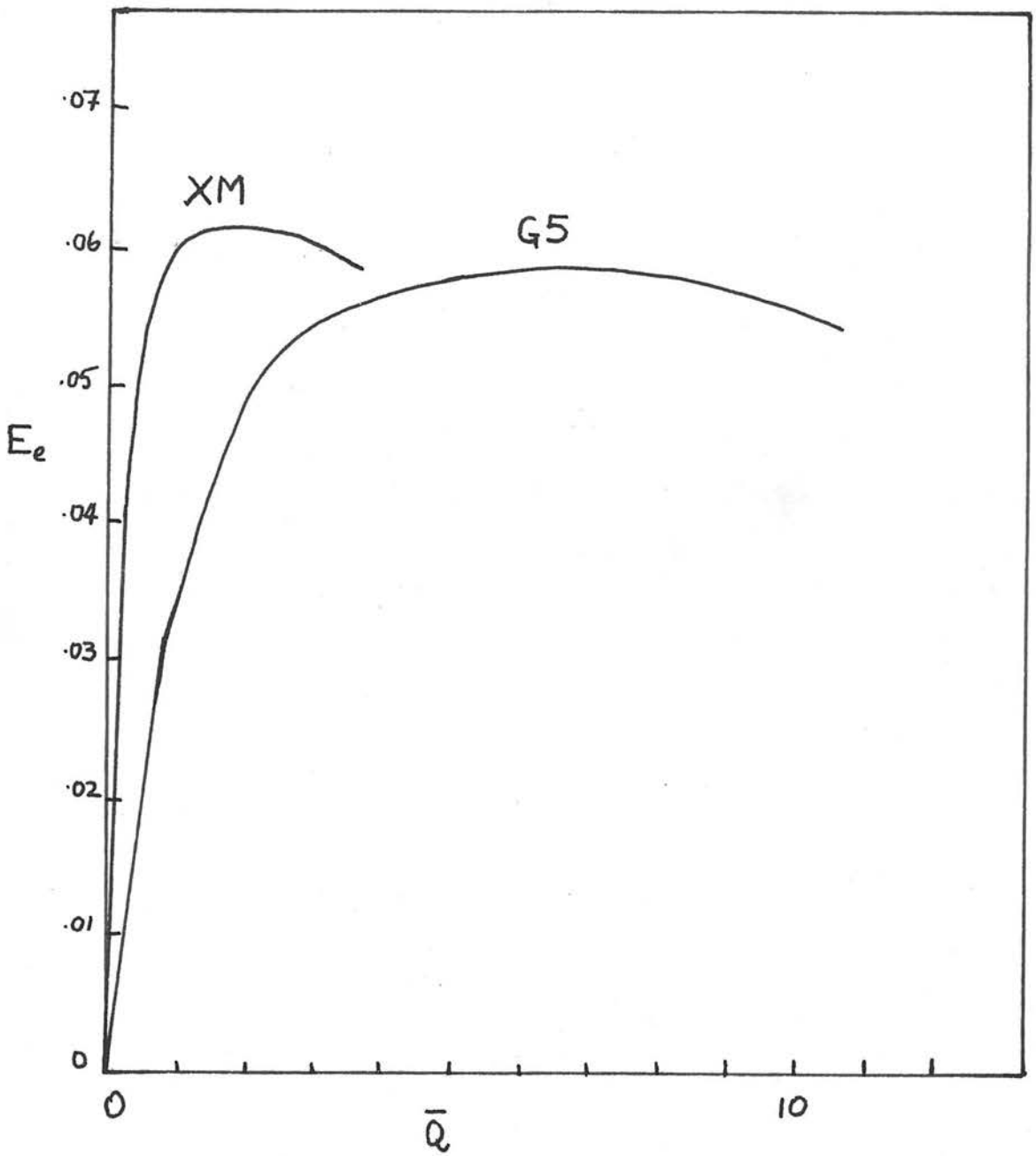

RESULTS Figure A Equivalent quantum efficiency of XM and G5 as a function of exposure

RESULTS OF PART I

The results of the preceding chapters may be collated to form the equivalent quantum efficiencies and photon storage (which note from equation (1.33) is equal to the information storage in bits, for signals small compared with noise). These performance parameters are resolvable into factors determining resolution (MTF) wavelength response (κ_λ), and saturation (D vs. exposure and n vs. D). Only the 'macroscopic' equivalent quantum efficiency and photon storage are given here, values at differing spatial frequencies being derived by multiplication with the value of the corresponding MTF, and at different wavelengths by multiplication by $\kappa_\lambda / \kappa_{420}$

The relevant relations are

$$N = \frac{(dD/d\bar{Q})^2 \bar{Q}^2}{n(o,o)}$$

$$E_e = \frac{(dD/d\bar{Q})^2 \bar{Q}}{n(o,o)}$$

The results for XM, G5 with the image tube and for unbaked IIaO are as follows (D is density above fog):

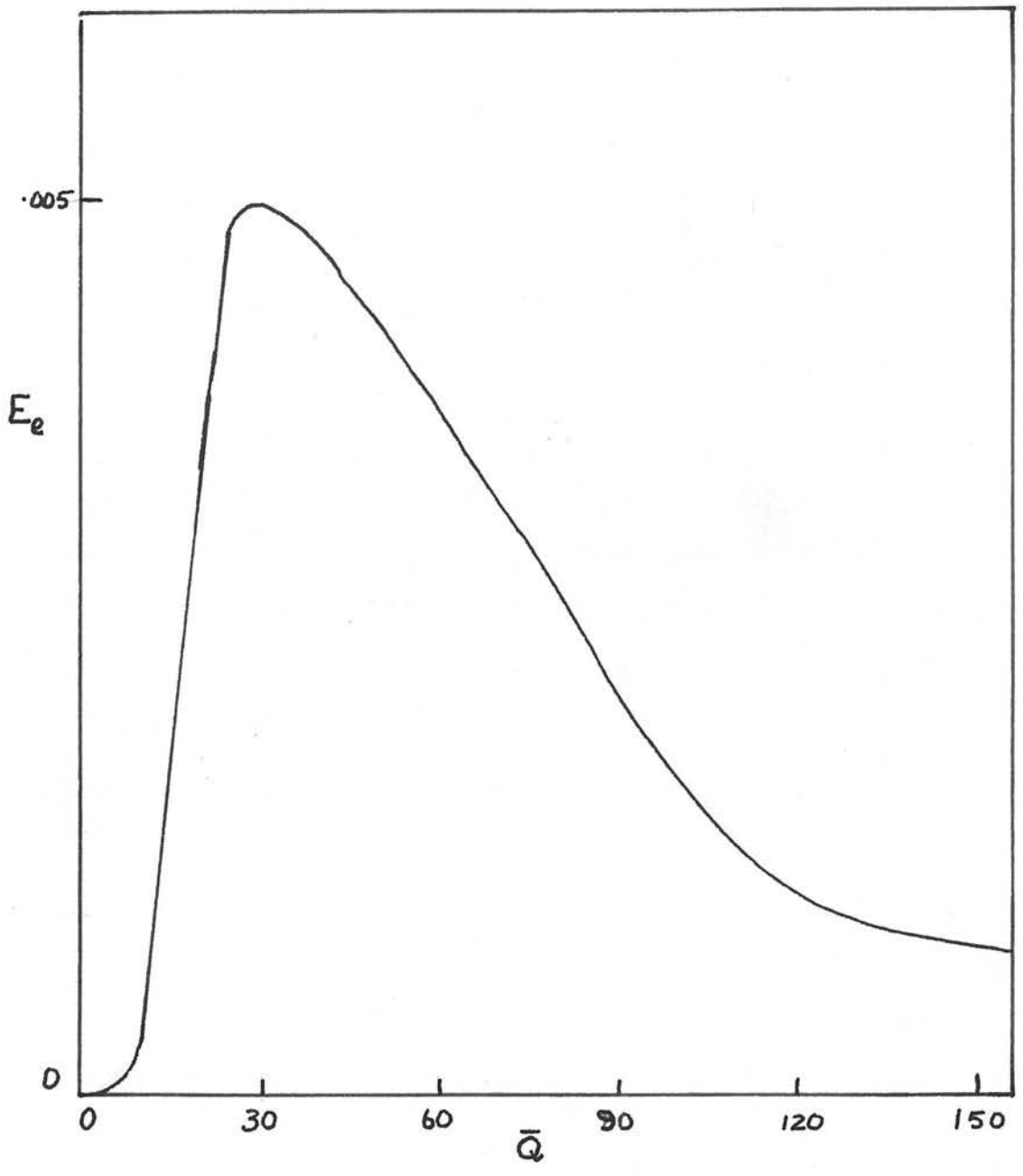

RESULTS Figure B Equivalent quantum efficiency of unbaked IIaO as a function of exposure

XM

$\bar{Q}$	D	N	$E_e = N/\bar{Q}$
0	0	0	0
.5	0.23	.025	.050
1	0.4	.060	.060
2	1.8	.122	.061
2.5	1.0	.150	.060

G5

0	0	0	0
1	.09	.039	.039
2	.18	.104	.052
4	.35	.228	.057
6	.52	.360	.060
8	.68	.472	.059
10	.84	.540	.054

IIaO

0	0	0	0
5	0	-	-
10	.01	.00145	.00015
20	.08	.048	.0024
30	.22	.146	.0049
40	.33	.190	.0047
60	.50	.210	.0035
80	.63	.208	.0026
100	.74	.186	.0019
150	.93	.116	.0008

These results are plotted in Figures A, B, C. Figure A shows E_e for XM and G5; Figure B that for unbaked IIaO; and in Figure C the results are plotted on a logarithmic scale, with the ordinate scale of the curve for IIaO increased by a factor 10.

From these graphs it may be seen that the peak efficiency of either XM or G5 is about twelve times that of unbaked IIaO. The resolution characteristics are

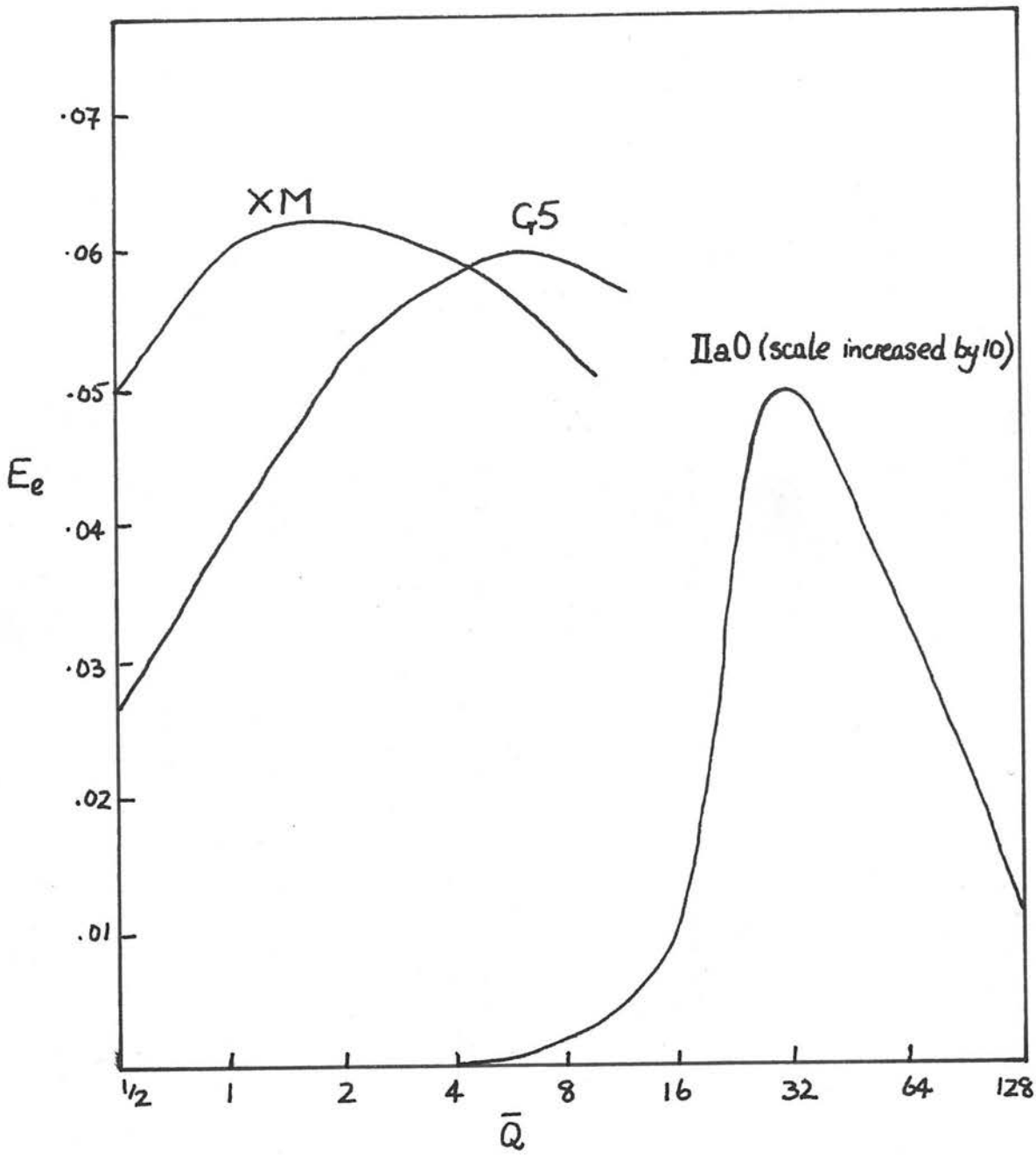

RESULTS Figure C Equivalent quantum efficiencies as a function of log exposure

not vastly different for the two detectors, but for a tube with full resolution capability the MTF of the tube with G5 will be considerably better than that with XM, and so considerably better than that of IIaO (basing estimates on Professor McGee's latest figures[3] the MTF 'radius of gyration' could probably be about twice that measured here). This will give an overall lead to G5, whose better linearity is possibly also an advantage. Notice that at very low exposures the relative gain of the tube over IIaO is virtually infinite (compare Lallemand[55]).

The results of equivalent quantum efficiency for the tube indicate a cathode quantum yield of about 10%.

Since, in terms of cathode quantum yield Y, mica transmission T and clump parameter m the equivalent quantum efficiency might be expected to be

$$E_e = \frac{T.Y}{1+1/m}$$

with m = 7, and T = .6[3]. This gives Y = 10%, at the wavelength of 420 n.m. This tallies well with estimates made at Imperial College.

P A R T II

CHAPTER V

Mounting on a Cassegrain Spectrograph

The use of the image tube in conjunction with the Observatory's 36" telescope posed many problems, which may be divided into three groups and will be so treated.

(i) Mechanical Design

The 36" telescope is a Cassegrain system, and has a spectrograph mounted behind the primary whose collimator, grating and cameras are of 4" aperture. The collimator is a Schmidt system, with the same aperture ratio as the telescope, f/18. In order to bring the cathode into the focal surface of the camera, the f/3 camera had to be used. This is a 6 component lens system, of not very efficient through-put. If the tentative figures for resolution of astronomical emulsions and the Spectracon are taken to be in the ratio of 1:2, and the seeing disc for a star is 2" (optimistic in this climate) so that this is 160μm at the slit, which must then be at least 120μm to pass most of the light from the star, then since the slit image will be 20μm wide, the astronomical emulsion will be approximately matched to the spectrograph, and the Spectracon miss-matched. Thus, cameras of very large aperture ratio are required, with a long working distance, in order to place the focal surface at the

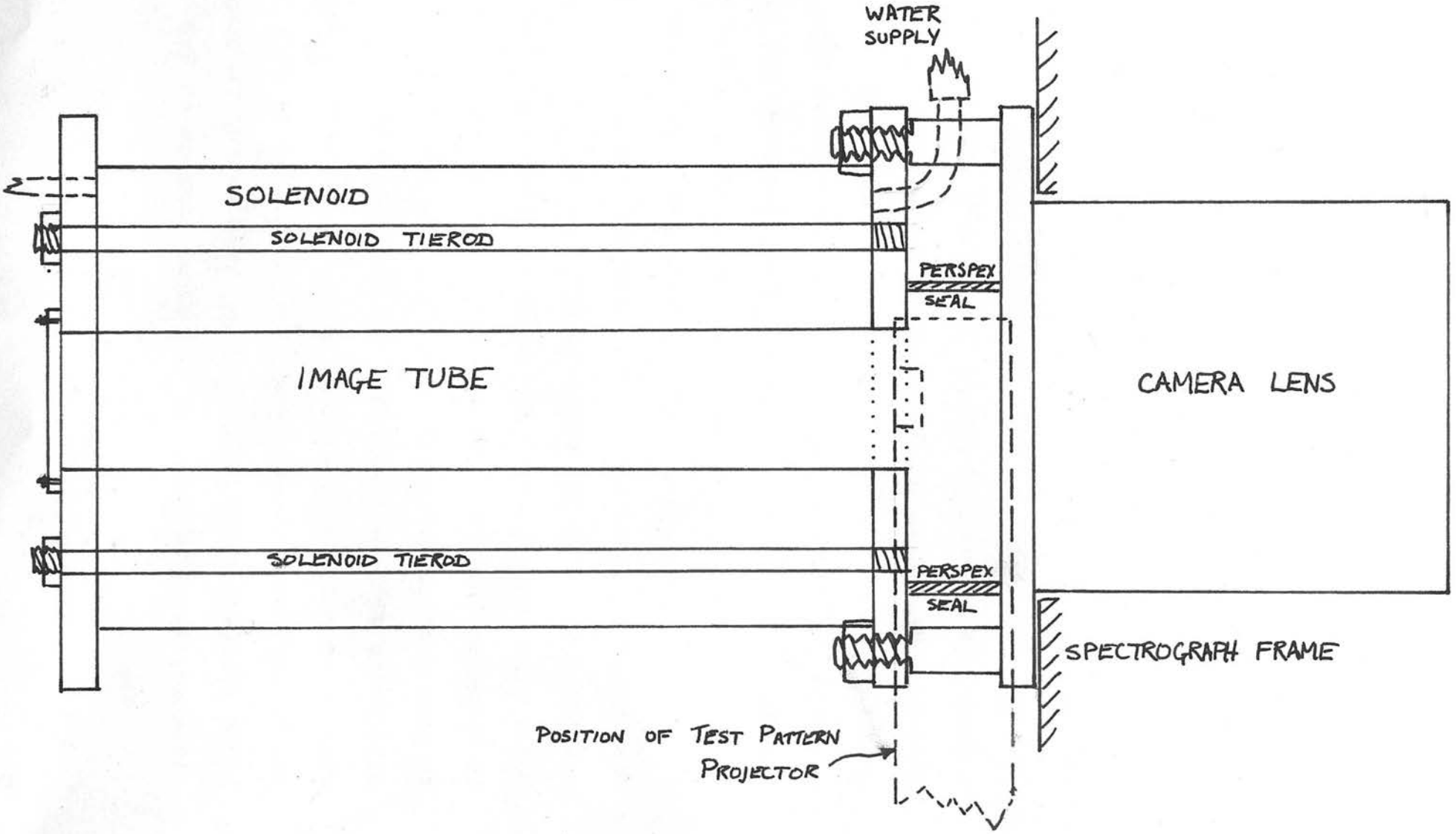

Figure 15 Design of solenoid mount (not to scale)

photocathode. These conflicting conditions are being studied intensively by the Carnegie Image Tube Committee[4], and Hiltner, for instance, has designed such a camera.[53] Meanwhile, this renders the poor resolving qualities of the tube used in the astronomical program less disadvantageous than they might have been with a camera matched to the best performance of the Spectracon.

The aluminium wire-wound focussing solenoid, weighing 7.3 Kg. was mounted between aluminium faceplates held together by tierods, and with circular holes cut on axis with their diameter equal to that of the Perspex casing of the image tube. A third plate of the same dimensions as the previous two was made with tapped holes to take the fixing bolts which normally secured the camera lens barrel to the camera back. In normal use the camera back is fastened with four bolts to the carcass of the spectrograph. Thus the third plate takes the place of this camera back, and serves as the spectrograph-located bed to which both the camera lens with focussing mechanism, and (by means of four stud bolts with $1\frac{1}{2}$" long collars) the solenoid are attached. The arrangement is shown in Figure 15. The $1\frac{1}{2}$" space between spectrograph and solenoid mount is necessary to permit access to camera focussing and the cooling tubes running through the solenoid, and to allow the EHT lead to reach the front of the image tube.

The system is very convenient in that the entire image tube apparatus can be removed from the telescope in moments by removing the nuts from the stud bolts, to allow maintenance, alterations or cleaning to be carried out on the tube, and to permit visual inspection of the focus.

The $1\frac{1}{2}$" gap has also permitted the following facility. Grooves were cut on the interior faces of the $1\frac{1}{2}$" faceplate sandwich to allow the snug fit of a $1\frac{3}{4}$" diameter tube extending across the axis of the image tube. A projector lens was fitted inside such an aluminium tube, by turning down its mounting till it was a sliding fit in the tube, and a spacer and prism also fitted in the tube at one end. Then a Baum[2] test pattern with an electroluminescent panel behind it was attached to a brass tube sliding over the other end of the aluminium tube and fastened to it with a lock nut. The rays from the pattern are focussed by the lens to give an image reduced by a factor of 5, and the image diverted by the prism to emerge from a slot in the top end of the tube.

By placing a stop on the outside of the aluminium tube, the axis of the image beam is caused to coincide with that of the image tube when the aluminium tube is pushed between the two plates at the front of the mounting.

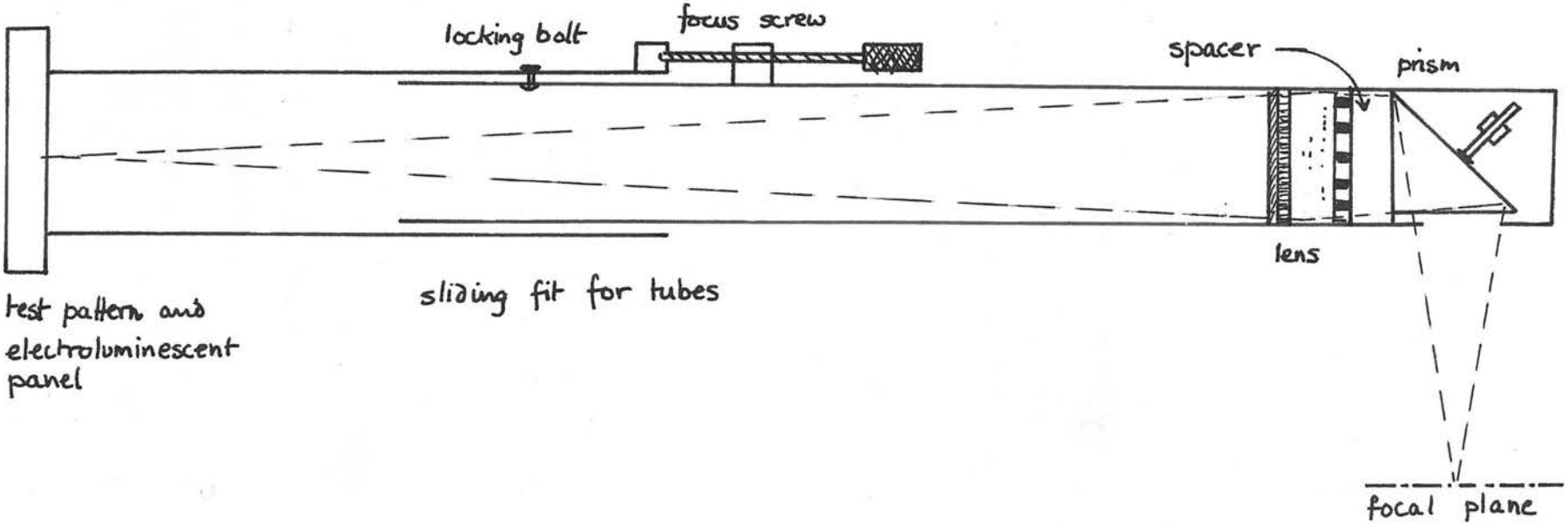

Figure 16 Design of test pattern projector (not to scale)

By suitable choice of aluminium tube length, and projector lens focal length, the image of the pattern coincides with the photocathode. Focussing is possible by means of a screw mounted on the aluminium tube and parallel to it, bearing against the sliding brass tube. This screw has about 10 turns per cm. and hence 1 turn moves the projected focal plane by $1/10 \times 1/5^2 = 40\mu m$. The aperture ratio of the image beam is about 1/10. This device is shown in Figure 16. By means of it, the image tube can be magnetically focussed *in situ*. Another such projector was constructed, but with these differences: the test pattern and lens were replaced by an Ilford 806 violet filter, light baffles and a small aperture covered with opal glass which can be illuminated by a small lamp. This device was used to check uniformity of cathode response *in situ*. By replacing the lamp and aperture with a small telescope, and reversing the prism at the other end, the spectrograph focal plane may also be examined without removing the image tube.

The image tube was located in the arrangement described by means of 4BA stud bolts projecting from the rear faceplate through the flange on the image tube's Perspex casing.

The ancillary equipment was mounted on a Dexion trolley which also served as the cradle for hoisting into the dome. The equipment consisted of a Brandenberg 40 KV EHT stabilised supply with a Pye 40 KV electrostatic voltmeter, a Brandenberg 400 mA current stabiliser, and a cooling system for the solenoid. This was a domestic refrigerator unit with the cooler immersed in a 5 gallon plastic tank filled with water. This was circulated by means of a Stuart and Turner centrifugal pump through plastic hoses attached to the ends of the cooling tube in the solenoid. The cooling system maintained room temperature at the outside of the coil for long periods, and in the dome at night it was found unnecessary to operate the refrigerator. The solenoid running at 400 mA produces 80 watts to be dissipated. If there were no heat exchange with the atmosphere, this would raise the temperature of the cooling tank by about 4 centigrade degrees per hour.

(ii) Insulation Failure

A persistent and difficult problem in the use of the image tube on the telescope was breakdown of the high voltage insulation due to damp, at various parts of the EHT circuit. After a lengthy series of attempts to eliminate it, the following arrangements were made.

A large airtight box was constructed to take the EHT supply and the electrostatic voltmeter. One side of the box is detachable for access. Perspex windows are let into relevant parts of the box to permit observation of the various dials and pilot lights, and to permit inspection for any corona discharge, for instance. The controls of the voltage supply were extracted and passed through the side of the box via a multi-way plug, and mounted on a separate part of the trolley. A rod, topped with a knurled knob was passed through a gland in the top of the box, and attached via a universal joint to the zeroing screw of the voltmeter. The EHT conductor, a coaxial cable stripped of its copper screening, was passed through a PVC tube attached to another gland in the top of the box. At the other end of this encased cable, a specially constructed PTFE plug was hermetically sealed to the PVC tube and the inner cable, so that the cable as far as this plug was in the same atmospheric environment as the interior of the airtight box. A removable rack of silica gel dessicators which may be sealed into the box was found to be sufficient to prevent any discharge trouble in this region(a gland for introducing dry nitrogen had been built in, but was never used). The PTFE plug was female, to avoid any risk of the cable parting while EHT was on, and coming into contact with earthed conductors,

or, indeed, observers. The male socket also in PTFE, formed the end of an intricately shaped Silastomer filled Perspex piece which was attached to the front of the solenoid faceplate, between it and the spectrograph, and contained the EHT lead to the front of the image tube.

The region between the front of the image tube and the back of the camera lens was also isolated by this Perspex piece, into which an airlock containing a Frigistor cooling device had been built. The Frigistor (1" x 2" x $\frac{1}{4}$"), a solid-state device, was backed with a water reservoir (supplied by means of a junction by the same pump as the solenoid) which cooled the hot side, while the temperature differential effect lowered the temperature of the face projecting into the volume in front of the photocathode to a possible -50°C. After a few minutes running at 15 amps, the device had condensed any moisture onto its face, and was withdrawn through the airlock, automatically closing it. It was found that the above procedure need be repeated only once per day at most to render the tube completely free of discharge.

During one of the many crises in this stage of the work when the electrostatic voltmeter suspension failed, as a temporary measure a small voltage was tapped from the feedback circuitry of the EHT supply to a digital

voltmeter. This has since proved a very useful antidote to drift in the electrostatic voltmeter, which tends to drift down by a reading of .3 KV from 38 KV during a warm-up period of 2 to 3 hours, while the digital voltmeter drifts up by 8 digits in 1,500 in the same period.

(iii) Magnetic Disturbances

The magnetic field experienced by the electrons is that created by the solenoid, and in addition any other magnetic field in the vicinity, such as the earth's field, and fields induced by the large iron components of a telescope.

If there are no disturbing fields, then the field structure in which the electrons move is

$$\underline{E} = E\underline{k} \qquad \underline{B} = B\underline{k} \tag{5.1}$$

and the solution to the Lorenz equation of motion is

$$x = x_o - \frac{Vm}{eB} \cos\left(\frac{eBt}{m} + \epsilon\right)$$

$$y = y_o + \frac{Vm}{eB} \sin\left(\frac{eBt}{m} + \epsilon\right) \tag{5.2}$$

$$z = \frac{1}{2} \frac{eE}{m} t^2 + w_o t$$

where the electron originates at $(x_o, y_o, 0)$ with initial velocity $(V\cos\epsilon, V\sin\epsilon, w_o)$.

Now a disturbance is formalised by a constant component in the x-direction (longitudinal components

will merely defocus by a small amount, and since the aperture ratio A of the beam is given by

$$\left.\frac{dr}{dz}\right|_{z=d} = V \circ \frac{B}{4\pi E} \qquad 5.3$$

where r is the radius of the converging beam at distance z, and V is the initial transverse velocity, and hence

$$A = .006\ T_t \qquad 5.4$$

where T_t is the kinetic energy in eV associated with the initial transverse velocity, and will be only a few electron volts. Thus the defocussing effect will be of second order only.)

The equation of motion then becomes

$$m\dot{\underline{v}} = e(Ek + \dot{\underline{v}} \wedge (Bk + bi)) \qquad 5.5$$

where b represents the disturbing magnetic field. The solution for the electron paths now becomes

$$\begin{aligned} x &= x_o - \frac{B}{B'}\frac{mA}{eB'}\cos\left(\frac{eB't}{m} + \epsilon\right) + \frac{bB}{B'^2}\frac{eE}{m}\frac{t^2}{2} + \frac{b}{B}Kt \\ y &= y_o + \frac{mA}{eB'}\sin\left(\frac{eBt}{m} + \epsilon\right) + \frac{bE}{B'^2}t \qquad 5.6 \\ z &= \frac{B^2}{B'^2}\frac{eE}{m}\frac{t^2}{2} - \frac{b}{B'}\frac{mA}{eB'}\left(\sin\left(\frac{eBt}{m} + \epsilon\right) - \sin\epsilon\right) + Kt \end{aligned}$$

where $B'^2 = B^2 + b^2$

if $b \ll B$, and the initial velocity is $(V\cos\psi, V\sin\psi, w_o)$ and $b = \eta B$, then

$$K = w_o + \eta V \sin\psi$$

$$A = V - \eta (E\cos\psi/B + w_o \sin\psi) \qquad 5.7$$

$$\epsilon = \psi + \eta \frac{\sin 2\psi}{2} \frac{E}{BV\cos\psi} - \frac{w_o}{V\sin\psi}$$

The (x,y) motion consists of

(a) an elliptic motion whose major axis is determined by the tube field, and whose eccentricity is determined by the disturbing field.

(b) a transposition of the image plane z = d.

$$\Delta x = \eta \frac{eE}{m} \frac{t^2}{2} \qquad \Delta y = \eta \frac{E}{B} t \qquad 5.8$$

and with $t = \pi m/eB$ at z = d

$$\frac{\Delta x}{d} = 2\pi \frac{\Delta y}{d} = \eta \qquad 5.9$$

(c) an astigmatism in the direction of the disturbance

$$\Delta x_{ast} = \eta K t = \eta \cdot w_o t \qquad 5.10$$

Of these (b) is the most important since, during a long exposure with η varying, the image will be smeared.

It has been mentioned that the spatial frequency response of the particular tube used for measurements of MTF, and for the astronomical program, was not as good as it should have been. This tube, by courtesy

of Professor McGee, was a hurried replacement for a tube whose sensitivity had dropped by a factor of ten but whose frequency response was much better. Resolution determined at Imperial College by eye for the Spectracon indicates an optimum of 80 c.p.mm. This subjectively determined response will correspond to signal:noise of the order of 5, and hence measurements will be significant up to frequencies of this order. Thus magnetic stabilisation must be such that during an exposure, $\Delta x < 1/160$ mm. From equation (5.9) with d = 280 mm, B = .016 webers/m^2

$$\Delta_B = 4 \times 10^{-7} \text{ webers/m}^2$$

$$\equiv 4 \text{ milligauss}$$

The induction earth's magnetic field is of the order of .5 gauss (in air).

Thus if the image tube mounted on the telescope is unshielded, under the worst conditions of alignment of the tube with the external field, exposures of more than a few minutes will smear the images, i.e. reduce the effective MTF of the tube. By aligning the slit of the spectrograph in the direction of smear this effect may be minimised, but it is obviously necessary to shield a tube in such an environment.

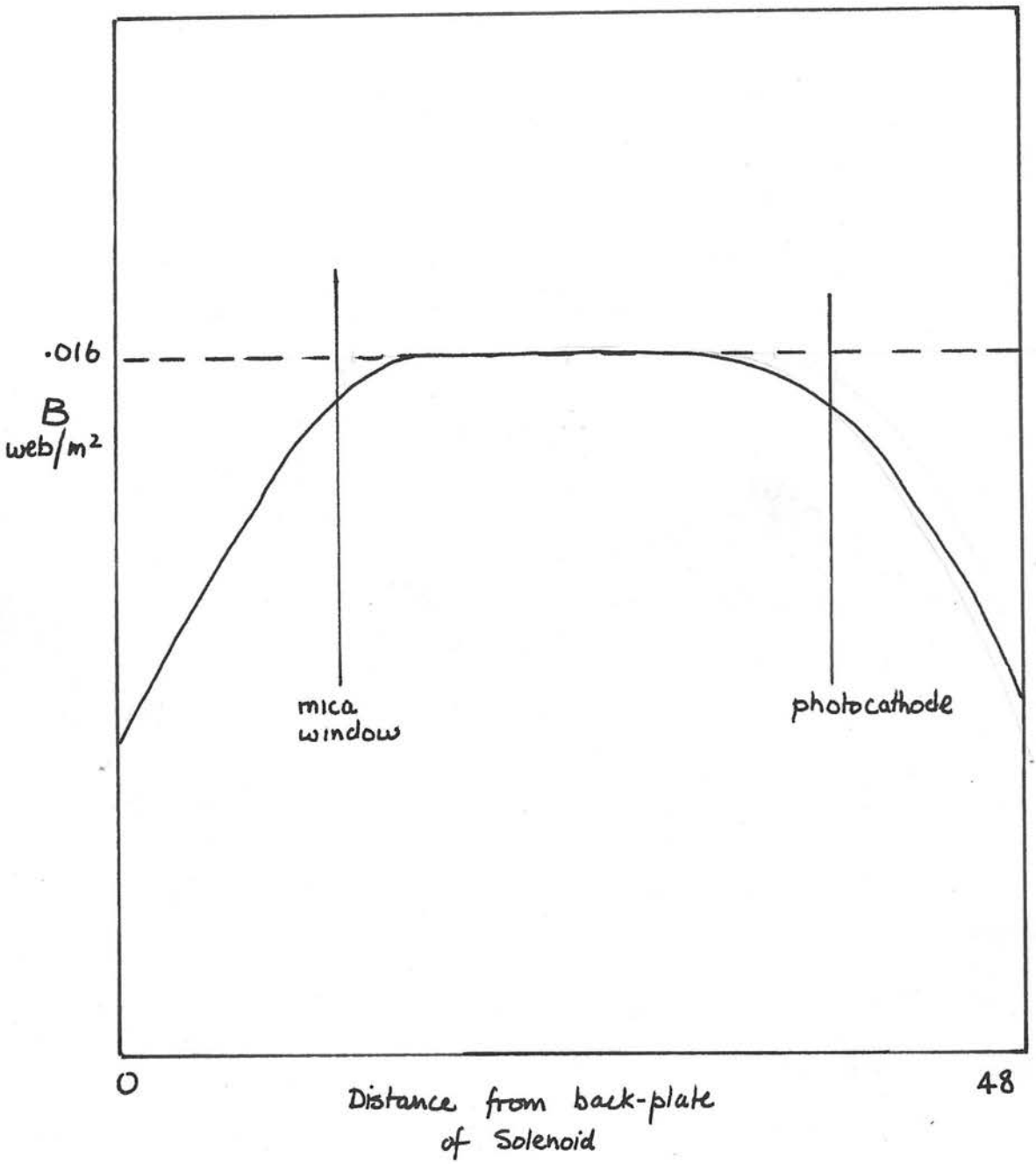

Figure 17 Magnetic field of solenoid

Since the group working under Professor McGee at Imperial College on the production of the Spectracon have been developing a compact shield and focussing solenoid assembly, this problem was not tackled.

Another limit on resolution imposed by the electron beam is that associated with the uniformity of the magnetic field produced in the accelerating region of the tube. Using a Hall effect probe run on stabilised D.C. current, the magnetic field of the solenoid used on the telescope was investigated.

The result of longitudinal measurement is shown in Figure 17. The position of the cathode as marked is determined by the focal surface of the spectrograph, and is further forward in the solenoid than it should be, were uniformity of field the sole criterion. This is probably the cause of slight S-distortion observed in spectra taken with the tube, as the helical trajectories of the electrons (typical radius $\frac{1}{4}$ mm.) tend to follow the lines of force of the field. Even so, the field strength drops by about 5% at each end of the coil, and compensating coils would benefit the field. Again, this problem has been solved at Imperial College, and so not much time was devoted to it here.

CHAPTER VI

Astronomical Program: Width of Profile of Interstellar Band λ4430

In order to prove the Spectracon in use, a program of astronomical observations was prepared. It was decided, in view of (a) the main interests in research at the Observatory, (b) spectral range of the tube (in terms of the length of photocathode and reciprocal linear dispersion of the spectrograph), and (c) the dubious resolution of the tube to be used for the observations, that a study of the interstellar band at λ4430 would be a good subject for study.

The Observatory has been studying the effects of the interstellar medium for some time, so expert knowledge was on hand. The band is an isolated feature, at a wavelength near the maximum wavelength sensitivity of the cathode, and is of the order of 50 A broad, and so satisfies requirements (b) and (c).

(i) λ4430

The absorption band λ4430 was first observed by Merrill in 1936.[56] Since then a deal of work has been done in attempting to identify the origin of the absorption. A recent discussion of results took place during the last meeting of the Royal Astronomical Society at the Observatory in 1963,[57] and still the material producing the feature has evaded identification.

A very recent paper by Seddon[58] describes what is possibly the most accurate determination of the profile to date. About 75 spectra of early-type stars were reduced, and the mean profile fitted with a double gaussian curve, the standard error being .003 magnitudes per fitted point.

(ii) Observational Program

Stars with λ4430 were selected from Duke's catalogue[59] on the basis (a) that the central absorption of λ4430 was greater than 3%, (b) the stars were brighter than 7^m, (c) the stars were in the region of the Milky Way between 20^h and 6^h. Criterion (b) was required to allow sufficiently short exposures that magnetic smearing (described in Chapter V) did not become a problem. Criterion (c) was dictated by the time of year for the observations. 25 such stars were selected, and spectra of 23, on G5 or XM, obtained.

The table below lists the HD number of the star, its magnitude (taken from the photographic magnitude in the HD catalogue), the central absorption as given by Duke, and the exposures obtained.

Exposures on G5 are denoted by G followed by the number of G5 spectra obtained; similarly X represents XM exposures. The stars are arranged in groups of increasing absorption, in which sequence the groups were later analysed.

HD	m	W_c	Exposures
23180	3.9	3.0	G2 X2
24760	3.0	3.8	G3 X2
24398	2.9	4.1	G3 X2
203064	5.0	6.0	G2
206165	4.9	7.0	G4 X3
12301	5.5	7.0	G3 X2
24912	4.0	7.2	G2
193237	4.9	7.2	G3
14489	5.2	7.5	G2 X3
2095	4.0	7.6	G4 X2
36371	4.9	7.9	G2 X2
21389	4.8	7.9	G3 X2
209481	5.5	8.0	G2
207198	6.0	8.2	G2
208501	6.0	8.3	G2
223385	5.6	8.5	G3 X2
41117	4.7	8.6	X2
198478	4.9	10.2	G2
13854	6.2	11.0	G2 X2
4841	6.9	11.0	X2
23675	6.6	11.6	G1 X2
35921	6.7	12.0	G1 X2
20041	5.9	12.5	G2 X3

Of these 50 spectra spanning the groups were selected for analysis.

(iii) Telescope Preparation

The spectrograph was set up with the No. 3 grating in position. This grating, blazed for blue light, gives, in conjunction with the f/3 camera, a reciprocal linear dispersion of 40 A/mm. It was found that, due to the way in which the grating was positioned in its mount, it was impossible to adjust the exit beam so

that the slit image was accurately perpendicular to the direction of dispersion, and at the same time the image was on the optical axis. However, since this effect was slight, it was tolerated, being compensated by rotating the scanning slit of the microphotometer. The problem only arises because of the small height of the cathode, which necessitates the spectrum being accurately on the optical axis. For conventional photography, the small deviation does not matter.

Preliminary investigations using the test pattern projector, and exposing the tube to the test pattern at different positions of the telescope had established the direction of drift due to external magnetic fields, and the spectrograph was rotated so that the drift was along, rather than across, the slit. However, it was deemed prudent to restrict the exposures to 15 minutes, to minimise drift effects. This restriction will of course not apply to later versions of the Spectracon provided with magnetic shielding.

Focussing was carried out using the test pattern projector for magnetic focus, and a mercury discharge lamp for camera lens focus.

The observations were made during a good spell in the weather in December and January, with occasional help from other observers. It seemed encouraging that

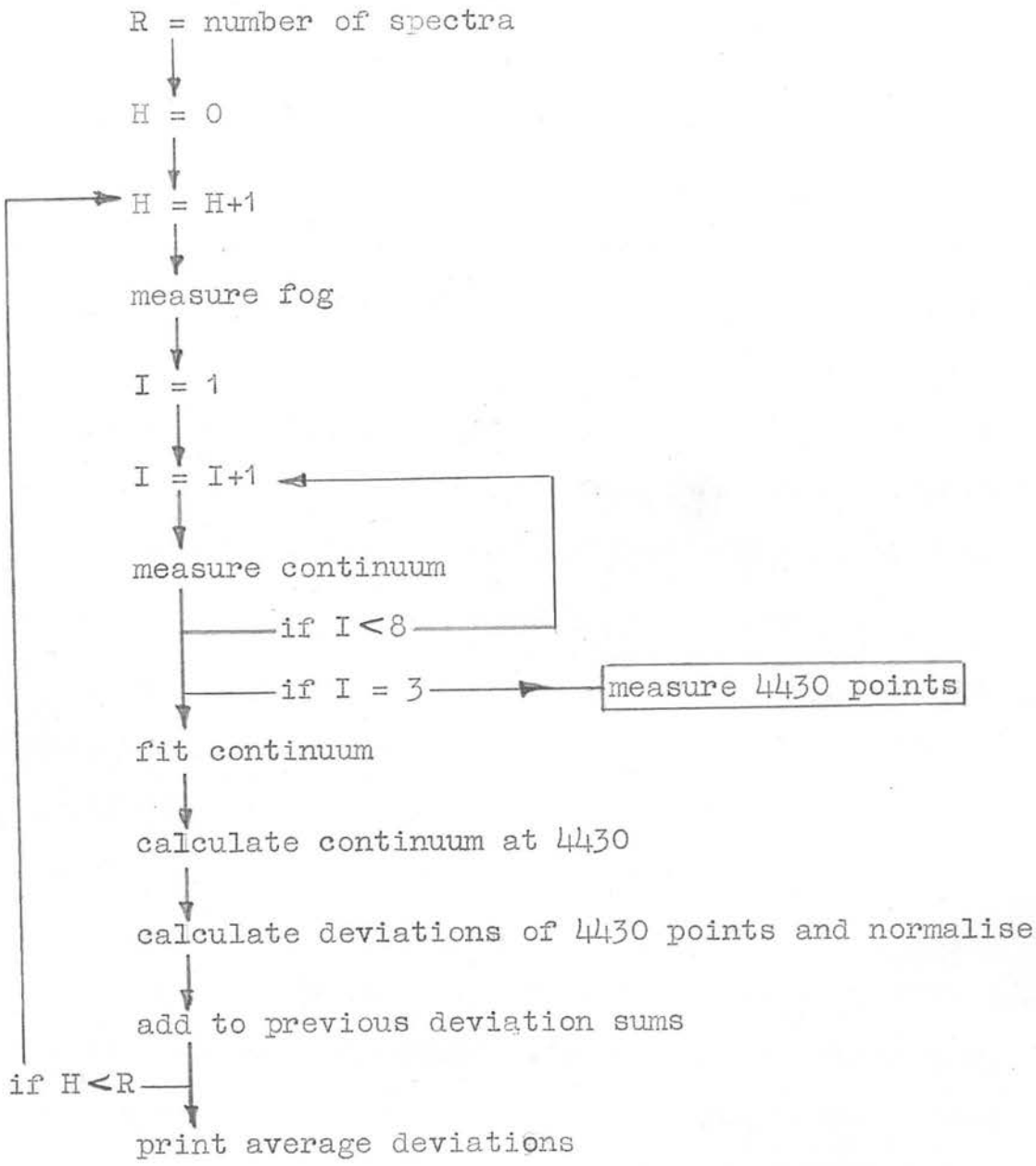

Figure 18 Flow diagram for "DM 4430"

they were impressed with the facility with which exposures could be made, using the Spectracon.

(iv) Reduction

The selected spectra were examined preliminarily using a Joyce-Loebl densitometer, in preparation for a spectrum reduction using digital output provided by the Hilger microphotometer.

Wavelength calibration of the Hilger was measured using the hydrogen Balmer lines Hγ and Hδ. From the calibration it was deduced that one $12\frac{1}{2}\mu$m step corresponded to .534 A. The zero point was chosen so that the 4430 A should occur at the 220th step. Eight regions of the spectrum between 4250 A and 4550 A which had few perceptible lines nearby were chosen to fit the continuum. Early attempts to fit a polynomial continuum were frustrated by lack of time and difficulties with computer handling of the obsolete Edsac output. In later versions of the program, a straight line is fitted as first approximation.

The data punched out consisted of groups of data for (a) fog level, (b) continuum points (10-20 data at each point), (c) 4430 region (steps 160-280). In all, 50 such data groups were punched, and transferred to 6 data tapes comprising the groups shown in the table above.

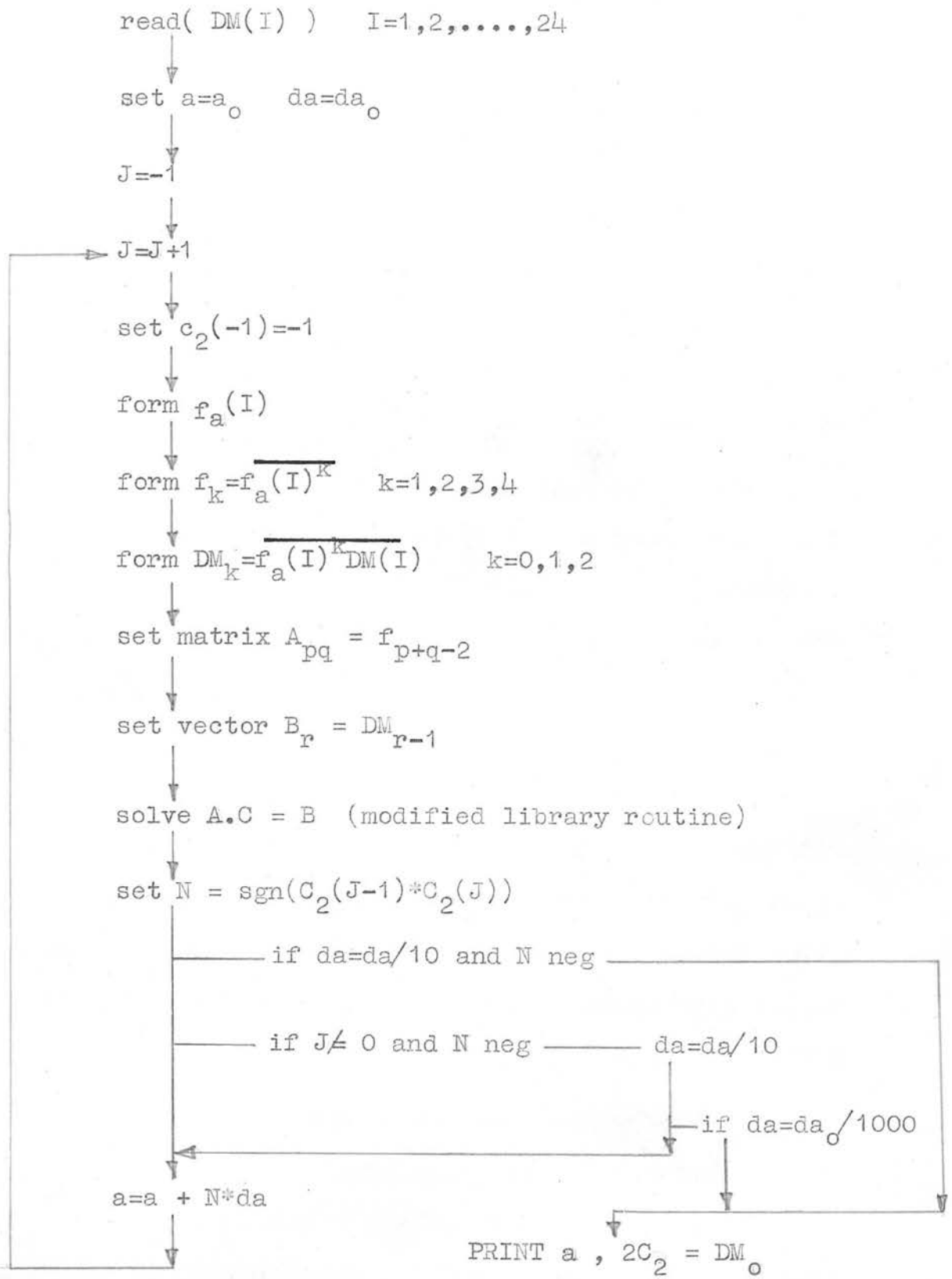

Figure 19 Flow diagram for "4430 FIT"

(v) Analysis

The data tapes were analysed by two programs ("DM 4430" and "4430 FIT") which respectively produced deviations from continuum for 24 points corresponding to the values of wavelength used by Seddon for fitting the profile to the absorption feature, and fitted his profile (with variable width) to the deviations. The aim of the analysis was to seek correlation between central depth and width of profile.

The results presented are preliminary. Trouble with continuum fit, and the moderate dispersion used both militate against accuracy. It appears, however, that if a correlation such as that sought exists, it is small. More sophisticated methods, and more data should provide a less ambiguous result.

The flow diagrams for the programs are shown in figures 18 and 19, and the relation derived between central depth DM_o and width 'a' is shown in Figure 20. The principle of the program "4430 FIT" is that of linear regression.

If the profile is given by f(x), and points x_i, y_i are given, and if it is assumed that these data are samples from a population distributed such that $\overline{Y}_i = f(x_i)$ then the regression between $f_i = f(x_i)$ and y_i will be linear. The profile f(x) depends on a parameter 'a'

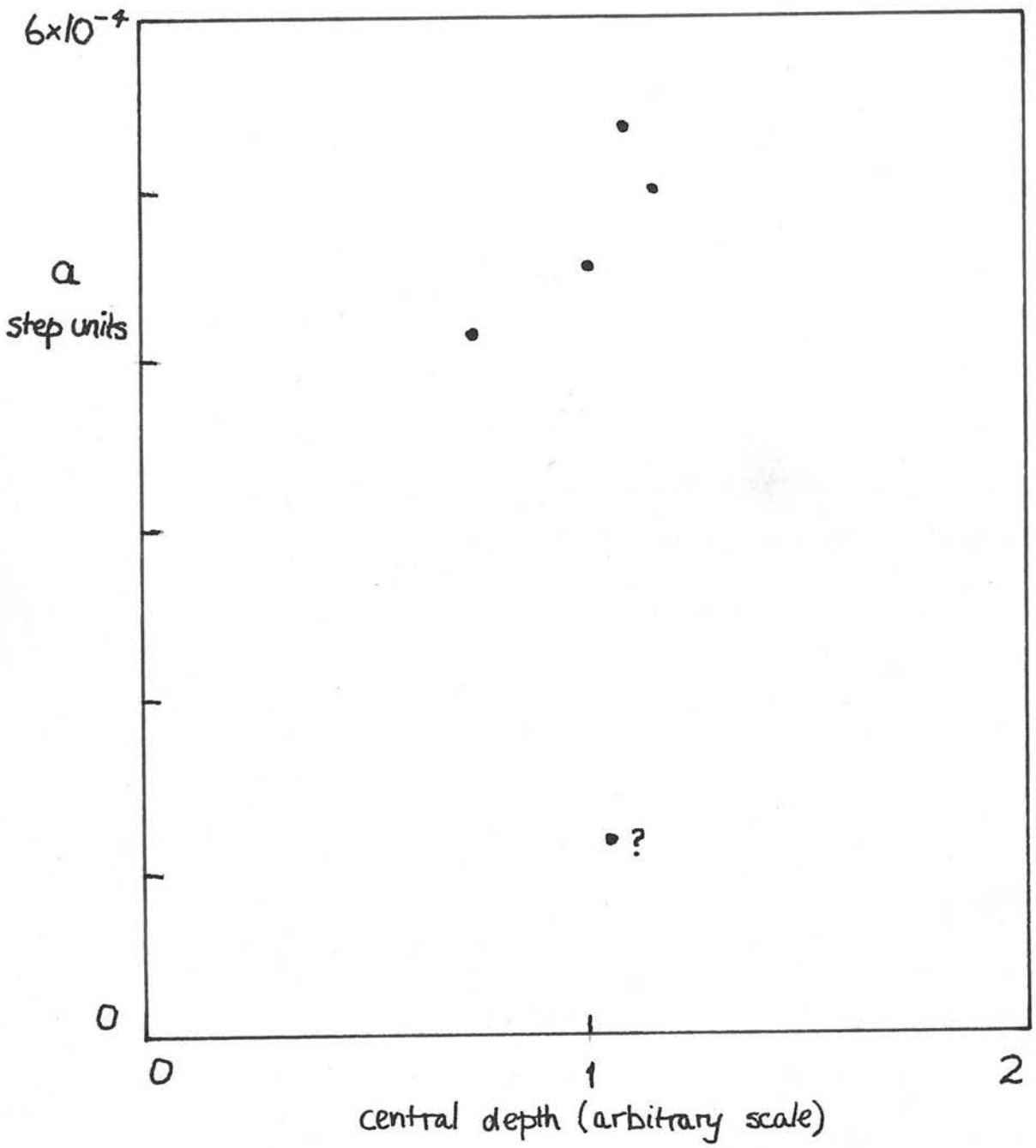

Figure 20 Width of fitted profile versus group central intensity

(which represents the width) and what program "4430 FIT" does is to least squares fit a second degree polynomial to y_i, f_i, and to vary the parameter in such a way as to cause the second degree coefficient to tend to zero. This is done by solving the normal equations for the regression, using a modified library routine to solve the matrix equation (EQN SOLVE 3). The program then measures the central intensity of the profile (note that it partially compensates for poor continuum choice), and prints this out with the final value of the parameter 'a'.

CONCLUSIONS

It is to be hoped that the methods described in the first part of this thesis will be extensively applied to imaging devices and to photographic emulsions, since this is the only way in which an unambiguous figure for the performance of the detector may be derived. Lack of attention to such concepts has produced many pitfalls, notably the enormous (and imaginary) gains reported earlier for various types of image tube, which, when they were not realised in practice, produced some considerable despondency.

The work of Shaw[60] on aerial films is an outstanding example of thorough application of Information Theory to the photographic process. His results are formally the same as those of Chapter I of this thesis.

The results derived enable a prediction of signal-to-noise-ratio (accuracy) and information gain for the image tube under any conditions of exposure. The results also point to the necessity of knowing, for instance, the MTF of the spectrograph used with the detector, in order to fully exploit the storage capacity of the detector.

Part II of this work has described the manner in which the Spectracon, as a particular example of an

astronomical image tube, may be brought into routine use as part of the observational astronomer's instrument capability.

Much is still to be achieved in this field. In particular, the emulsions are in no way comparable in standard (understandably, they are still a laboratory - rather than commercial - commodity) with the best astronomical emulsions. Similarly, such is the experimental complexity in building a tube, that to produce a flawless cathode and window (and both are focal surfaces) is asking a great deal. But it is not asking for the impossible, and it is foreseeable that in time such difficulties will be eliminated.

There remains the problem of the small area of the cathode. In effect, while the information storage capacity of the image tube is considerably greater than that of astronomical emulsions, its limited area rather nullifies this advantage in that, with suitable coding, all the information in the small cathode area could be spread onto one large astronomical plate. However, to do this the exposing intensity must be reduced, and this, because of the nonlinearity of the photographic process, reduces the efficiency.

Thus the crucial advantage in using an image tube must be in exploiting its higher detecting efficiency. If programs consist in looking at small regions of spectrum (or of sky), then the advantages of the image tube are obvious.

Some of this work has already been reported in a paper read to the 3rd Symposium on Photoelectronic Imaging Devices.[3]

APPENDIX

FACSIMILE PROGRAMS

PHOTOGRAN

FILTER

MTF

MODEL G5 COEFFS

MODEL SPREAD FN,MTF

DM 4430

4430 FIT

"FILTER"

```
%BEGIN
%INTEGER I,N
%REAL LAMBDA,DELTA,MX,MI,MIS,RMSI,F,G,K,T,X
%ARRAY E(0:17)

E(0)=.879
E(1)=1.69
E(2)=3.085
E(3)=5.247
E(4)=8.448
E(5)=12.90
E(6)=19.09
E(7)=26.77
E(8)=37.03
E(9)=49.25
E(10)=64.87
E(11)=81.36
E(12)=101.7
E(13)=124.9
E(14)=149.3
E(15)=177.4
E(16)=207.8
E(17)=240.3

READ(K);        !CONST FACTOR IN T
READ(LAMBDA);   !WAVELENGTH AT I=0 IN NM.
READ(DELTA);    !WAVELENGTH INTERVAL PER I
READ(N)

MX=0;MI=0;MIS=0
%CYCLE I=1,1,N-1
  READ(T)
  G=(LAMBDA-380+I*DELTA)/20
  F=E(INTPT(G))+FRACPT(G)*(E(INTPT(G)+1)-E(INTPT(G)))
  X=T*F
  X=.5*X %IF I=1 %OR I=N-1
  MX=MX+X
  MI=MI+I*X
  MIS=MIS+I↑2*X
%REPEAT
MI=MI/MX
MIS=MIS/MX
RMSI=SQRT(MIS-MI↑2)

%CAPTION MEAN WAVELENGTH=;PRINT(LAMBDA+MI*DELTA,4,0);%CAPTION NM.
%CAPTION RMS DEVN=;PRINT(RMSI*DELTA,3,0);%CAPTION NM.;SPACES(2)
%CAPTION PHOTONS/SEC.SR.NM=;PRINTFL(MX*DELTA*K,3);%CAPTION *10↑13

%ENDOFPROGRAM
```

```
            "MODEL G5 COEFFS"


%BEGIN
%INTEGER N

N=6

%BEGIN
%INTEGER K,D,J
%ROUTINESPEC NEST(%INTEGER J)
%REALFNSPEC F(%INTEGERNAME D)
%ARRAY S(1:7)
%INTEGERARRAY I(1:N)
%REAL SUM

S(1)=.205
S(2)=.391
S(3)=.554
S(4)=.693
S(5)=.805
S(6)=.885
S(7)=.951

%CYCLE K=1,1,N
   %CAPTION Y(;PRINT(K,1,0);%CAPTION )=
   SUM=0
   NEST(K)
   PRINTFL(SUM*1.2533/(2.5065)↑K,4)
   NEWLINE
%REPEAT

%ROUTINE NEST(%INTEGER J)
   ->1 %IF J=0
   %CYCLE I(J)=1,1,7
      NEST(J-1)
   %REPEAT
   %RETURN
   1:SUM=SUM+F(K)
%END

%REALFN F(%INTEGERNAME D)
   %INTEGER P
   %REAL X
   X=0
   %CYCLE P=1,1,D
      X=X+1/S(I(P))
   %REPEAT
   %CYCLE P=1,1,D
      X=X*S(I(P))
   %REPEAT
   %RESULT =1/SQRT(X)
%END


%END

%ENDOFPROGRAM
```

```
                "PHOTOGRAN Y"

%BEGIN
%INTEGER B,D,I,J,K,L,M,P,R
%REAL T,U,SMT,SUMSQT,SUMUT,G,H
%INTEGERARRAY A(0:64),IT,C(1:5)
%INTEGERFNSPEC EDREAD

%COMMENT        NO.OF FILMS=B,IT NOS. STORED IN IT(M),NO.OF
%COMMENT        STRIPS PER FILM STORED IN C(M)

B=2
IT(1)=215;C(1)=7
IT(2)=216;C(2)=8

A(0)=-2
A(1)=-2
A(2)=-3
A(3)=0
A(4)=-2
A(5)=7
A(6)=2
A(7)=-2
A(8)=-3
A(9)=8
A(10)=5
A(11)=-2
A(12)=9
A(13)=-2
A(14)=-2
A(15)=-2
A(16)=-2
A(17)=4
A(18)=3
A(19)=-2
A(20)=6
A(21)=-2
A(22)=-2
A(23)=-1
A(24)=1

%CYCLE J=25,1,64
  A(J)=-2
%REPEAT


M=0;   ! M COUNTS FILMS
1:M=M+1
%CAPTION IT;PRINT(IT(M),3,0);NEWLINE

D=0;     !D COUNTS STRIPS
2:D=D+1
```

```
SUMSQT=0;SUMUT=0;T=EDREAD;T=EDREAD %IF M=1 %AND D=1
SMT=T
%CYCLE J=0,1,1000
  U=EDREAD;  ->3 %IF U=1600;                    ! *
  SMT=SMT+U
  SUMSQT=SUMSQT+U*U
  SUMUT=SUMUT+U*T
  T=U
%REPEAT

3:NEWLINE
%CAPTION NO␣OF␣VALUES␣OF␣TRANS␣=;PRINT(J,4,0);NEWLINE
PRINT(SMT/J,3,3);SPACES(3);PRINT(SUMSQT/J,5,1);PRINT(SUMUT/J,5,1)
H=.4343*LOG(SMT/J) %IF D=1
SPACES(4)
%CAPTION DENSITY=;PRINT(H-.4343*LOG(SMT/J),1,3)
SPACES(3)
%CAPTION SIGMA␣SQD␣D=;PRINTFL(J*(SUMSQT-SUMUT)/(SMT*SMT),3)
NEWLINES(3)

%STOP %IF M=B %AND D=C(B)                     ;!DATA ENDS
->4 %IF U=1600

%COMMENT SEEK DATA BLOCK MARKER,BINARY32
P=0
%CYCLE L=1,1,5000
  READBINARY(P)
  ->4 %IF P=32
  %STOP %IF P=63                              ;!DATA TERMINATOR
%REPEAT
%CAPTION DATA␣OVERRUN;    !NO MARKER FOUND
%STOP
4:->1 %IF D=C(M)
->2


%INTEGERFN EDREAD
%INTEGER I,J,K
1:J=0;  K=0
READBINARY(I)
%IF I=32 %THENRESULT =1600;                    ! *
%STOP %IF I=63                                ;!DATA TERMINATOR
->1 %UNLESS A(I)=0 %OR A(I)=1
K=1
J=A(I)
2:READBINARY(I)
->1 %IF I<3 %OR I>24 %OR A(I)=-2 %OR I=8 %OR I=23
K=K+1
J=A(I)+J*10
%IF K=4 %THENRESULT =J
->2
%END


%COMMENT     *   BINARY32 TRANS. TO 1600 ALLOWS PRINTOUT OF DATA
%COMMENT         FROM INCOMPLETE STRIP


%ENDOFPROGRAM
```

```
                    "DM 4430"

%BEGIN

%INTEGERFNSPEC EDREAD
%REALFNSPEC MEAN TRANS(%INTEGERNAME N)
%ARRAY TR(0:7),M(0:7),ML,MP,XL,DIFM,DM(1:24)
%INTEGER J,P,H,R,L,Q
%INTEGERARRAY A(0:64),Y(0:9)
%REAL K

A(0)=-2
A(1)=-2
A(2)=-3
A(3)=0
A(4)=-2
A(5)=7
A(6)=2
A(7)=-2
A(8)=-3
A(9)=8
A(10)=5
A(11)=-2
A(12)=9
A(13)=-2
A(14)=-2
A(15)=-2
A(16)=-2
A(17)=4
A(18)=3
A(19)=-2
A(20)=6
A(21)=-2
A(22)=-2
A(23)=-1
A(24)=1

%CYCLE J=25,1,64
  A(J)=-2
%REPEAT

%COMMENT HILGER COORDS FOR 4430 FIT
XL(1)=164
XL(2)=165
XL(3)=173
XL(4)=180
XL(5)=181
XL(6)=192
XL(7)=201
XL(8)=209
XL(9)=220
XL(10)=230
XL(11)=231
XL(12)=232
XL(13)=233
XL(14)=234
XL(15)=235
XL(16)=252
XL(17)=264
XL(18)=265
XL(19)=266
```

```
XL(20)=267
XL(21)=268
XL(22)=269
XL(23)=270
XL(24)=275

%CYCLE J=1,1,24
   DM(J)=0
%REPEAT

R=9
H=0
5:H=H+1

%COMMENT VALUES OF DATA MARKERS
Y(0)=33
Y(1)=34
Y(2)=35
Y(3)=36
Y(4)=37
Y(5)=38
Y(6)=39
Y(7)=40
Y(8)=41
Y(9)=42

%CYCLE Q=1,1,500
   READBINARY(P)
   ->10 %IF P=Y(0)
%REPEAT
%CAPTION NO START;%STOP

%COMMENT CALC. DENS. AT X(J) FOR CONTINUUM FIT
10:%CYCLE J=0,1,7
   P=10;P=2P %IF J=0 %OR J=1 %OR J=7
   TR(J)=MEAN TRANS(P);PRINT(TR(J),3,2);NEWLINE
   ->9 %IF J=0
   TR(J)=TR(0)/TR(J)
   M(J)=LOG(TR(J))
   ->8 %IF J=2
9:%REPEAT

%COMMENT FIT CONTINUUM
%BEGIN
%INTEGER J
%REAL MSUM,XSUM,C1,X2
%ARRAY X(1:7)

%COMMENT HILGER COORDS FOR CONTINUUM FIT
X(1)=10
X(2)=50
X(3)=305
X(4)=460
X(5)=475
X(6)=510
X(7)=550

MSUM=0;XSUM=0
```

```
%CYCLE J=1,1,7
   MSUM=MSUM+M(J)/7
   XSUM=XSUM+X(J)/7
%REPEAT
%CYCLE J=1,1,7
   M(J)=M(J)-MSUM
   X(J)=X(J)-XSUM
%REPEAT

%COMMENT C1=MX/X2BAR  Y=C1*X
C1=0;X2=0
%CYCLE J=1,1,7
   C1=C1+M(J)*X(J)/7
   X2=X2+X(J)*X(J)/7
%REPEAT
C1=C1/X2
K=MSUM+C1*(220-XSUM)
%CYCLE J=1,1,24
   DIFM(J)=(ML(J)-(C1*(XL(J)-XSUM)+MSUM))/K
   DIFM(J)=0 %IF ML(J)=0
%REPEAT

%END

%CYCLE J=1,1,24
   DM(J)=DM(J)+DIFM(J)          ;!AVERAGE 4430 DEVIATIONS
%REPEAT
->5 %UNLESS H=R
%CYCLE J=1,1,24
   DM(J)=DM(J)/H
   NEWLINE;PRINTFL(DM(J),4)     ;!PRINT 4430 DEVIATIONS
%REPEAT
->100

%COMMENT CALC DENS AT XL(J)
8:%BEGIN
%ROUTINESPEC MISS(%INTEGER C)
%INTEGERFNSPEC EDREAD
%INTEGERARRAY L(1:24),N(1:24)
%INTEGER T,J

N(1)=4
N(2)=0
N(3)=7
N(4)=6
N(5)=0
N(6)=10
N(7)=8
N(8)=7
N(9)=10
N(10)=9
N(11)=0
N(12)=0
N(13)=0
N(14)=0
N(15)=0
N(16)=16
N(17)=11
```

```
N(18)=0
N(19)=0
N(20)=0
N(21)=0
N(22)=0
N(23)=0
N(24)=4

%CYCLE J=1,1,24
   MISS(J)
   T=EDREAD
   %IF T=Y(4) %THENCAPTION BLOCK␣8␣NUTS␣J=
   PRINT(J,2,0) %IF T=Y(4)
   ->2 %IF T=Y(4)
   ML(J)=0 %IF T=-1;%IF T=-1 %THENCAPTION DUD␣ML␣J
   ;PRINT(J,2,0) %IF T=-1
   ->1 %IF T=-1
   ML(J)=LOG(TR(0)/T)
1:%REPEAT
%CYCLE J=1,1,500
   READBINARY(T)
   ->2 %IF T=Y(4)
%REPEAT
%CAPTION NO ␣Y(4);%STOP

%ROUTINE MISS(%INTEGER D)
   %INTEGER Q,P
   ->1 %IF N(D)=0
   %CYCLE Q=1,1,7N(D)
      READBINARY(P)
      %IF P=Y(4) %THENCAPTION MISS␣Y;%STOPIF P=Y(4)
   %REPEAT
1:%END

%INTEGERFN EDREAD
%INTEGER I,J,K,L
L=0
1:%RESULT =-1 %IF L=5;READBINARY(I)
L=L+1;->1 %UNLESS A(I)=0 %OR A(I)=1
K=1
J=A(I)
2:READBINARY(I);%IF A(I)<0 %THENRESULT =-1
J=10J+A(I)
K=K+1
%IF K=4 %THENRESULT =J
->2
%END

2:%END

->9

%REALFN MEAN TRANS(%INTEGERNAME N)
%REAL TRANS
%INTEGER I,R,T
TRANS=0;R=0
Y(J+1)=Y(J+1)+1 %IF J>2;SPACES(10);PRINT(J,1,0)
PRINT(Y(J+1),2,0);NEWLINE
```

```
%CYCLE I=1,1,N
    T=EDREAD;R=R+L
    ->1 %IF T=Y(J+1)
    %IF R>=N %AND I<3 %THENCAPTION NOREAD;%STOPIF R>=N %AND I<3
    TRANS=TRANS+T
3:%REPEAT
%CYCLE I=1,1,10
    T=EDREAD;NEWLINES(2);PRINT(T,4,0)
    ->2 %IF T=Y(J+1)
%REPEAT
%CAPTION OVERRUN;%STOP
2:%RESULT =TRANS/N
1:PRINT(I,2,0);%CAPTION L=;PRINT(L,2,0);%RESULT =TRANS/(I-1)
%END

%INTEGERFN EDREAD
%INTEGER J,K,Q
%INTEGERARRAY I(1:6)
L=-1
1:L=L+1
READBINARY(K)
%RESULT =K %IF 32<K<43
%STOPIF K=63
->1 %UNLESS K=23
2:%CYCLE Q=1,1,6
    READBINARY(I(Q));L=L+1 %IF I(Q)=23;->2 %IF I(Q)=23
%REPEAT
->1 %UNLESS A(I(1))=0 %OR A(I(1))=1
J=0
%CYCLE Q=1,1,4
    ->1 %UNLESS -1<A(I(Q))<10
    J=A(I(Q))+J*10
%REPEAT
%RESULT =J
%END

100:%ENDOFPROGRAM
```

"4430 FIT"

```
%BEGIN
%ROUTINESPEC EQN SOLVE 3(%ARRAYNAME A,B)
%REAL DM0,AL,A0,DA,DA0,K,F1,F2,F3,F4,DMB0,DMB1,DMB2
%ARRAY A(1:3,1:3),B(1:3),B3(-1:200),F,DM,XL(1:24)
%INTEGER I,J

10:NEWLINES(4)
K=6.895
A0=.007053
DA0=.0002

XL(1)=164
XL(2)=165
XL(3)=173
XL(4)=180
XL(5)=181
XL(6)=192
XL(7)=201
XL(8)=209
XL(9)=220
XL(10)=230
XL(11)=231
XL(12)=232
XL(13)=233
XL(14)=234
XL(15)=235
XL(16)=252
XL(17)=264
XL(18)=265
XL(19)=266
XL(20)=267
XL(21)=268
XL(22)=269
XL(23)=270
XL(24)=275

%CYCLE I=1,1,24
   READ(DM(I));%IF DM(I)=1000 %THEN %STOP
%REPEAT
DA=DA0;AL=A0;J=-1;B3(-1)==-
1:J=J+1;F1=0;F2=0;F3=0;F4=0;DMB0=0;DMB1=0;DMB2=0
%CYCLE I=1,1,24
   F(I)=EXP(-AL*(XL(I)-220)↑2)+EXP(-K*AL*(XL(I)-220)↑2)
   F1=F1+F(I)/24
   F2=F2+F(I)*F(I)/24
   F3=F3+F(I)*F(I)*F(I)/24
   F4=F4+F(I)*F(I)*F(I)*F(I)/24
   DMB0=DMB0+DM(I)/24
   DMB1=DMB1+DM(I)*F(I)/24
   DMB2=DMB2+DM(I)*F(I)*F(I)/24
%REPEAT

A(1,1)=1; A(1,2)=F1;A(1,3)=F2; B(1)=DMB0
A(2,1)=F1;A(2,2)=F2;A(2,3)=F3; B(2)=DMB1
A(3,1)=F2;A(3,2)=F3;A(3,3)=F4; B(3)=DMB2
```

```
EQN SOLVE 3 (A,B)

B3(J)=B(3)
->4 %IF DA=.1DA0 %AND B3(J)*B3(J-1)<1@-9
->3 %IF J≠0 %AND B3(J)*B3(J-1)<1@-9
2:AL=AL+DA*B3(J)/MOD(B3(J));%CAPTION 2ND;PRINTFL(B3(J),3);SPACES(2)
->1
3:DA=.1DA0;  PRINT(J,2,0);%CAPTION =NO.OF␣STEPS␣TO␣PARITY␣CHANGE
NEWLINE;%CAPTION B3=;PRINTFL(B3(J),3)
->4 %IF DA=.001DA0
->2
4:NEWLINES(2);%CAPTION A=;PRINTFL(AL,6);SPACES(3)
              %CAPTION DMO=;PRINTFL(2B(2),6)
->10


%ROUTINE  EQN SOLVE 3 (%ARRAYNAME A,B)
%REAL  AMAX, CH, DET
%INTEGER  I,J,J MAX,S
DET = 1
%CYCLE  I = 1,1,2
A MAX = 0 ; J MAX = 0
%CYCLE  J = I,1,3
-> 4 %IF  MOD(A(J,I))<= A MAX
A MAX = MOD (A(J,I)); J MAX = J
4: %REPEAT
-> 5 %IF  J MAX = I
DET=-DET
-> 6 %IF  J MAX ≠ 0
DET = 0 ; -> 2
6: %CYCLE  J = I,1,3
CH=A(I,J)
A(I,J)=A(J MAX,J)
A(J MAX,J)=CH
%REPEAT
CH=B(I)
B(I)=B(J MAX)
B(J MAX) = CH
5: CH=A(I,I)
DET = DET*CH
%CYCLE  J = I+1,1,3
A MAX = A(J,I)/CH
%CYCLE  S=I+1 ,1,3
A(J,S)=A(J,S)-A(I,S)*A MAX
%REPEAT
B(J)=B(J)-B(I)*A MAX
%REPEAT
%REPEAT
CH=A(3,3)
DET=DET*CH
-> 2 %IF  DET = 0
B(3)=B(3)/CH.
%CYCLE  I=2,-1,1
CH=B(I)
%CYCLE  J=I+1,1,3
CH=CH-A(I,J)*B(J)
%REPEAT
B(I)=CH/A(I,I)
%REPEAT
2: %END


%ENDOFPROGRAM
```

REFERENCES

1. Lallemand, C.R. 203 243 (1936)

2. 2nd Symposium on Photoelectronic Imaging Devices. Advances in Electronics and Electron Physics 16 (1962)

3. 3rd Symposium on Photoelectronic Imaging Devices. Advances in Electronics and Electron Physics 22 (1966)

4. Annual Report of the Committee on Image Tubes for Telescopes, Carnegie Institution, Washington D.C. 1965-66

5. Frederick, Lowell Obs. Bul. 114 149 (1961)
A.J. 71 384 (1966)

Reference 3. p. 723

Livingston & Lynds, A.J. 68 284 (1963)
Ap.J. 140 818 (1964)
Reference 3. p. 705

Ford & Rubin, A.J. 71, 396 (1966)

Dunham, Reference 3. p. 729

6. Shannon, Bell Syst. Tech. J. 27 623 (1948)

7. Beckman, Thesis (Oxford) 1965

8. Reference 2. p. 37

9. Khogali, Thesis (Imperial College) 1963

10. Rose, J.S.M.P.E. 47 273 (1946)

11. Fellgett, M.N.R.A.S. 118 224 (1958)

12. Clark Jones, Phot. Sci. Eng. 2 57 (1958)

13. Lewis, Proc. Phys. Soc. 59 32 (1947)

14. Selwyn, Phot. J. 75 571 (1935)

15. O'Neill, J.O.S.A., 48 945 (1945)

16. Jones & Higgins, J.O.S.A. 35 435 (1945)
36 203 (1946)
37 217 (1947)
38 398 (1948)
41 41, 64, 192 (1951)
45 107 (1955)

17. Fellgett, J.O.S.A. 43 271 (1953)

18. Clark Jones, J.O.S.A. 45 799 (1955)

19. Marriage & Pitts, J.O.S.A. 46 1019 (1956)

20. Zweig, J.O.S.A. 46 805, 812 (1956)
49 238 (1959)

21. Schade, J.S.M.P.T.E. 73 81 (1964)

22. Woodward, "Probability and Information Theory, with Applications to Radar" (Pergamon Press, 1953)

23. Wiener, Acta Math. 55 118 (1930)

24. Fellgett & Linfoot, Phil. Trans. R.S. 247 46 (1955)

25. Carson, Bell Syst. Tech. J. 10 374 (1931)

26. Tamura & Kubota, J. Appl. Phys. (Japan) 26 92 (1957)

27. Wall & Steel, J. Phot. Sci. 12 34 (1964)

28. Nutting, Phil. Mag. 26 423 (1913)

29. Higson, Phot. J. 60 161 (1920)

30. Arens, Eggert & Heisenberg, Z. f. Wissenshaft. Phot. 28 31 (1930)

31. Silberstein, J. Frank. Inst. 251 359 (1951)

32. Trivelli, J. Frank. Inst. 241 1 (1946)

33. Seddon, Publ. Roy. Obs. Edin. 5 No. 6 (1966)

34. Thompson, Publ. Roy. Obs. Edin. 5 No. 12 (1967)

35. Kenney & Keeping, "Mathematics of Statistics II" (Van Nostrand, 1951)

36. Lynds & Aikens, P.A.S.P. 77 347 (1965)

37. Romer, I. Zhur. Nauch. Priklad. Fot. i Kin. 5 225 (1960)

38. Langner, Phot. Korr. 11 177 (1963)

39. Haugh, J. Phot. Sci. 11 65 (1963)

40. Levi, Rogers, et al., Mat. Fys. Medd. Dan. Vid. Selsk. 33 5 (1963)

41. Ilford Data Sheet Y44.1

42. N.P.L. Private Communication

43. Langner, J. Phot. Sci. 11 150 (1963)

44. Baker, Control 282 (1963)

45. Lamberts, J.O.S.A. 49 425 (1959)

46. O'Neill, "Introduction to Statistical Optics" (Addison Wesley, 1963)

47. Booth, "Numerical Methods" (Butterworth, 1955)

48. Kahan, Private Communication

49. Zajac & Ross, Nature 163 923 (1948)
164 311 (1949)

50. Mees, "Theory of the Photographic Process" (Macmillan, 1966)

51. Chandrasekhar, Rev. Mod. Phys. 15 1 (1943)

52. Young, Phys. Rev. 103 292 (1956)
J. App. Phys. 28 524 (1957)

53. Millington & White, Proc. Roy. Soc. 128A 701 (1928)

54. Hiltner, U.S. Govt. Res. Dev. Dept. AD 623914 41 (1966)

55. Lallemand, C.R. Acad. Sc. Paris 262 838 (1966)

56. Merrill, Ap. J. 83 126 (1936)
Merrill & Humason, P.A.S.P. 50 212 (1938)

57. Publications of the Royal Observatory Edinburgh 4 (1964)

58. Seddon, Nature 214, 257 (1967)

59. Duke, Ap. J. 113 100 (1951)

60. Shaw, J. Phot. Sci. 11 199 (1963)
11 313 (1963)
13 308 (1965)